GCA TECHNICAL REPORT NO. 64-14-N

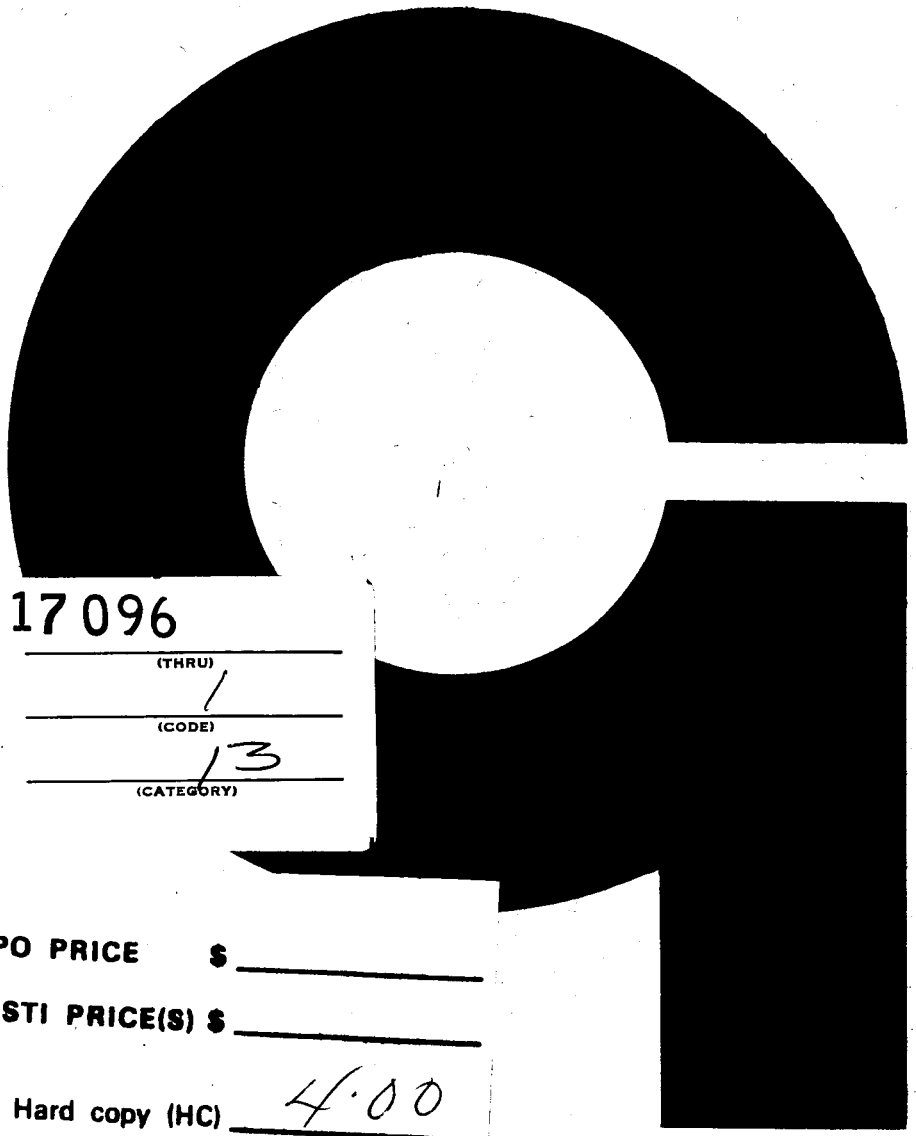

MEASUREMENTS IN THE IONOSPHERE DURING A SOLAR ECLIPSE

L. G. SMITH L. H. WEEKS C. A. ACCARDO P. J. McKINNON

FINAL REPORT
CONTRACT NO. NASw-500

PREPARED FOR
NATIONAL AERONAUTICS AND SPACE ADMINISTRATION
HEADQUARTERS
WASHINGTON 25, D. C.

AUGUST 1964

GEOPHYSICS CORPORATION OF AMERICA BEDFORD, MASSACHUSETTS

GCA Technical Report No. 64-14-N

MEASUREMENTS IN THE IONOSPHERE DURING A SOLAR ECLIPSE

L. G. Smith
L. H. Weeks
C. A. Accardo
P. J. McKinnon

FINAL REPORT

Contract No. NASw-500

August 1964

GEOPHYSICS CORPORATION OF AMERICA
Bedford, Massachusetts

Prepared for

NATIONAL AERONAUTICS AND SPACE ADMINISTRATION
Headquarters
Washington 25, D.C.

SUMMARY

The behavior of the inosphere up to 200 km was observed in a series of rocket flights at Fort Churchill, Manitoba, during the solar eclipse of 20 July 1963. Six Nike Apache rockets were instrumented to measure electron density, electron temperature, Lyman-α radiation and a band of X-rays (44-60Å). The electron density in the E-region (90-160 km) was reduced during the eclipse without any significant change in the shape of the profile. The rocket data show a time lag between the minimum area of the visible solar disc and the minimum electron density of much less than 3 minutes. Comparison with ionosonde data indicates a minimum value of 1×10^{-7} cm^3 sec^{-1} for the effective recombination coefficient of the E-layer. The rocket observations also indicate that the ionizing radiation causing the E-layer is reduced during the eclipse in proportion to the intensity of the measured band of X-rays. The variation of electron temperature in the E-region due to the eclipse is found to be small. The electron density in the D-region (50-90 km) shows a more complex variation. Between 79 and 89 km a time lag of about 3 minutes is indicated, but at lower heights, as at greater heights, the time lag is much smaller. Below 72 km the effect of the eclipse on electron density is much more pronounced than at greater heights for the observations taken with 8% and 15% of the disc visible, but not for the observation taken with 60% of the disc visible.

TABLE OF CONTENTS

LIST OF ILLUSTRATIONS

LIST OF ILLUSTRATIONS (continued)

INTRODUCTION

A series of six sounding rockets (Nike Apache) were launched from Fort Churchill, Canada, during the eclipse of 20 July 1963. These rockets were instrumented to measure electron density and electron temperature by a probe technique and solar radiation in the UV and X-ray regions of the spectrum by means of narrow band detectors.

The importance of solar eclipses in ionospheric studies was brought out at an international symposium held in London in 1955 [1].* At the time of the conference no rockets had been used in eclipse work; the measurements presented were ground-based, principally the ionosonde (ionospheric sweep-frequency sounder). Later, in October, 1958, the incident solar radiation in the UV and X-ray regions of the spectrum was measured by rockets fired during an eclipse [2]. The present direct measurements of electron density in the ionosphere during an eclipse are believed to be the first such measurements.

The value of eclipse observations is principally in the D-, E- and F_1-regions of the ionosphere, that is, the regions below 250 km. There are two main reasons why the ionosphere above 250 km (F_2-region) is considered to be of minor interest in an eclipse: First, the F_2-region is considerably less regular in its behavior even on magnetically quiet days, so that any disturbance associated with the eclipse is difficult to identify positively, and second, the time constants appropriate to the decay of electrons are sufficiently great that only a relatively small effect in the F_2-region would be observed. Only below 250 km is it likely that rocket measurements can produce results of immediate significance.

The E-layer, at about 110 km, being the most regular of the ionospheric layers, shows the most clearly defined eclipse effect. The occasional occurrence of sporadic E interferes with the interpretation of ionosonde records but this is no problem in rocket measurements of electron density. It is found that the electron density decreases as the sun's disc is gradually obscured but even in total eclipses of the maximum possible duration (about 7 minutes) the electron density decreases to no less than one third of its normal value.

The first generally accepted explanation of this remarkable observation was that, although the ionizing radiation from the sun had been removed from the region, the relaxation time appropriate to the process by which electrons were removed (recombination) did not allow the electron density to decay to zero during the eclipse. It was found that a recombination coefficient of $2 \times 10^{-8} cm^3 sec^{-1}$ would allow a reasonable explanation of the minimum value of electron density. The calculations

*Numbers in [ ] throughout text indicate reference numbers.

also showed that there must be a time lag of about 5 minutes between the end of totality and the minimum of electron density. However, the most careful observations show that this time lag is not always present. In addition this value of recombination coefficient is smaller than recent laboratory and theoretical studies indicate.

An alternative and, currently, the most acceptable explanation is that the ionizing radiation is not, in fact, reduced to zero during a total eclipse. This is supported by the 1958 rocket measurements which showed that a significant fraction of the solar X-ray flux was present at totality. Thus the measurement of solar X-rays becomes an important part of the design of the present experiment.

The F_1-layer (or ledge) at about 180 km, when present at the time of an eclipse, shows a variation which is closely similar to that of the E-layer. In particular the electron density is reduced by the same factor and the time lag is usually the same for both layers. The higher value of electron density (almost twice that of the E-layer) consequently leads to smaller values of recombination coefficient when the "sluggishness" hypothesis is used. The hypothesis is equally unacceptable for this part of the ionosphere as for the E-layer. The alternative "residual radiation" hypothesis has not yet been applied to the F_1-layer. The importance of the layer leads to the requirement of a vehicle for this program which has an apogee altitude of at least 180 km.

The D-region (60-90 km has received relatively little attention in eclipse investigations largely due to the difficulty of obtaining a direct measurement of the electron density profile. The complex structure of the region is gradually being resolved and eclipse measurements from rockets have a particular value. In addition to determining the electron density profile, rocket-borne instruments can obtain the incident flux and absorption profile of Lyman-α, the only solar UV radiation of any significance in this part of the ionosphere.

The recent development of the so-called direct measurement techniques for measuring electron and ion density in the ionosphere including the Langmuir probe, radio-frequency probe and ion-traps means that it is now possible to design an experiment in which the incident ionizing radiations and the ions they produce can be measured simultaneously by a rocket sent into the ionosphere. The Langmuir probe technique is felt to be the most powerful of the direct-measurement methods for electron density while ion chambers and Geiger counters are available for the measurements of Lyman-α and X-rays respectively.

The eclipse of 20 July 1963 provided the opportunity to make rocket measurements relevant to the ionosphere up to 200 km. The path of totality of the eclipse passed about 220 km from Churchill, Manitoba, as shown by the map, Figure 1. At 2106 UT, (1506 Central Standard Time) Churchill was deep in the penumbra, 94% of the area of the disc being covered by

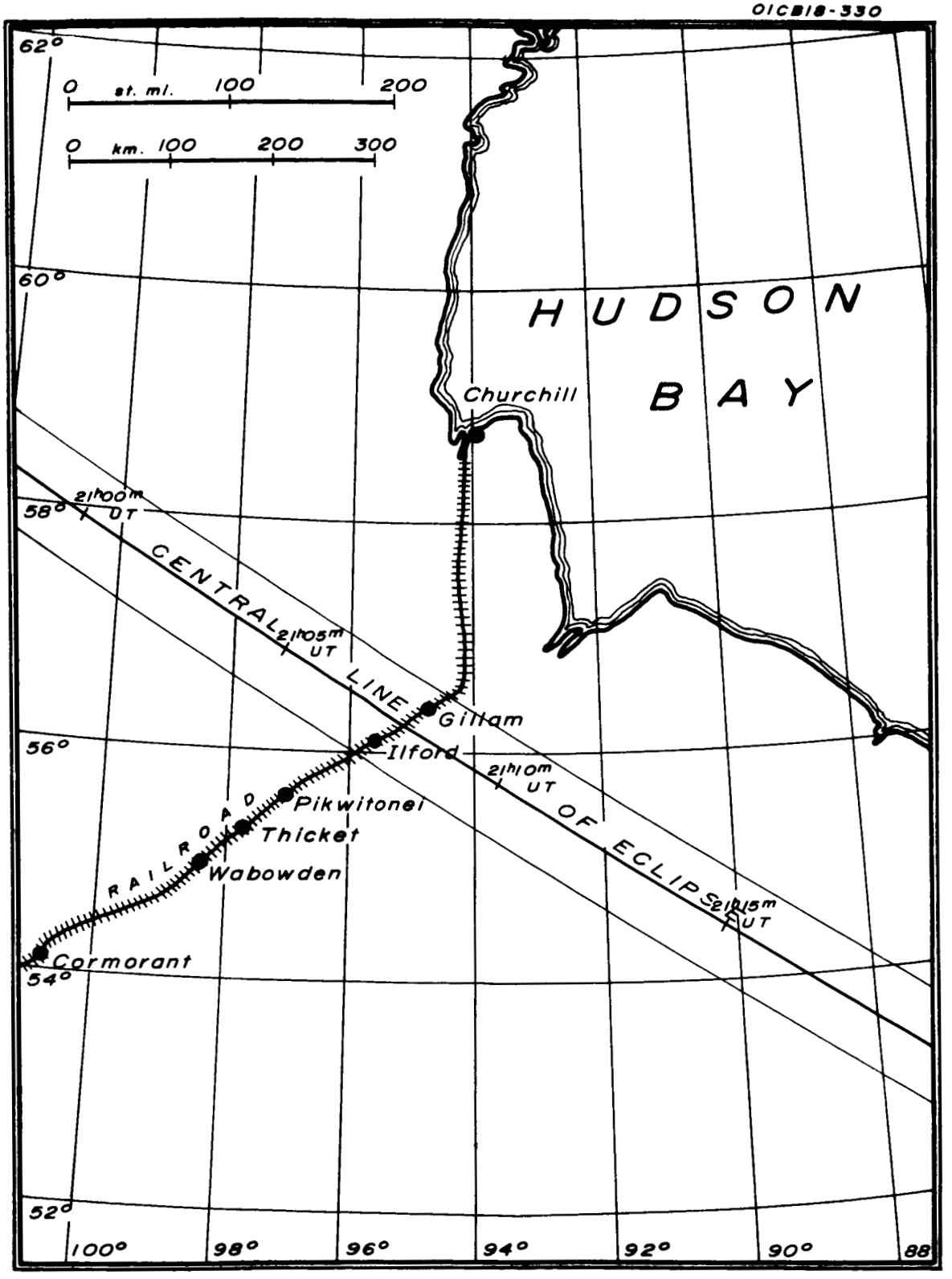

Figure 1. Eclipse of 1963 July 20.

the moon. At higher altitudes the magnitude of the eclipse was slightly less, as seen from the geometric circumstances represented in Figure 2. At Churchill the eclipse lasted 2 hours 18 minutes, first and last contacts occurring respectively at 1955 UT and 2213 UT.

The launch times were selected to give maximum information in the event of the failure of any particular vehicle or instrument. The primary vehicles were the ones at (or close to) first contact (Nike Apache 14.89, launch time 2000 UT), maximum phase (Nike Apache 14.91, 2103 UT) and last contact (Nike Apache 14.94, 2110 UT). A vehicle was launched ten minutes after maximum phase (Nike Apache 14.92, 2113 UT) and at two intermediate times (Nike Apache 14.90, 2030 UT, and Nike Apache 14.93, 2140 UT).

The vehicles were all launched within two seconds of the specified time with all instrumentation working. Two of the flights (14.89 and 14.90) ended in complete failure with explosion of the Nike stage about three seconds after launch. The excellent performance of the four subsequent vehicles, starting with the maximum phase of the eclipse, largely compensates for the failure of the first two. The telemetry transmitter of 14.91 failed late in the flight resulting in some loss of data and the doors covering the sensors failed to eject on 14.93 resulting in loss of solar radiation data. As will be seen in the later sections of the report, the data obtained in the series of flights was sufficient and the scientific objectives of the project were not compromised.

On 14 July 1963, six days prior to the eclipse, Nike Apache 14.88 was launched (at 2103:28 UT) to obtain background at data and to test the system. This flight was only partially successful with respect to the stated objectives, partly because of poor vehicle attitude and partly because of a minor absorption event which disturbed the ionosphere. The data has been analysed and is presented separately from the eclipse observations.

Earlier in the program two flights were made as a test of the instrumentation. These were Nike Apache 14.86, launched on 27 February 1963 at 1430 EST (1930 UT), and Nike Apache 14.87, launched 28 March 1963 at 1560 EST (2006 UT), both from Wallops Island.

The following technical reports were prepared during the course of the project.

(1) L.H. Weeks, "Useful Ranges of Some Solar Detectors," GCA Technical Report No. 63-5-N, February 1963. [3]

(2) C.A. Accardo, H.G. Gross and L.H. Weeks, "A Rocket-Borne 44-60 Å Geiger Counter," GCA Technical Report No. 63-14-N, May 1963. [4]

(3) L.H. Weeks, "A Survey of the Lower Ionosphere during Solar Eclipses," GCA Technical Report No. 63-20-N, July 1963. [5]

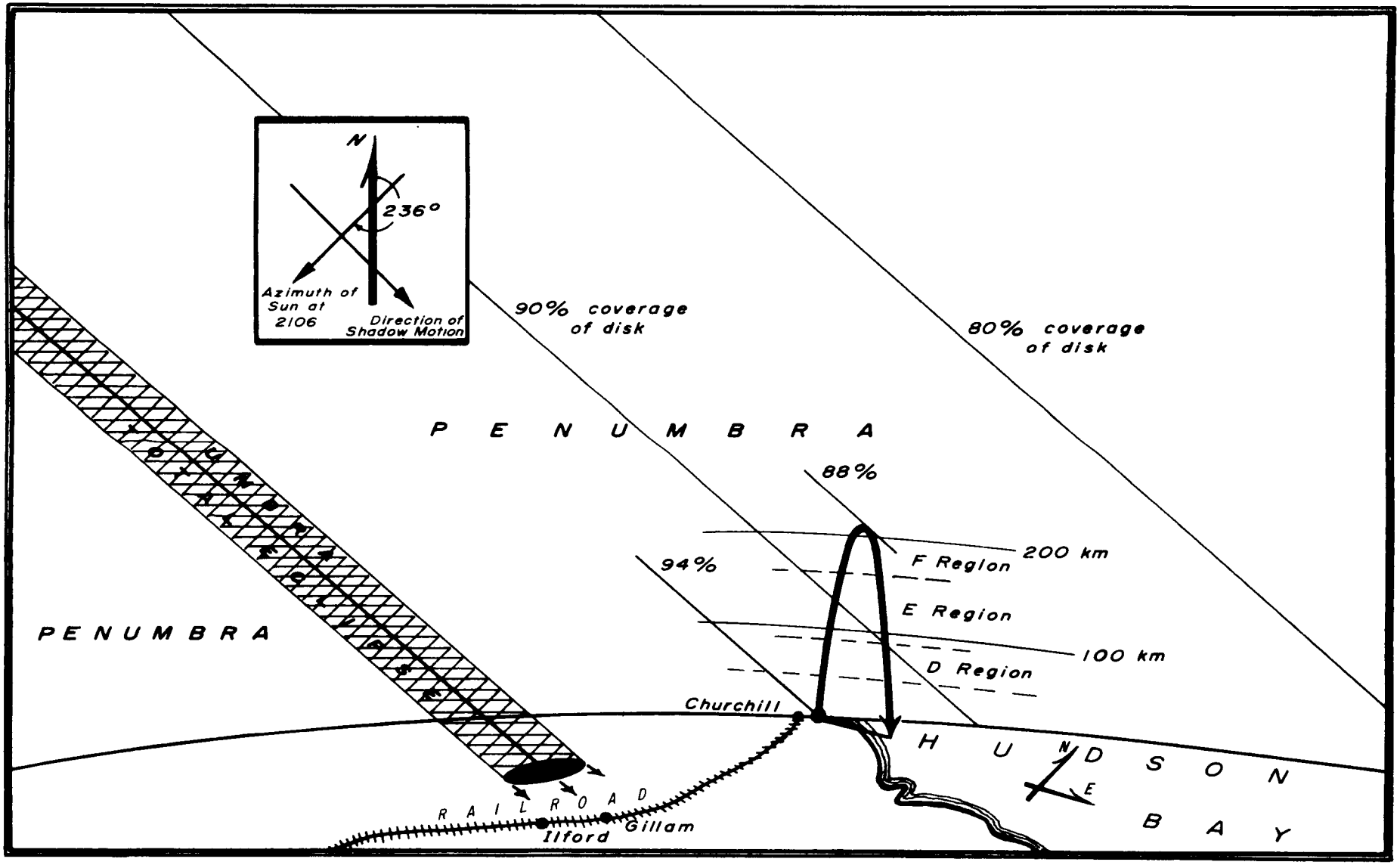

Figure 2. Diagram showing the relation of the solar eclipse to rocket trajectory at Churchill, Manitoba - 2106 universal time 20 July 1963.

(4) L.G. Smith, C.A. Accardo, L.H. Weeks and P.J. McKinnon, "Rocket Measurements in the Ionosphere during the Eclipse of 20 July 1963," GCA Technical Report No. 64-11-N, May 1964. [6] Paper presented at the Fifth International Space Science Symposium of COSPAR, Florence, May 1964.

In addition to the presentation at COSPAR, the results of the eclipse measurements were presented at the AGU Annual Meeting, Washington, D. C., April 1964.

The two following reports were, in part, prepared during the course of this project.

(1) L.G. Smith, "A DC Probe for Rocket Measurements in the Ionosphere," GCA Technical Report No. 63-19-N, June 1963. Included in COSPAR Information Bulletin No. 17, Ed. K. Meada, February, 1964. [7]

(2) P.J. McKinnon and L.G. Smith, "A Solar Aspect Sensor for Sounding Rockets," GCA Technical Report No. 64-12-N, July 1964. [8] Paper presented at the IEEE Region 3 Annual Meeting and Technical Conference, Clearwater, Florida, May 1964.

Reference will be made to these reports in the appropriate sections of this report.

PAYLOAD INSTRUMENTATION

The scientific instrumentation of the payload consists of the Langmuir probe, two Lyman-α ion chambers and the X-ray Geiger counter. Supporting instrumentation consists of two solar aspect sensors and a magnetic aspect sensor. Figure 3 is a photograph of one of the payloads. The general arrangement of these components in the payload is shown in Figure 4. The interconnection of the major assemblies is shown schematically in Figure 5. Some details of the payload are given on the following pages.

DC Probe

The DC probe consists of three main parts, namely, (1) the nose electrode and connector, (2) the program unit, and (3) the electrometer.

The nose electrode, which replaces the nose tip of the rocket, is insulated from the body of the rocket and its potential is swept from -2.7 volts to +2.7 volts by the program unit. The variation of current with voltage is then analyzed in the manner of the Langmuir probe technique to obtain electron temperature. The sweep which has a duration of 0.5 second is programmed onto the probe at intervals of 2 seconds. Between sweeps the electrode is held at a constant potential of +2.7 volts (with respect to the body of the rocket), The probe current is found to be proportional to electron density. Although its use in the D-region below about 85 km is without theoretical basis, the technique does appear to give reasonable values of electron density as low as 55 km. The particular value of the fixed voltage method of measurement is that it permits observations of the fine structure of the electron density profile. The construction and use of the instrument has been described in reference [7] which should be consulted for further details.

The program unit also includes a mechanical commutator which is used to commutate data from the magnetometer, the baroswitch, and payload monitor voltages. It is electrically independent of the probe circuit.

Lyman-α Ion Chamber

A view of a Lyman-α ion chamber before assembly is given in Figure 6. The gold plated ceramic envelope and gold plated silver flange shown in the figure are identical to the design described by Stober [8a]. The spectral response of the ion chamber (1050-1240Å) is limited at low wavelengths end by the transmission cutoff of the 2 mm thick lithium fluoride windows. The high wavelength limit is determined by

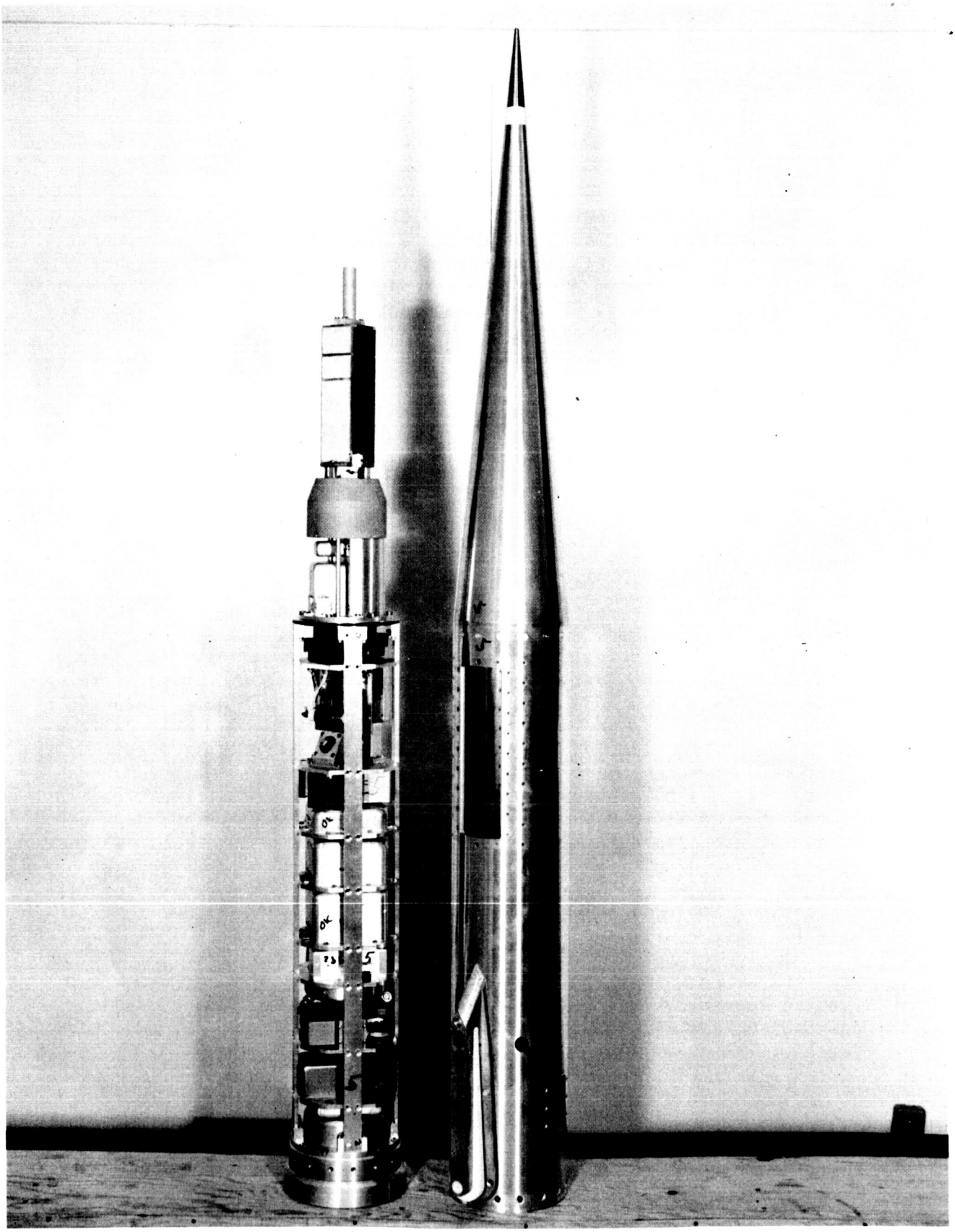

Figure 3. One of six Nike Apache payloads launched during the solar eclipse of 20 July 1963 at Fort Churchill.

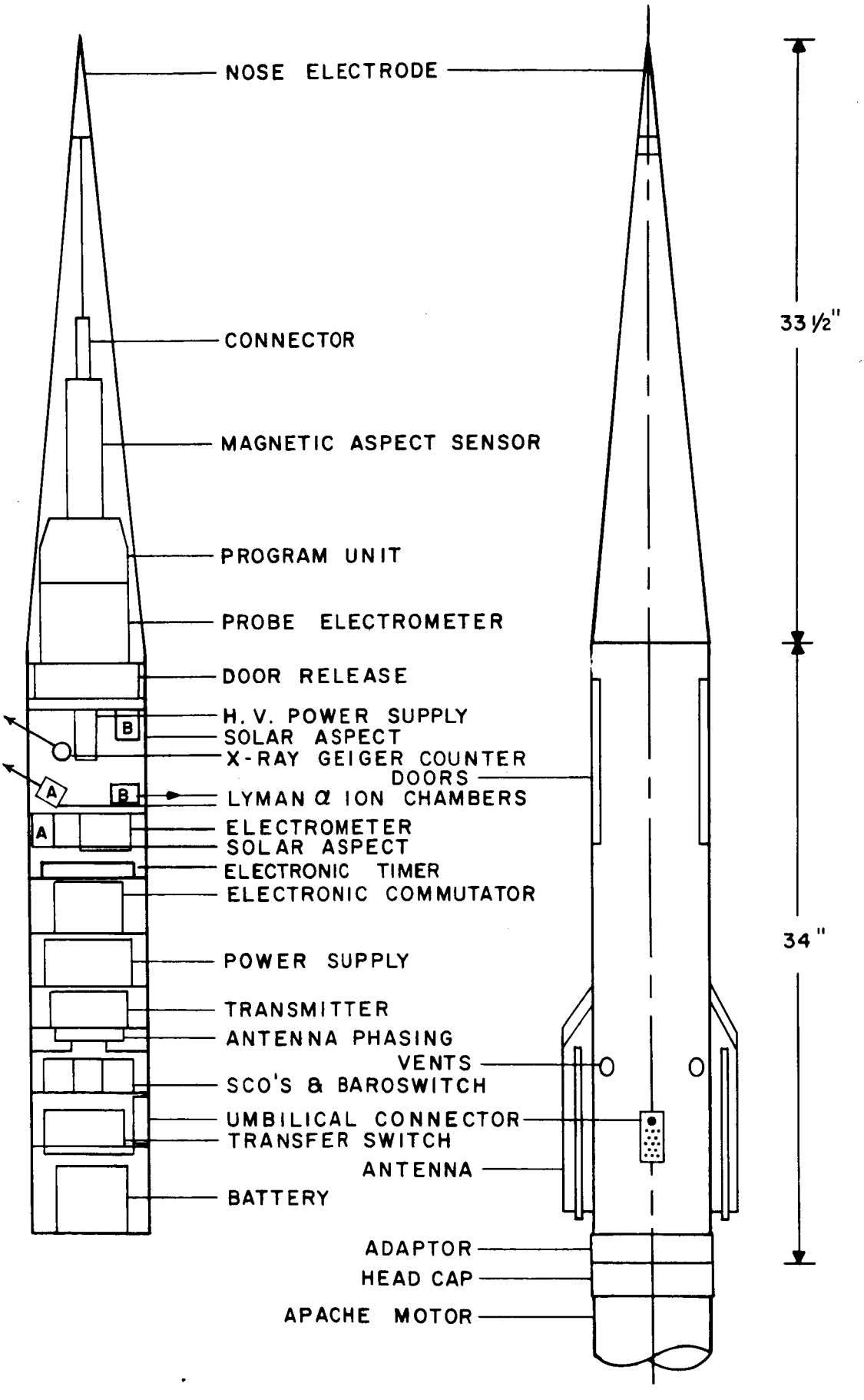

Figure 4. Payload configuration for Nike Apaches 14.86 to 14.94.

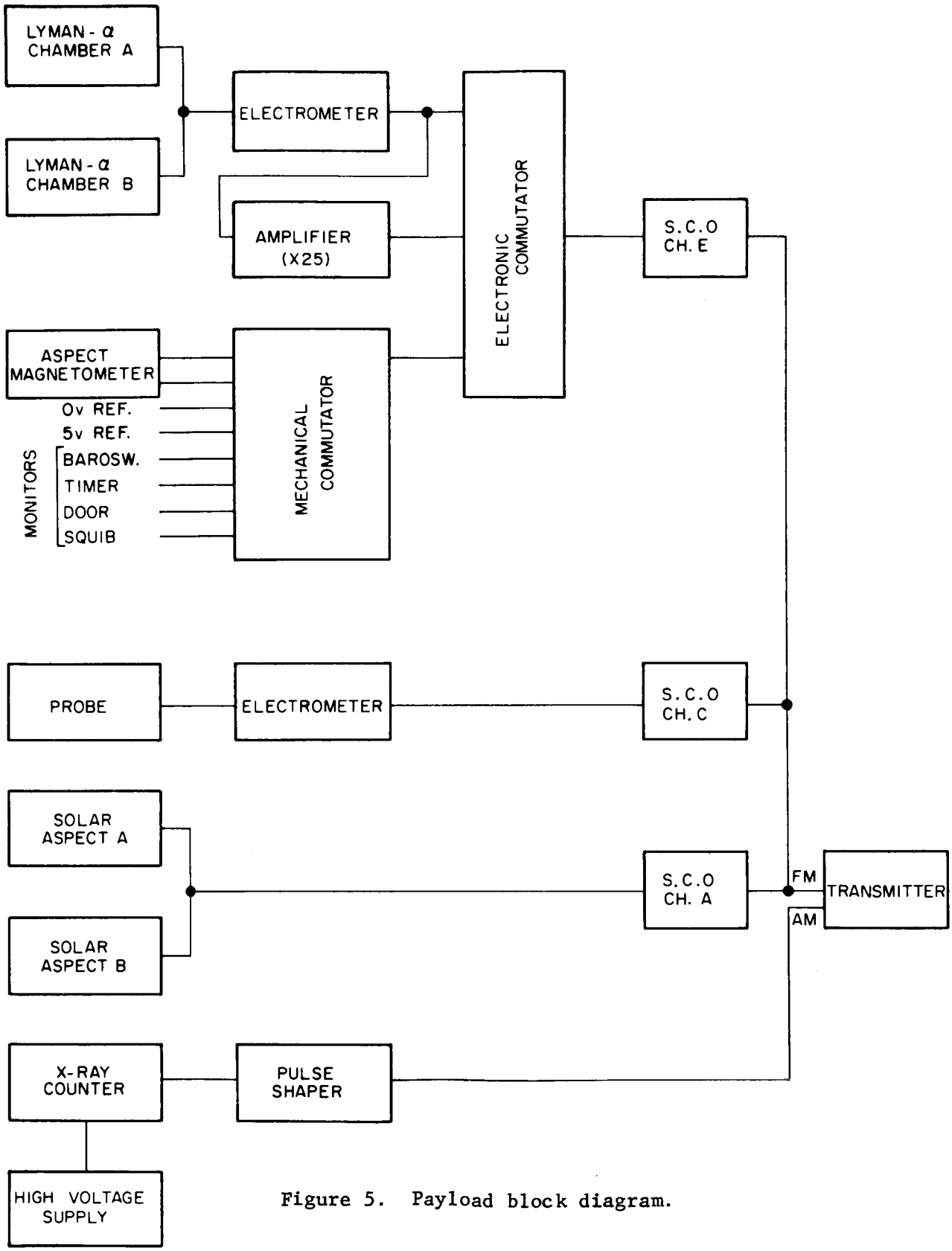

Figure 5. Payload block diagram.

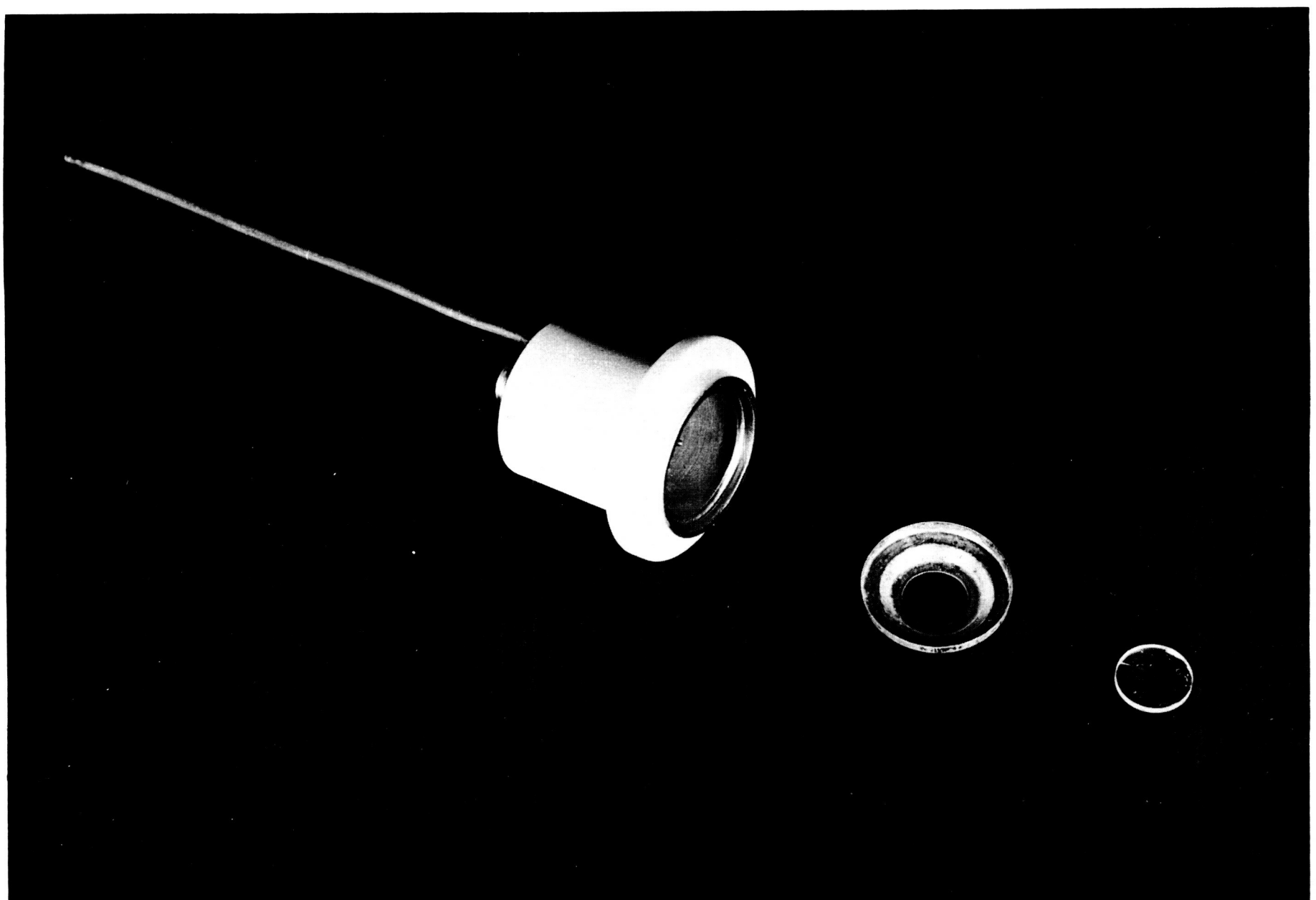

Figure 6. Ceramic-metal envelope subassembly with flange and lithium fluoride window for an ion chamber.

the photoionization onset of the gas fill, carbon disulphide (15 mm pressure). The more frequently used nitric oxide gas has a somewhat lower efficiency and a higher wavelength photoionization onset (1350Å). For this reason carbon disulphide was considered preferable. The use of carbon disulphide in such an ion chamber has been discussed by Stober [8b]. In the wavelength range measured by the ion chamber, Lyman-α contributes 80 percent or more to the total response at the top of the atmosphere, and in the D-region the contribution of Lyman-α is even greater. Preflight laboratory calibrations of the ion chambers at Lyman-α are made with a spectrograph, using a standard ion chamber to establish the flux.

Each payload is instrumented with two ion chambers, one oriented at 60° with respect to the rocket axis and the other perpendicular to the rocket axis (except Nike Apache 14.86 in which the second was at 120° to the axis). The additional ion chamber is added as a cross check for the data analysis, and also to serve as a spare in case of a failure.

X-Ray Geiger Counter

A complete description of these Geiger counters is presented by Accardo et al.[4]. The orientation of a Geiger counter in the payload is shown in Figure 7. Also shown in this figure is a Lyman-α ion chamber directly below the Geiger counter and a solar aspect sensor. The Geiger counter is oriented at 60° with respect to the rocket axis.

SOLAR ASPECT SENSOR

The solar aspect sensor is designed to measure the angle between the longitudinal axis of a spin stabilized rocket and the sun-rocket line for angles between 20° and 160° with an accuracy of $\pm 1^{\circ}$.

Its primary purpose is to provide aspect data to correct the measured response of solar radiation detectors to conditions of normal incidence.

The technique involves a diamond-shaped aperture with a light detector placed a fixed distance behind the center of the aperture. The sensor is mounted with the long axis parallel to the spin axis of the rocket. As the rocket spins, the detector, indicating the intersection of the sun detector line and the aperture, functions as an off-on switch. The aspect angle is obtained from the time interval between the two pulses generated in the device by the spin of the rocket. Figure 8 is an exploded view of the assembly.

In addition to its primary purpose, the instrument provides valuable information on vehicle motion. The most readily determined value is spin rate. The included angle and period of the precession cone are also obtained.

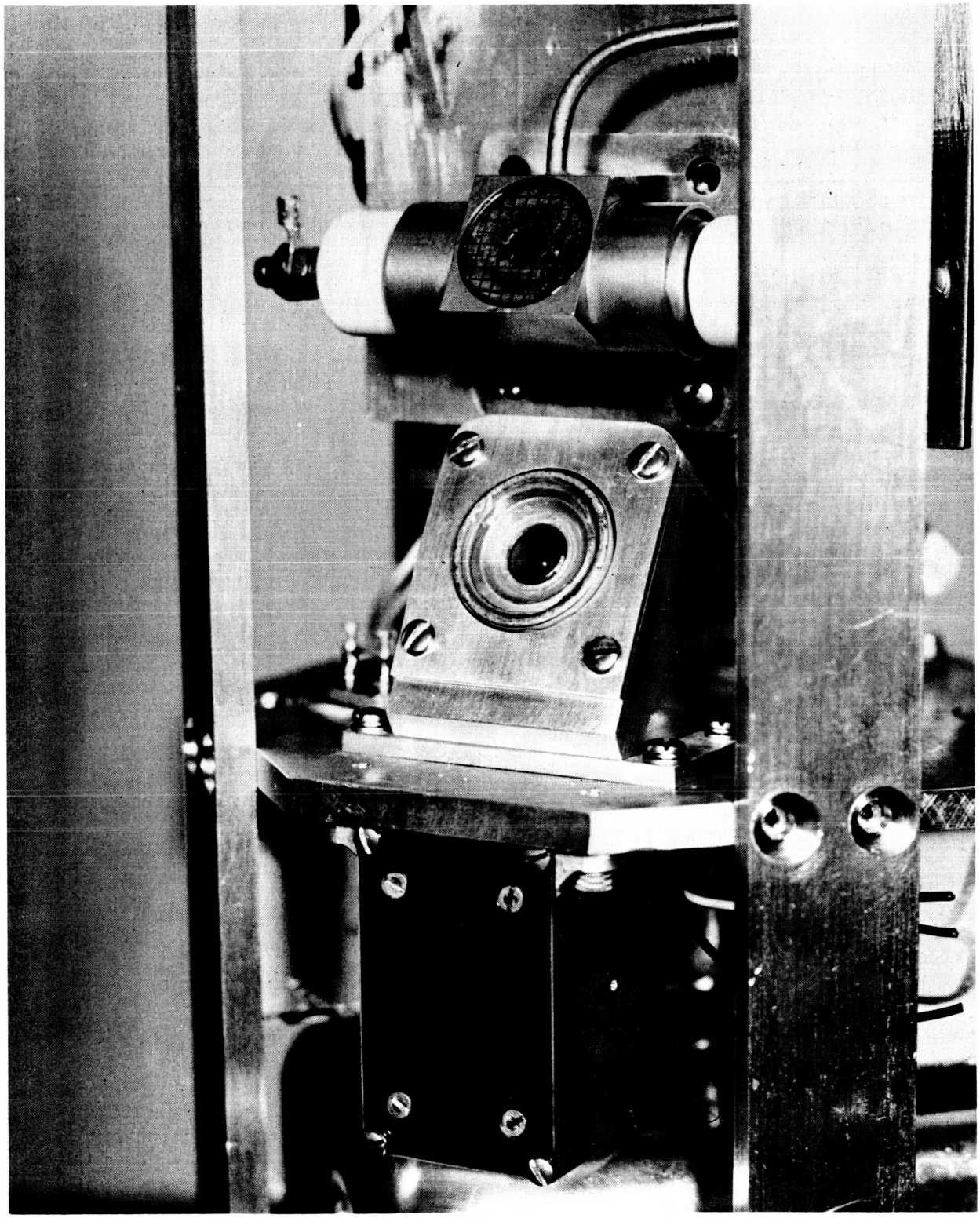

Figure 7. Orientation of Geiger counter.

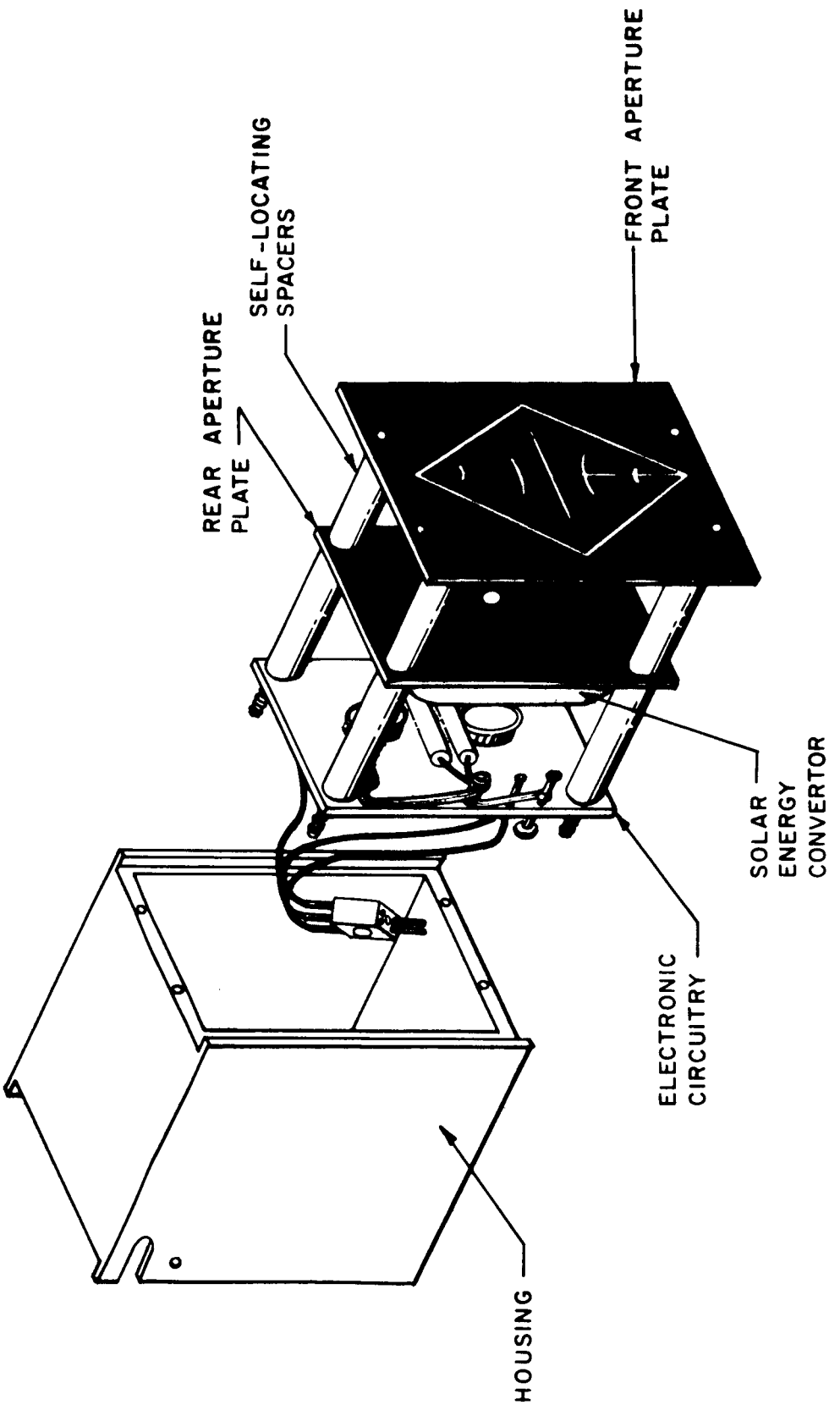

Figure 8. Exploded view of solar aspect sensor.

The construction and use of this instrument has been described in reference [8] which should be consulted for further detail.

Magnetic Aspect Sensor

One magnetic aspect sensor (Schonstedt, Model RAM-3) is mounted along the longitudinal axis of the vehicle primarily to sense precessional motion. Prior to solar aspect sensor exposure at T+50 seconds, this aspect sensor is the sole means of determining vehicle motion. In the vehicle performance section of the report the discussion of magnetometer aspect sensor data of Nike Apache 14.89 and 14.90 will point up the usefulness of the instrument.

Dual Door Release

The dual door release mechanism, whose function is to release two oppositely located panels in the payload housing, is shown in Figure 9. A bellows actuator (Hercules BA31K2) is used for initiating release. Each door is fastened to the end of a split bar by means of a screw that passes through a clearance hole in the door and threads into a tapped hole in the split bar. When the split bar is caused to spread the tapped hole in each end opens up approximately 1/4 inch, thereby disengaging the door screw and allowing rapid simultaneous ejection of each door. The doors rotate about their base hinge approximately 30^{o} when complete disengagement from the payload occurs.

The ejectable doors, covering the solar radiation sensors during launch phase, are released at 150,000 feet. The circuit is armed at 70,000 feet by the baroswitch. This initiates an electronic timer set for 20 seconds delay. A relay closure results in the firing of the bellows actuator which releases the doors. A schematic of the firing circuit is shown in Figure 10.

Power

The system is powered by a 34-volt "one shot" battery (Eagle-Picher No. 1025-V) which is capable of delivering 2 amp for 1 hour. The payload in flight requires 1.8 amp. The battery is connected directly to a voltage regulator set for 28 volts. All instrumentation obtains power through this regulator. A DC to DC converter provides 200 volts for the transmitter and -28 volts for the electrometers used in the probe and UV experiments.

Telemetry

The telemetry system uses a 2-watt FM/FM transmitter (Telechrome, Model 1483-A16) , shown in Figure 11, which is modulated by three

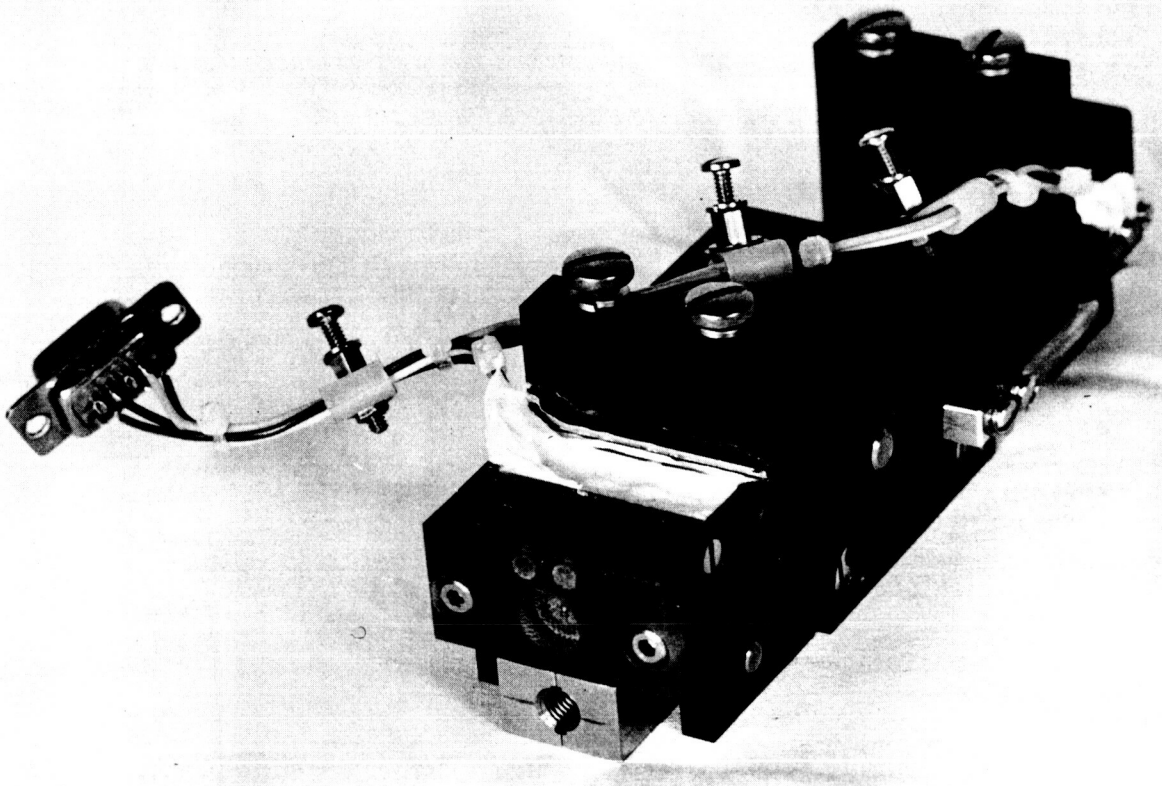

Figure 9. Door release mechanism.

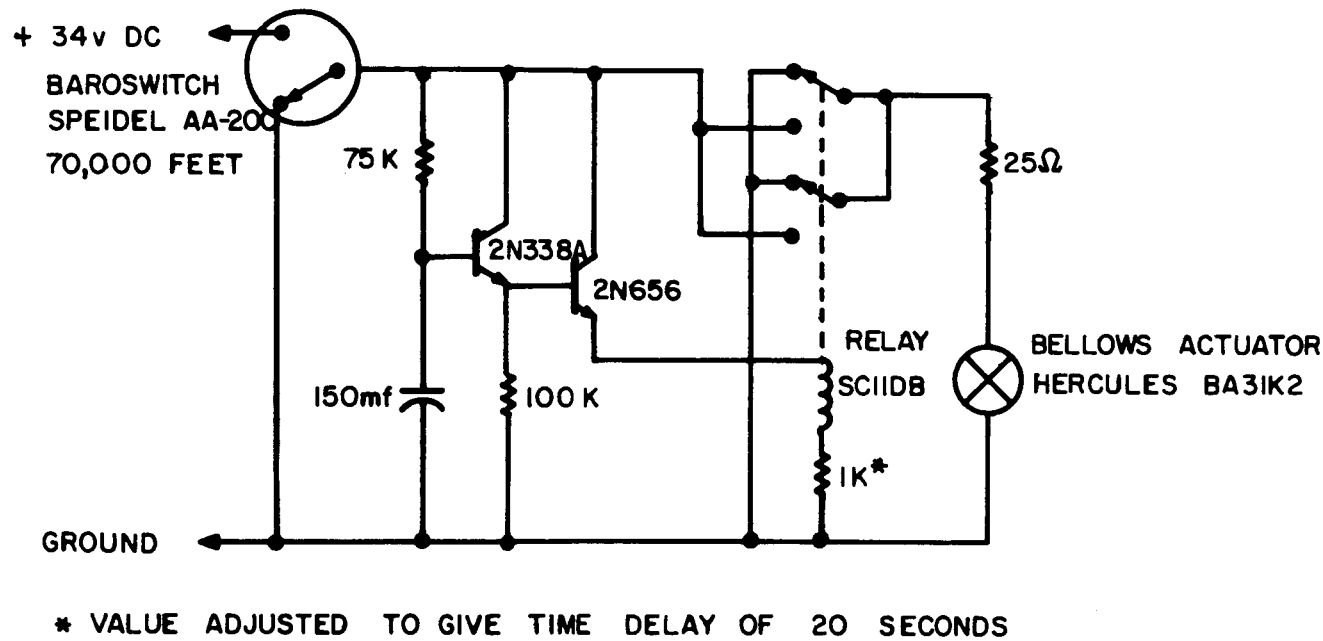

Figure 10. Circuit of timer.

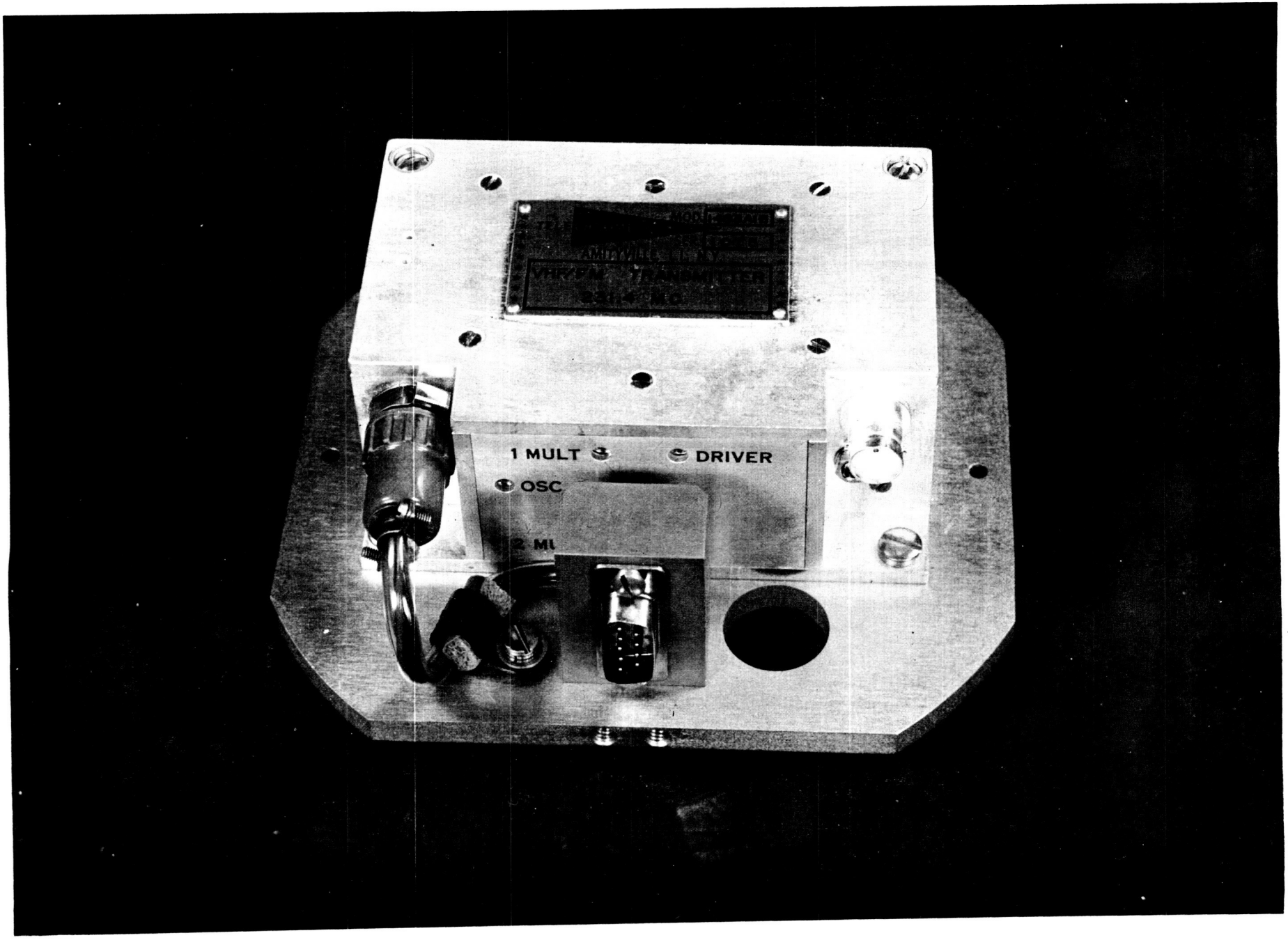

Figure 11. Typical transmitter deck.

subcarrier oscillators, IRIG Channels A(22 kc/sec), C(40 kc/sec), and E(70 kc/sec), and AM modulated by pulse data from the X-ray Geiger counter. Quarterwave quadraloop antennas replace the standard turnstile type to reduce aerodynamic drag. Since six vehicles were launched during the two-hour period of the eclipse, alternate payloads operated at different carrier frequencies (229.9 mc/sec or 231.4 mc/sec) to permit simultaneous tracking and prelaunch checkout without RF interference.

The Geiger counter electronics provides data to the telemetry in the form of pulses at a maximum rate of 6000 counts per second. Because the experiment is conducted on a vehicle which is not equipped with a pointing control by an instrument which is aspect-dependent, the highest degree of accuracy in determining the true count rates was obtained by transmitting each individual Geiger pulse. The most straightforward technique for transmitting the wideband Geiger counter data and the data from the other experiments in real time without using two transmitters is to amplitude modulate the FM/FM transmitter. The technique is implemented by properly coupling the positive going pulses of the Geiger counter wave shaping circuitry to the cathodes of the two transmitter output tubes which are grounded-grid amplifiers connected in push-pull. The positive pulses pull the tubes toward cutoff, having the effect of momentarily reducing transmitter output. The modulation percentage of the carrier is 30 percent to produce a signal-to-noise ratio of 12 db at the receiver output. Figure 12 is a graph of modulating input voltage versus percent modulation, empirically determined for these transmitters. The FM/FM carrier includes an undesirable effect referred to as incidental AM resulting from other than flat frequency response in the multipliers of the transmitter. A typical range of values of incidental AM is 3 to 5 percent. The output signal of the AM detector at the ground station receiver is characterized by three parts, (1) the intelligence, (2) the incidental AM, and (3) noise. The effect of the latter two is reduced by limiting the bandwidth of the receiver video output to 30 kc/sec.

The electronic commutator operates at a commutation rate of 700 samples per second, except in Nike Apache 14.86 where the rate was 2100 samples per second. The novel method used to obtain the commutated information is made possible through the development of the Inch (National Semiconductor), an integrated chopper. The Inch, serving as a relay, is connected in the collector circuit of each of a series of multivibrators. The number of channels determines the number of multivibrators. An oscillator provides a timing pulse to the first multivibrator at a frequency equal to the sampling rate per channel. The first multivibrator changes state when triggered by the timing pulse. The Inch is activated, allowing information to be transmitted. The read-out time for each sample is set by the time constant of the multivibrator. As the first multivibrator returns to the off state, the action is coupled over to trigger the second multivibrator, etc. At the end of the sequence, the oscillator triggers the first multivibrator again.

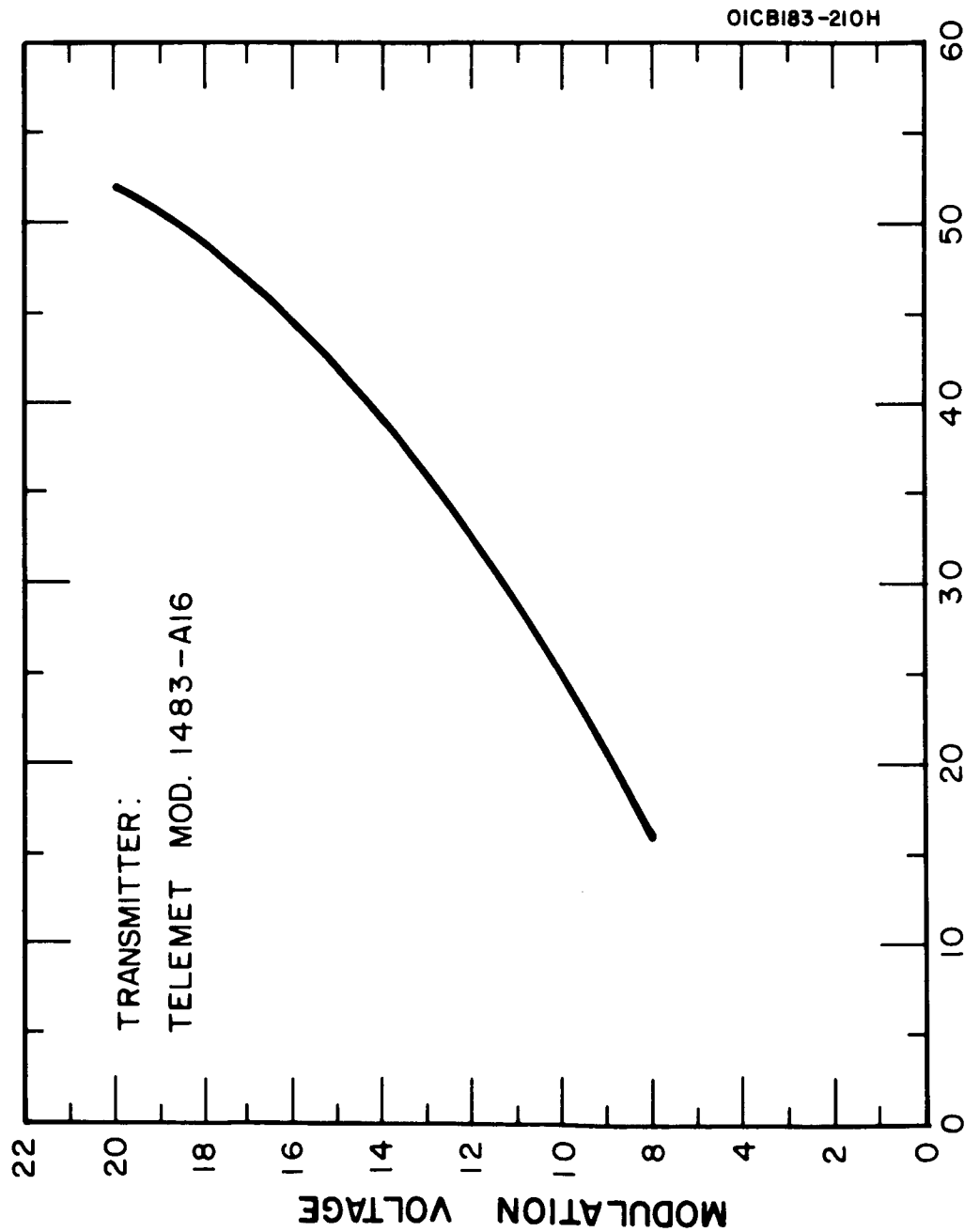

Figure 12. Amplitude modulation of transmitter.

The three inputs fed to the electronic commutator are

(1) Lyman-α high gain channel

(2) Lyman-α low gain channel

(3) Output of the mechanical commutator.

Baroswitch

The use of a baroswitch (Speidel Model AA-200, 70,000 ft.) for obtaining approximate apogee of the vehicle represents a form of low-cost tracking back-up. Excellent apogee correlation with radar skin track has been obtained in past Nike Apache and Cajun flights. In the event of tracking failure or limited radar tracking facilities the vertical component of rocket trajectory is obtained to an accuracy of better than 1 km in height. The payload is vented by four holes in the payload shell. The holes, 1 inch in diameter and 90° apart, are placed close to the level of the baroswitch.

The use of the baroswitch is described in reference [9]. An example of the method of trajectory calculation is given in a later section of this report.

Ground Instrumentation and Payload Controls

The payload is controlled and monitored prior to launch from the ground control console to which it is connected by the umbilical cable. The system is arranged so that the status of the instrumentation may be determined at any time without turning on the transmitter.

Figure 13 illustrates the ground control console and one of the eclipse payloads. The following design features characterize the console: (1) Payload experiment functions are displayed on an oscilloscope; sequential checks of the experiments can be rapidly performed and controlled at the push-button control panel. (2) Payload monitor functions (e.g., battery voltage, transmitter B + voltage, etc.) are displayed on meters; (3) Umbilical release is controlled from the control console; (4) Continuity test of umbilical release circuit can be performed.

The control deck of the payload is shown in Figure 14. The deck contains the cutoff relay, control relay, motor-driven transfer switch, and a 20-pin male umbilical connector. The female umbilical connector is attached to the payload by an explosive bolt (Holex No. 2503-10).

In the transfer switch, a 1 rpm motor, geared down a ratio of 3:1 is used to drive a series of cam-actuated switches. Power is normally supplied to the motor from the DC power supply in the console but can be

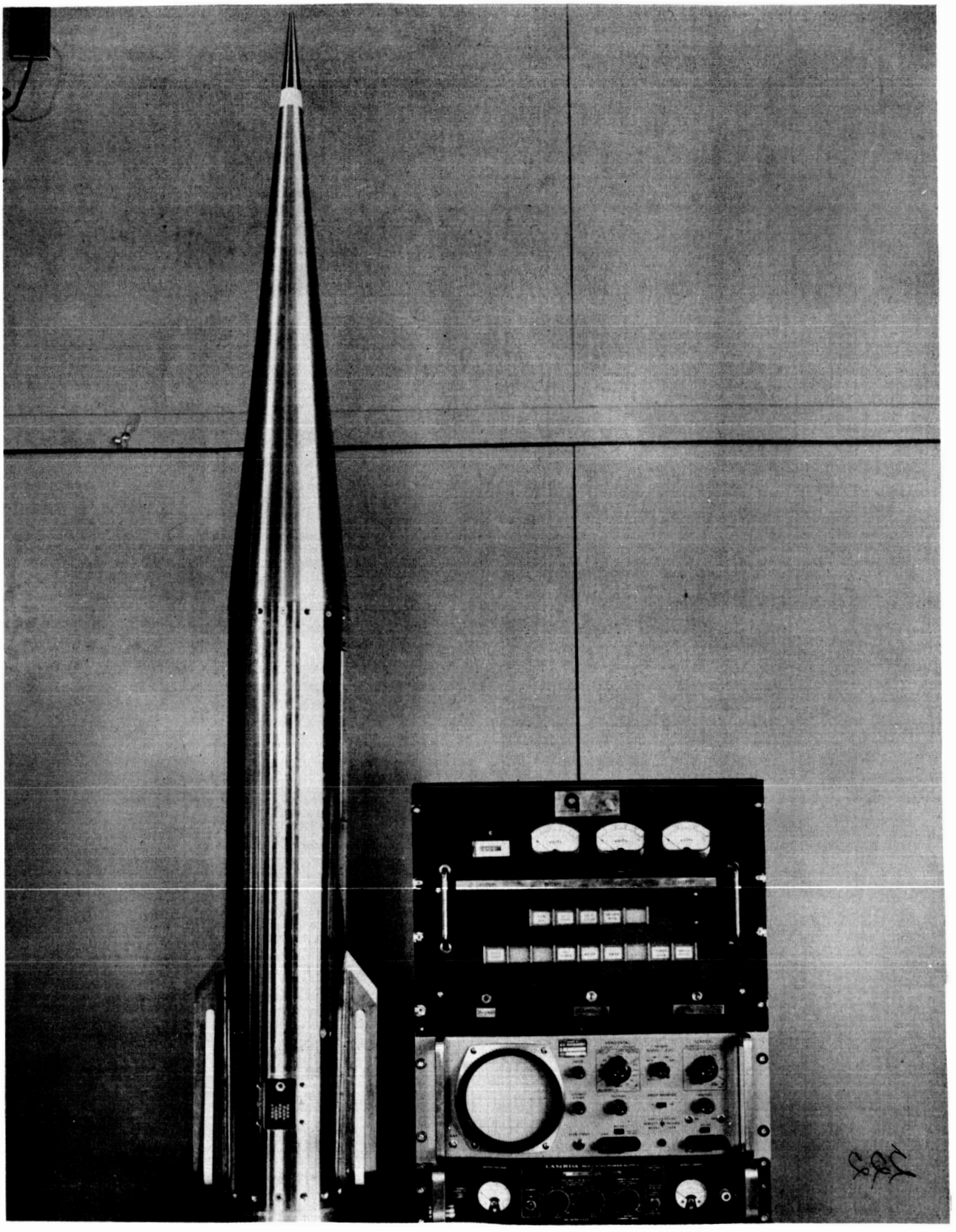

Figure 13. Nike Apache payload with ground checkout console.

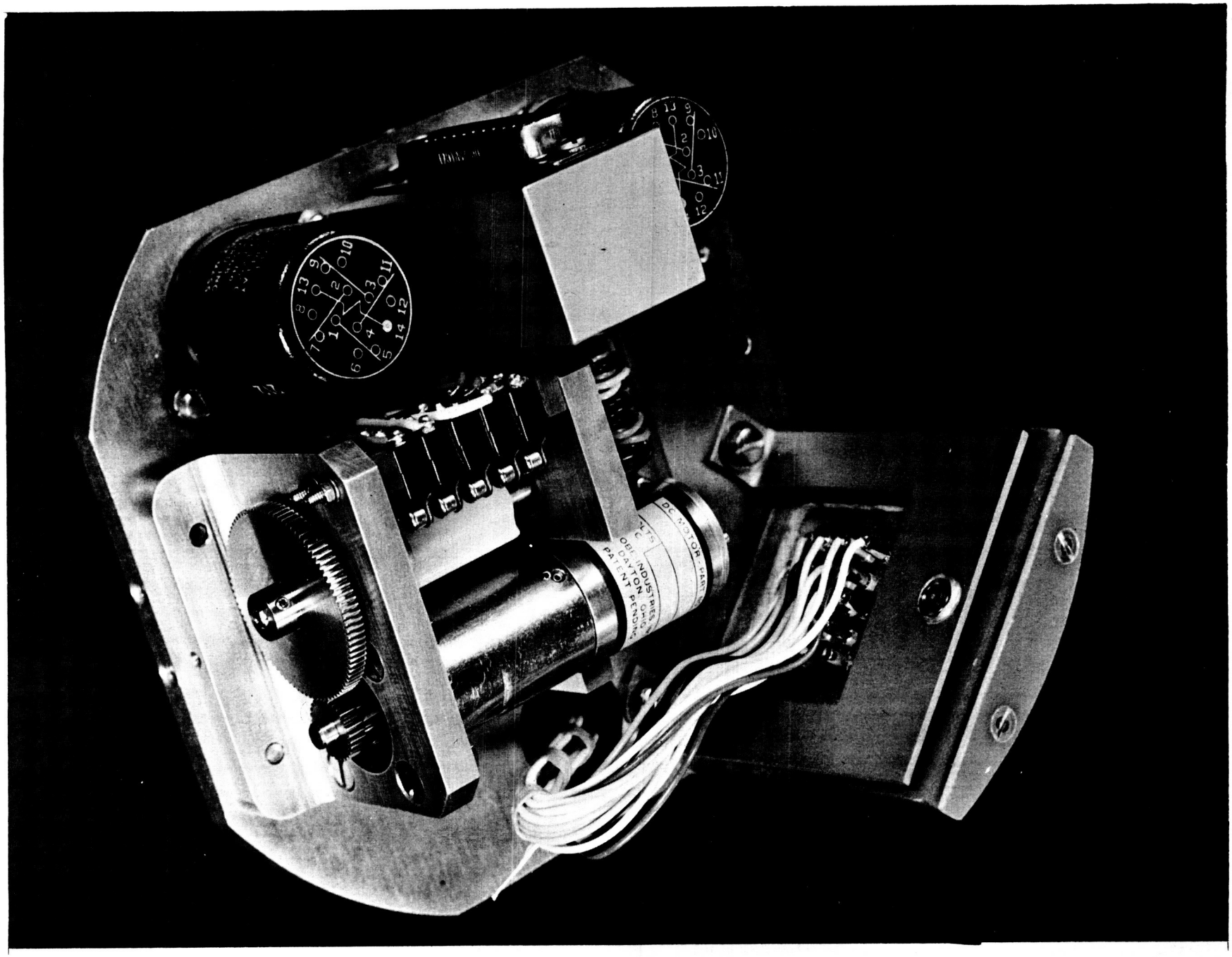

Figure 14. Transfer switch assembly.

switched to emergency battery power if line voltage is lost at the blockhouse. Figure 15 is a schematic of power transfer and the umbilical release circuits. When power is transferred to internal, power is fed back through the umbilical to energize an interlock relay and a signal light at the ground control console. This safety feature serves two purposes: (1) to prevent accidental or premature release of the umbilical and (2) to verify to the console operator that power transfer has been accomplished.

A two-pole control relay is used to independently control the high voltage to the transmitter as shown in Figure 16. This feature is extremely desirable in that all payload instrumentation can be operated for checkout during a period when permission to radiate cannot be granted for reasons of pad safety or RF interference.

The cutoff relay, a four-pole unit energized from the console, is inserted between the outputs of the payload instrumentation and the monitoring lines of the umbilical cable. When the umbilical is released, the relay opens so as to remove voltage from all pins of the umbilical connector. This was done originally to prevent disturbance of the vehicle potential in flight but also protects the payload should the umbilical connector be damaged at launch.

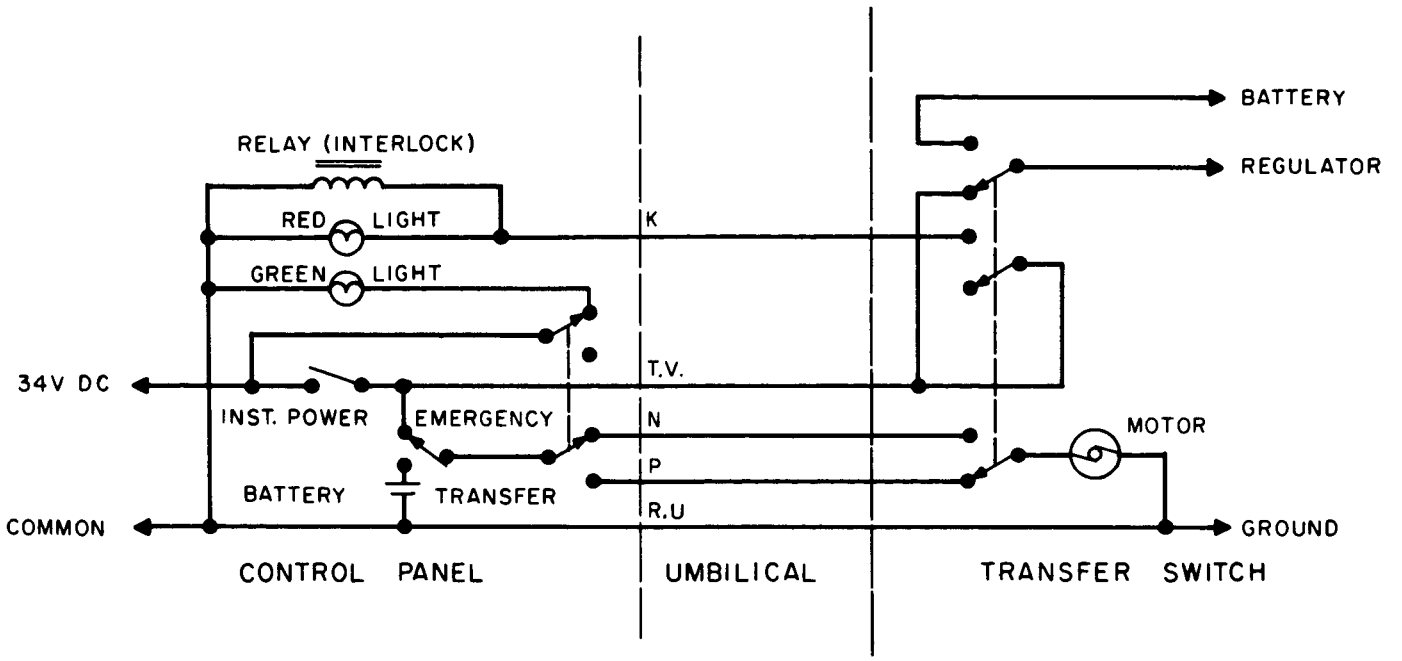

(a) POWER TRANSFER CIRCUIT

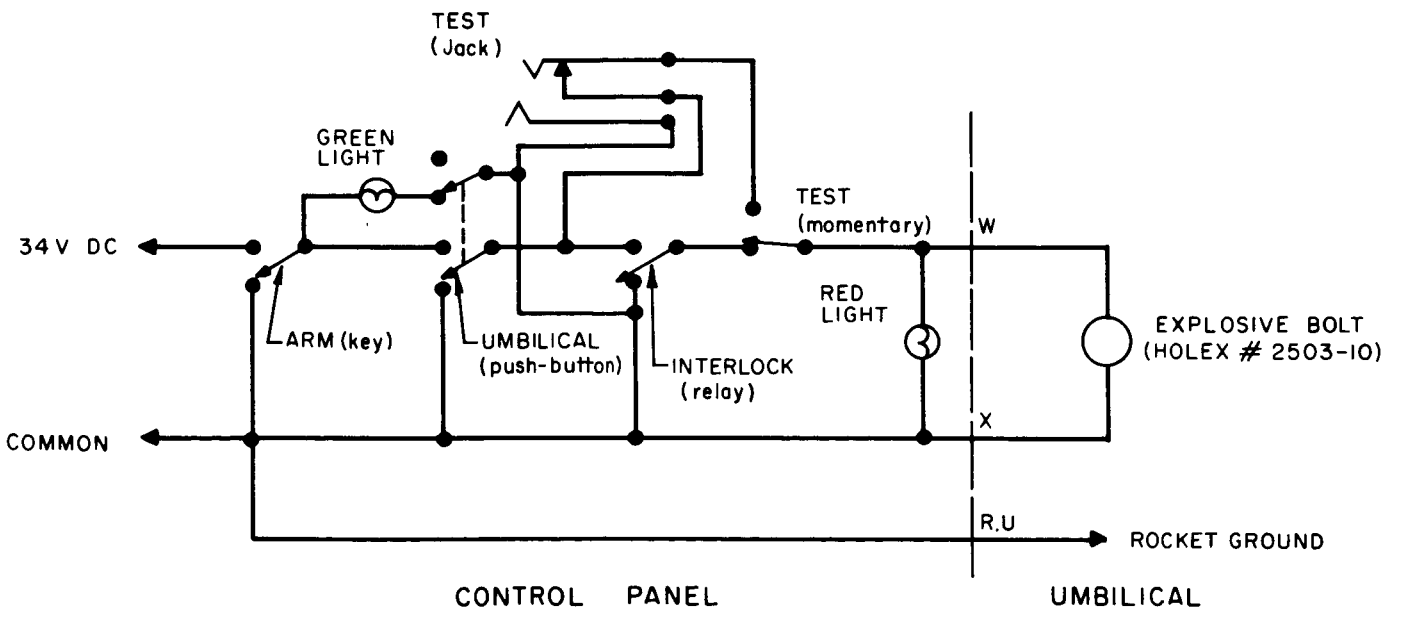

(b) UMBILICAL RELEASE CIRCUIT

Figure 15.

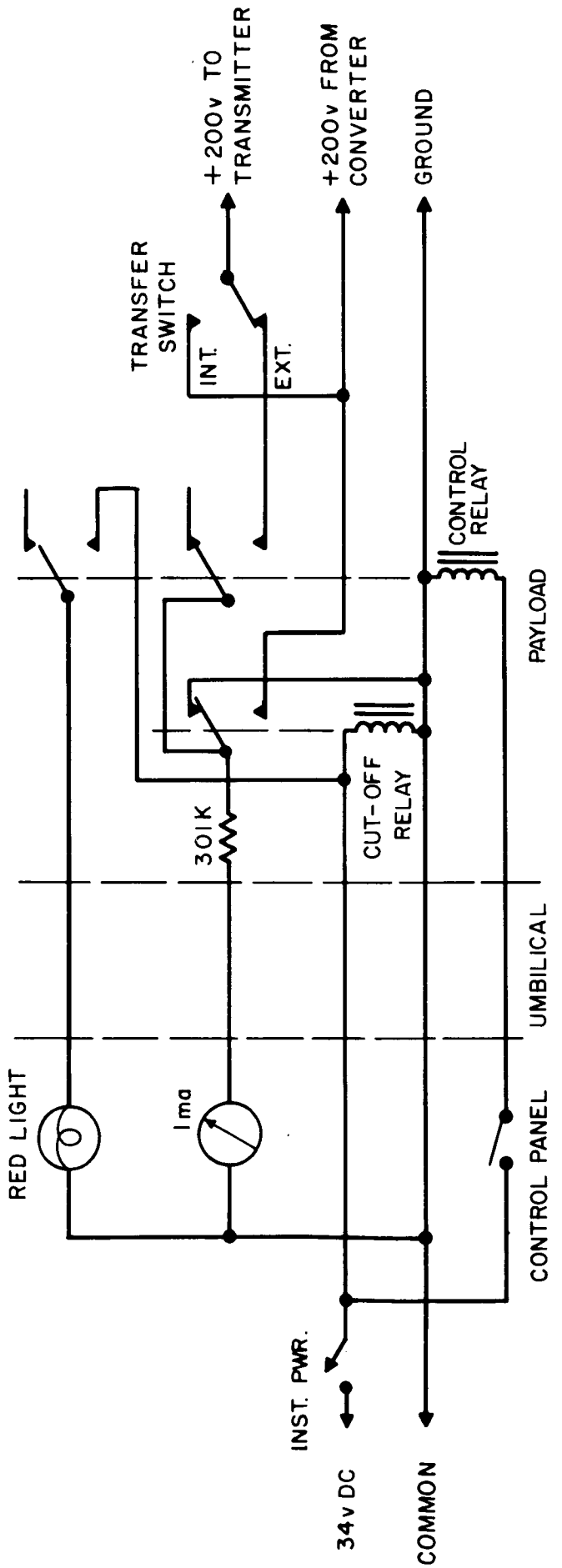

Figure 16. Transmitter control circuit.

TEST FLIGHTS AT WALLOPS ISLAND

Nike Apache 14.86 was launched from Wallops Island, Virginia, at 1430 EST on 27 February 1963. The launch time was chosen to obtain a solar zenith angle of 56°, which is the same angle as the end of the Fort Churchill eclipse. It also is the same solar zenith angle as two previous shots (Aerobee 4.48 and Nike Apache 14.31) in which the electron density profile was obtained.

The performance of the vehicle was lower than predicted. Apogee was at 151 km compared with the predicted value of about 190 km. One contributing factor was low performance of the Nike booster which burned for 3.1 seconds compared with the normal time of 3.5 to 3.6 seconds. The altitude stability of the vehicle was exceptional; no precessional motion was indicated by the magnetic aspect sensor, the two solar aspect sensors or the ion chamber. The excellent stability was due to the relatively high spin rate (set for 6 rps at second stage burnout) and to careful balancing of the payload.

The instrumentation was satisfactory with the exception of the Geiger counter which produced an unacceptably high count rate with no dependence on aspect angle. Subsequent testing of an identical payload (for Nike Apache 14.87) indicated that the probable cause was RF interference from the telemetry transmitter. The circuit associated with the counter was modified in this and subsequent payloads to eliminate any possible RF interference.

Several other minor modifications were made in the payload as a result of this first flight.

(1) One Lyman-α ion chamber was changed in position to give better angular coverage. In 14.86 the two sensors looked in directions making 60° and 120° with the forward axis of the payload. In 14.87 the larger angle was reduced to 90°, the other being unchanged.

(2) The aperture mask of the solar aspect sensors was redesigned to reduce the effect of scattered light within the instrument.

(3) The sampling rate of the electronic commutator was reduced from 2100 samples per second to about 700 samples per second to improve the appearance of the telemetry record.

(4) Although there is no evidence from the 14.86 flight that the mylar window did not survive, it was decided to use a wire mesh support for the mylar window on the 14.87 Geiger counter. This serves to prevent pressure reversals between the inside of the counter and the outside environment from placing any unnecessary strain on the mylar.

The second payload was launched from Wallops Island, on Nike Apache 14.87, at 1506 EST, 28 March 1963. The operation of the Geiger counter was satisfactory. The Cobalt 60 source attached to the protective doors

provided 8 counts per second during early phases of the flight. A general increase in count rate was observed on ascent due to the increase in cosmic ray background. The soft X-rays were first detected at an altitude of 81 km. The rocket, unfortunately, executed a large precession cone due to a low spin rate (2 rps). The Lyman-α data was also unsatisfactory due to unfavorable vehicle orientation and it was not possible to obtain the absorption profile for either X-rays or Lyman-α.

Some data from the Langmuir probe experiment was lost in the height range 53 to 74 km, both on ascent and descent. This is believed to be due to intermittent RF breakdown at the telemetry antennas. The power of the transmitter had been increased for this shot to 5 watts; it was reduced to 2 watts in subsequent shots. Apart from this height range good data was obtained from the probe.

FIELD OPERATIONS AT FORT CHURCHILL

A meeting at Fort Churchill was held during April 1963 to discuss problems associated with the launch schedule for the eclipse. The attendees included representatives of GCA, NASA, USAF, Canadian Army and the range contractor (Pan American Airways). There were a total of eight vehicles to be launched during the eclipse; a NASA Aerobee and a USAF Black Brandt in addition to the six Nike Apaches. The major problem at Churchill concerned timing, i.e., scheduling the various telemetry checks and launches. Another problem concerned frequency allocations.

Further meetings were held at Fort Churchill during May and June, 1963. At the second organizational meeting held at Fort Churchill in May 1963, it became clear that the facilities at the telemetry station at the Churchill Range were barely adequate for the eclipse program. It was suggested to the Sounding Rocket Group at GSFC that some additional telemetering equipment should be sent to Churchill. This produced some rapid action and a fully instrumented telemetry van was sent to Churchill for the duration of the project.

Prior to shipment of equipment to Fort Churchill, the payloads were taken to Goddard Space Flight Center for interference tests (i.e., checking the complete system including telemetry) and for spin-balancing. Project personnel met the equipment at Fort Churchill and re-tested the payloads using the facilities of the telemetry station. The equipment was found to be in perfect working order.

Some time at Fort Churchill was spent discussing the count-down and other features of the eclipse launches. In order to provide experience for the project crews it was agreed that the complete operation would be rehearsed one week prior to the eclipse (i.e., July 13), with all vehicles complete on the launchers. The vehicles were then removed from the launchers and the final preparations on the payloads began.

A photograph taken from the blockhouse of five of the six Nike Apaches on launchers with their protective covers still in place is shown in Figure 17. From left to right the vehicles are 14.94, 14.92, 14.90, 14.93 and 14.89. The other Nike Apache, 14.91, was mounted on the permanent (covered) launcher, a military (or rail) launcher similar to those used for all other Nike Apaches except 14.93 which was launched from the "zero-length" Black Brandt launcher. This can be identified in the photograph by the distinctive boom.

The Black Brandt launcher is on fixed azimuth, 108.3^{o} from true North. The military launchers are adjustable in azimuth, but because of the nature of the operation the final launcher settings were computed and set on all launchers before the first launch and the predicted impact points computed prior to each launch to determine that the impact was

Figure 17. Nike Apaches on launchers at Fort Churchill.

within the range. The launcher settings were calculated for an effective azimuth of 110° from true North and an effective elevation above the horizontal of 85°. The actual launcher settings used were:

Azimuth	14.89-14.94 (except 14.93)	115.8° from true North.
Elevation	14.89-14.94	84.3° above horizontal.

The six payloads were controlled from two ground consoles in the blockhouse, the umbilical cables being connected sequentially to alternate consoles.

VEHICLE PERFORMANCE

The times of stage ignition and burnout and impact (loss of signal) are given in Table 1. A notable feature of this data is the late ignition of the second stage, for the Churchill flights, ranging from 22.0 to 22.9 seconds after launch compared with the nominal 20 seconds.

The altitude and time of apogee for the vehicles is given in Table 2, except for Nike Apache 14.89 and 14.90. The data for the Churchill flights are derived on the basis of the time-of-flight above a reference altitude as indicated by a baroswitch. The method has been discussed in an earlier report [9]. The actual calculation of trajectory is illustrated in the following section.

The observed impact points of the four vehicles Nike Apache 14.91-14.94 given in Table 3 were obtained from sound ranging. The computed azimuth and range were calculated using the wind measurements at the time of each launch. The mean horizontal velocity is obtained by dividing the observed impact range by the total flight time.

The first two vehicles of the eclipse series were complete failures. The telemetry signal from Nike Apache 14.89 was lost 3.2 seconds after launch. The longitudinal magnetometer record, Figure 18 indicates that the payload broke off the second stage (Apache) motor shortly before the signal was lost. The payload was later recovered and found to have the Apache head-cap attached. The Apache motor was also found and was without either head-cap or fin assembly.

The second vehicle Nike Apache 14.90 failed in a manner closely resembling the previous failure. The record of the longitudinal magnetometer reproduced in Figure 19 shows that the vehicle began to turn at about 3.2 seconds after launch. Gaps in the record are caused by commutation of the magnetometer signal. The slowing down on the mechanical commutator and bursts of microphonic noise on the two electrometers indicates that the payload broke from the Apache and began tumbling at 3.6 seconds. The FM signal was lost at 3.88 seconds but the carrier and AM signal (Geiger counts) continued until 67.6 seconds, presumably ending at impact. The Apache was subsequently found unburnt and without either fins or head-cap. The Nike first stage was found in two parts with no fins. It is presumed that the Nike malfunctioned at about 3.2 seconds after launch, damaging the Apache fins and resulting in the head-cap and payload breaking from the Apache.

The evidence appears to indicate that in both cases the Nike stage exploded shortly before burnout. This is an extremely rare mode of failure and is believed to be due to physical damage sustained by the two stages in shipment. These two unsuccessful rockets (14.89 and 14.90) gave no scientific data. The payload of 14.89, which was recovered, has

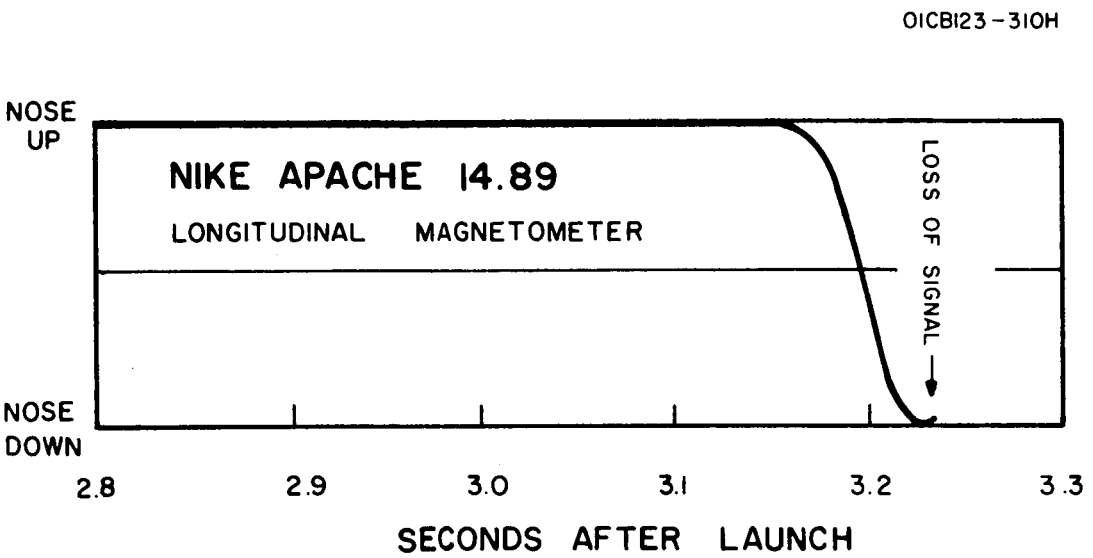
01CB123-310H
NOSE UP
NIKE APACHE 14.89
LONGITUDINAL MAGNETOMETER
LOSS OF SIGNAL
NOSE DOWN
2.8
2.9
3.0
3.1
3.2
3.3
SECONDS AFTER LAUNCH

Figure 18.

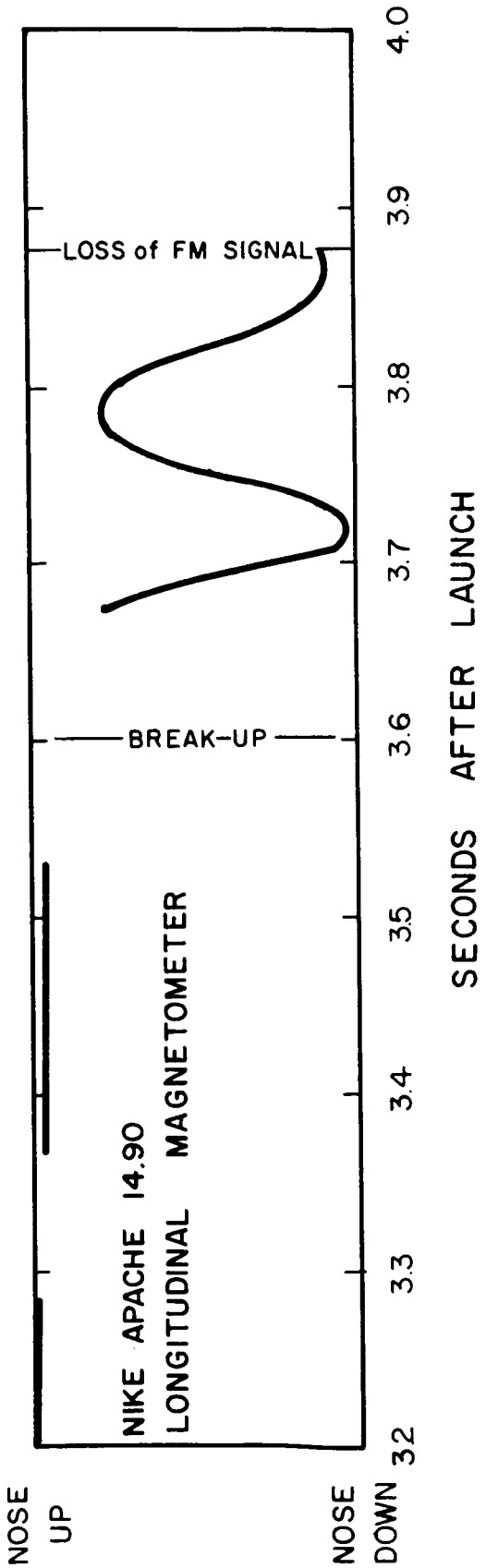
NOSE UP
NOSE DOWN
NIKE APACHE 14.90
LONGITUDINAL MAGNETOMETER
BREAK-UP
LOSS of FM SIGNAL
3.2
3.3
3.4
3.5
3.6
3.7
3.8
3.9
4.0
SECONDS AFTER LAUNCH

Figure 19.

TABLE 1. Rocket Launch Data

Nike-Apache 14.86

Date: 27 February 1963
Place: Wallops Island, Virginia
Data obtained from telemetry record:

Nike Ignition	1930:00.1 UT	(T)
Nike Burnout	1930:03.2 UT	(T + 3.1 sec)
Apache Ignition	1930:21.1 UT	(T + 21.0 sec)
Apache Burnout	1930:27.9 UT	(T + 27.8 sec)
Impact (Loss of Signal)	1936:21.4 UT	(T + 381.3 sec)

Nike-Apache 14.87

Date: 28 March 1963
Place: Wallops Island, Virginia
Data obtained from telemetry record:

Nike Ignition	2006:00.1 UT	(T)
Nike Burnout	2006:03.7 UT	(T + 3.6 sec)
Apache Ignition	2006:21.0 UT	(T + 20.9 sec)
Apache Burnout	2006:27.7 UT	(T + 27.6 sec)
Impact (Loss of Signal)	2012.33.9 UT	(T + 393.8 sec)

Nike-Apache 14.88

Date: 14 July 1963
Place: Fort Churchill, Manitoba
Data obtained from telemetry record:

Nike Ignition	2103:27.3 UT	(T)
Nike Burnout	2103:31.1 UT	(T + 3.8 sec)
Apache Ignition	2103.50.2 UT	(T + 22.9 sec)
Apache Burnout	2103:56.9 UT	(T + 29.6 sec)
Impact (Loss of Signal)	2110:14.0 UT	(T + 406.7 sec)

Nike-Apache 14.89

Date: 20 July 1963
Place: Fort Churchill, Manitoba
Data obtained from telemetry record:

Nike Ignition	2000:01.7 UT	(T)
Loss of Signal	2000:04.9 UT	(T + 3.2 sec)

TABLE 1. (Continued)

Nike-Apache 14.90

Date: 20 July 1963
Place: Fort Churchill, Manitoba
Data obtained from telemetry record:

Nike Ignition	2030:00.3 UT	(T)
Loss of FM Signal	2030:04.2 UT	(T + 3.9 sec)
Loss of AM Signal	2031:07.9 UT	(T + 67.6 sec)

Nike-Apache 14.91

Date: 20 July 1963
Place: Fort Churchill, Manitoba
Data obtained from telemetry record:

Nike Ignition	2103:00.5 UT	(T)
Nike Burnout	2103:04.0 UT	(T + 3.5 sec)
Apache Ignition	2103:23.1 UT	(T + 22.6 sec)
Apache Burnout	2103:29.8 UT	(T + 29.3 sec)
Impact (Loss of Signal)	2110:12.9 UT	(T + 432.4 sec)

Nike-Apache 14.92

Date: 20 July 1963
Place: Fort Churchill, Manitoba
Data obtained from telemetry record:

Nike Ignition	2113:00.0 UT	(T)
Nike Burnout	2113:03.7 UT	(T + 3.7 sec)
Apache Ignition	2113:22.6 UT	(T + 22.6 sec)
Apache Burnout	2113:29.2 UT	(T + 29.2 sec)
Impact (Loss of Signal)	2120:16.2 UT	(T + 436.2 sec)

Nike-Apache 14.93

Date: 20 July 1963
Place: Fort Churchill, Manitoba
Data obtained from telemetry record:

Nike Ignition	2140:00.0 UT	(T)
Nike Burnout	2140:03.6 UT	(T + 3.6 sec)
Apache Ignition	2140:22.0 UT	(T + 22.0 sec)
Apache Burnout	2140:28.6 UT	(T + 28.6 sec)
Impact (Loss of Signal)	2147:15.4 UT	(T + 435.4 sec)

TABLE 1. (Continued)

Nike-Apache 14.94

Date: 20 July 1963
Place: Fort Churchill, Manitoba
Data obtained from telemetry record :

Nike Ignition	2210:00.8 UT	(T)
Nike Burnout	2210:04.4 UT	(T + 3.6 sec)
Apache Ignition	2210:23.0 UT	(T + 22.2 sec)
Apache Burnout	2210:29.7 UT	(T + 28.9 sec)
Impact (Loss of Signal)	2217:09.5 UT	(T + 428.7 sec)

TABLE 2. Apogee Altitude and Time

1. Apogee altitude and time obtained from radar data:

Nike Apache 14.86

Altitude	150.9 km	
Time	1933:17 UT	(T + 197.0 sec)

Nike Apache 14.87

Altitude	161.4 km	
Time	2009:20 UT	(T + 200.0 sec)

2. Apogee altitude and time obtained from time of flight above reference level (21.3 km):

Nike Apache 14.88

Altitude	171.6 km	
Time	2106:56.2 UT	(T + 208.9 sec)

Nike Apache 14.91

Altitude	196.0 km	
Time	2106:42.4 UT	(T + 221.9 sec)

Nike Apache 14.92

Altitude	198.8 km	
Time	2116:43.5 UT	(T + 223.5 sec)

Nike Apache 14.93

Altitude	199.7 km	
Time	2143:43.4 UT	(T + 223.4 sec)

Nike Apache 14.94

Altitude	192.6 km	
Time	2113:40.5 UT	(T + 219.7 sec)

Accuracy of altitude estimated to be $\pm$ 0.5 km.
Accuracy of time estimated to be $\pm$ 0.5 sec.

TABLE 3. Impact Points

Nike Apache	Computed Azimuth	Observed Azimuth	Computed Range	Observed Range	Horizontal Velocity
14.91	102°	120°	106 km	92 km	0.21 km/sec
14.92	110°	113°	83 km	96 km	0.22 km/sec
14.93	76°	90°	74 km	112 km	0.26 km/sec
14.94	106°	110°	113 km	114 km	0.27 km/sec

been tested and found to be in excellent condition although the structure is slightly distorted. Even the Mylar-window Geiger counter together with its high-voltage power supply and pulse-forming circuits were found to be in perfect working order.

The telemetry records were analysed to give data on the spin rate of the vehicles up to 40 seconds from launch. The data is actually obtained from the AGC record: the strength of the signal received at the ground station shows modulation at a frequency equal to twice the spin rate. No AGC record is available for Nike Apache 14.86, which was a satisfactory flight, nor for 14.89 and 14.90, both of which exploded shortly after launch. Otherwise good data is available on the six other vehicles in the program: Nike Apaches 14.87, 14.88, 14.91, 14.92, 14.93 and 14.94.

The payloads were identical and each contained a magnetic aspect sensor arranged longitudinally and therefore sensitive only to precessional motion, and two solar aspect sensors which were, however, not uncovered until 50 seconds after launch. These instruments show unambiguously that Nike Apaches 14.87 and 14.88 precessed into a flat spin (i.e., a precession cone of about 90^{o} half-angle) whereas the other five flights (14.86, 14.91, 14.92, 14.93 and 14.94) were stabilized with small precession cones.

The period and cone angles of the precessional motion in mid-flight are given in Table 4.

TABLE 4. Precessional Motion

Nike Apache	Period	Cone Angle
14.86	40 sec	$\approx 5^{o}$
14.91	45	10.5^{o}
14.92	52	11.0^{o}
14.93	67	$\approx 20^{o}$*
14.94	55	6.5^{o}

*Magnetic aspect sensor data.

The plot of spin rate against time from launch, Figure 20 shows a striking difference between the two "unstabilized" vehicles 14.87 and 14.88, and the stabilized vehicles 14.91, 14.92, 14.93 and 14.94 beginning at 12 seconds after launch. Up to that time the curves are closely similar, rising to a maximum at about 10 seconds then decreasing slowly. After 12 seconds the spin rate of the unstabilized vehicles continues to decrease while that of the stabilized vehicles increases to a peak at

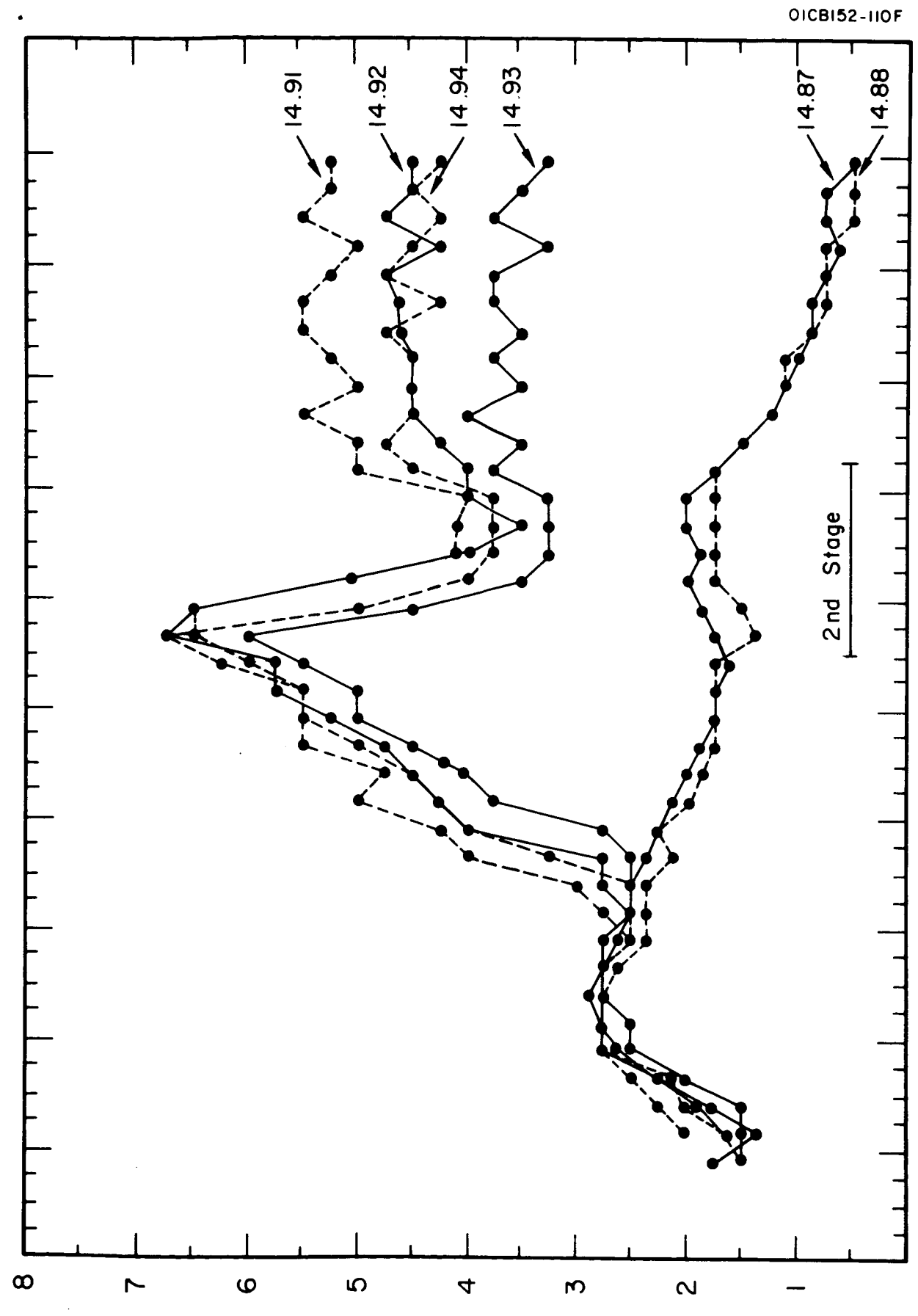

Figure 20. Nike Apache spin rates.

second stage ignition. Note that the rate of increase of spin rate between 4 and 8 seconds is about the same as the rate between 12 and 22 seconds. This suggests that the spin wedges become ineffective at 8 seconds and may or may not become effective again at 12 seconds.

No explanation of these observations can be offered at the present time. However an aerodynamic problem is indicated, and in view of the importance in other sounding rocket programs, a thorough investigation of the problem should be undertaken at an early date.

CALCULATION OF TRAJECTORY

The baroswitches, nominally set for 70,000 ft, are individually calibrated for decreasing pressure (ascent) and increasing pressure (descent). Due to the differential travel in the microswitch these two readings differ by an amount equivalent to about 1 or 2 km in altitude and, in practice, neither is exactly at the nominal setting of the baroswitch. The first step in computing the trajectory is to correct the observed switching times to the reference altitude of 70,000 ft (21.3 km).

The procedure for correcting the baroswitch and computing the apogee altitude and time is illustrated in Table 5 by the data from Nike Apache 14.92. Lines 1 to 4 identify the flight. Line 5 gives the values of the constants g' and z_o. Line 6 gives the baroswitch calibration determined prior to the flight. Line 7 gives the corresponding altitudes obtained from the 1959 ARDC Model Atmosphere. Line 8 gives the actual times of switching observed during the flight. The difference between these, (t_2-t_1), gives the time of flight uncorrected for the baroswitch altitude error. This first approximation to the time of flight is used to compute the vertical component of velocity at the reference level, as shown in line 10. The corrections to be applied to the observed switching times to bring them to the reference altitude are obtained by dividing the height error by the vertical velocity. The values given in line 11 are to be added to and subtracted from the times observed on ascent and descent respectively, giving the corrected switching times, line 12. The corrected time of flight is the difference between these two times (t_4-t_3), line 13. Apogee altitude is immediately obtained, line 14, assuming the effective value of g' determined previously. Apogee time, line 15, is determined as being 0.5 sec earlier than the mid-point of the time of flight. Comparison of altitudes and times obtained from the baroswitch with these obtained by radar skin-track, in earlier flights, indicates that the probable error in altitude is $\pm$ 0.5 km and in time is $\pm$ 0.5 sec.

Knowing the apogee altitude z' and time t' the trajectory (altitude z versus time t) is easily computed using the formula

$$z = z' - \frac{g'}{2}(t-t')^2.$$

The calculation is convenient for a desk computer. The first six lines of the tabulation for the trajectory of Nike Apache 14.92 are shown in Table 6. The trajectory is then plotted and a smooth curve drawn through the points. It is found that the ten-second interval of the computation is sufficient.

TABLE 5. Computation of Apogee Altitude and Time

1. Rocket: Nike Apache 14.92
2. Date: 20 July 1963
3. Time: 2113:00 UT
4. Place: Fort Churchill, Manitoba
5. Constants used: $g' = 935$ cm/sec^2; reference altitude, $z_o = 21.3$ km
6. Baroswitch calibration: ascent 36.5 mm Hg; descent 45.0 mm Hg.
7. Baroswitch altitude: ascent 20.8 km; descent 19.5 km
8. Switching time: ascent (t_1) 2113:28.9 UT; descent (t_2) 2119:59.8 UT
9. Time of flight (first approximation): $(t_2-t_1) = 390.9$ sec
10. Velocity at reference altitude:
    $g'(t_2-t_1)/2 = 467.5 \times 10^{-5} \times 390.9 = 1.83$ km/sec
11. Time correction: ascent $0.5/1.83 = 0.3$ sec (add);
    descent $1.8/1.83 = 1.0$ sec (subtract)
12. Switching times (corrected): ascent (t_3) 2113:29.2 UT;
    descent (t_4) 2119:58.8 UT
13. Time of flight (corrected): $(t_4-t_3) = 389.6$ sec
14. Apogee altitude: $z' = z_o + \frac{g'}{2}\left[\frac{t_4-t_3}{2}\right]^2 = 21.3 + 1.169\ 10^{-3}$
    $(389.6)^2 = 198.8$ km
15. Apogee time: $t' = (t_3 + t_4)/2 - 0.5$ sec = 2116:43.5 UT

TABLE 6. Computation of Trajectory

Rocket: Nike Apache 14.92

Constants used: $\frac{g'}{2} = 4.675\ 10^{-3}$ km/sec^2;

$z' = 198.8$ km;

$t' = 2116{:}43.5$ UT

t UT	$\lvert t-t' \rvert$ sec	$\lvert t-t' \rvert^2$ sec^2	$\frac{g'}{2} \lvert t-t' \rvert^2$ km	Z km
2113:30	193.5	$3.744\ 10^4$	175.0	23.8
40	183.5	3.367	157.4	41.4
50	173.5	3.010	140.7	58.1
2114:00	163.5	2.673	125.0	73.8
10	153.5	2.356	110.1	88.7
20	143.5	2.059	96.3	102.5
etc.	etc.	etc.	etc.	etc.

INSTRUMENTATION PERFORMANCE

The instrumentation had been thoroughly tested in the two flights at Wallops Island (Nike Apaches 14.86 and 14.87) and no problems were encountered in the preparation of the subsequent payloads at Fort Churchill. The performance of the instrumentation in flight was satisfactory though some partial failures were encountered.

Telemetry - The signal was excellent and continuous from launch to impact on Nike Apaches 14.88, 14.92, 14.93 and 14.94. Signal was lost at vehicle break-up (T + 3.2 sec) on Nike Apache 14.89. The FM signal of Nike Apache 14.90 was lost shortly after vehicle break-up (T + 3.9 sec) but the carrier continued with the amplitude modulation (Geiger counter pulses) until impact at T + 68 sec.

A partial failure of the telemetry system occured on Nike Apache 14.91. The FM signal was lost at T + 300 sec (at an altitude of 168 km on descent). The carrier and AM signal continued, as on Nike-Apache 14.90. The FM signal reappeared at T + 413 sec for a period of 0.4 sec, then at T + 418 sec continuing to impact (T + 433 sec). The similarity of the mode of failure in Nike Apaches 14.90 and 14.91 appears to indicate a weakness in the modulation stage of the transmitter. There is no evidence of any malfunction of the subcarrier oscillators. The temporary loss of telemetry signal resulted in loss of the descent profiles of Lyman-α.

Lyman-α - The anomalous behaviour in varying degrees of all the Lyman-α ion chambers detracted from the quality of the data. No evidence of malfunction in the associated circuits has been found.

The anomaly consists of an apparent decrease in sensitivity when the chamber is first exposed to the unattenuated solar flux followed by various degrees of recovery. This is illustrated in Figure 21 which shows the ion chamber current as a function of time. The initial peak occurs at an altitude of about 95 km. The rise in current observed in the middle part of the figure for Nike Apache 14.91 and 14.92 is much greater than the change in incident flux due to the decreasing obscuration of the solar disc.

No satisfactory explanation of the behaviour of the ion chambers has been found. It is felt that future measurement of Lyman-α should be made with NO as the gas in the ion chamber rather than CS_2.

Geiger Counter - Satisfactory operation of the X-ray Geiger counters is indicated for all vehicles except Nike Apache 14.94 where a reduction of sensitivity is implied, the cause of which is not known.

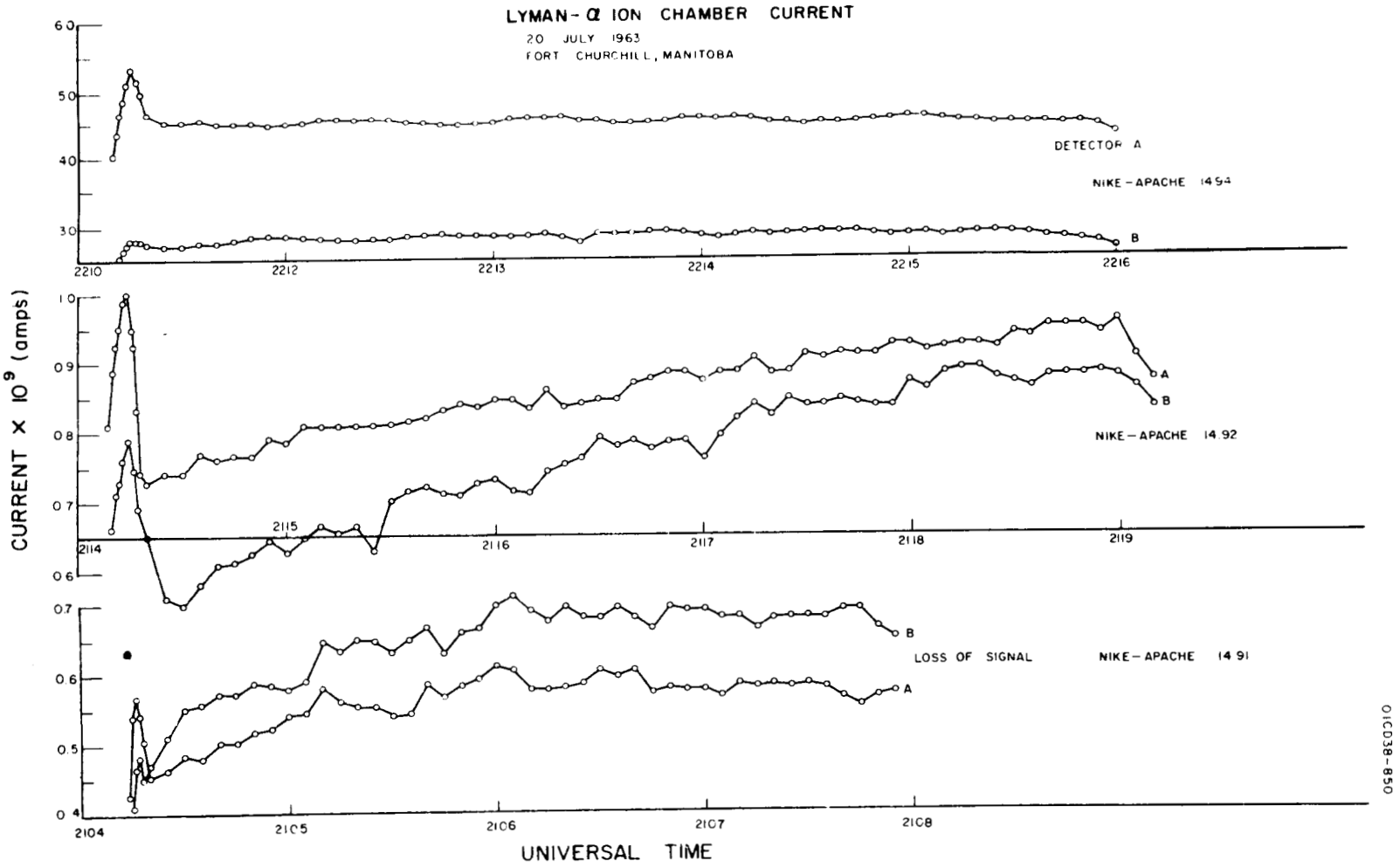
LYMAN-α ION CHAMBER CURRENT
20 JULY 1963
FORT CHURCHILL, MANITOBA
DETECTOR A
NIKE-APACHE 14.94
B
NIKE-APACHE 14.92
A
B
LOSS OF SIGNAL
NIKE-APACHE 14.91
A
CURRENT × 10⁹ (amps)
UNIVERSAL TIME
2210
2212
2213
2214
2215
2216
2114
2115
2116
2117
2118
2119
2104
2105
2106
2107
2108
OIC038-850

Figure 21.

Probe - The probe operation was excellent and electron density profiles were obtained on all flights except for the two vehicle failures (14.89 and 14.90). Descent profiles were not obtained on 14.91 - 14.94 due to the high launch angle; as has been found before when the tip probe descends in the rarefied wake of the vehicle the current to the probe is reduced. This is not considered a loss of data.

Door Mechanism - The doors failed to eject on Nike Apache 14.93 causing loss of Lyman-α and X-ray data. The monitor circuits in the payload show that the bellows actuator received voltage and fired. It is not known why the mechanism failed to release the doors.

Aspect Sensors - The performance of the solar and magnetic aspect sensors was satisfactory. The position of the magnetic aspect sensor almost parallel to the magnetic field line resulted in rather poor sensitivity to vehicle precessional motion.

Other Instrumentation - The power supplies and electronic and mechanical commutators performed satisfactorily with no evidence of malfunction.

CALCULATION OF MAGNITUDE OF ECLIPSE

The percentage of obscuration of the eclipse at altitudes above Churchill, Manitoba (Latitude 58° 48'N, Longitude 94° 12'W) have been made available by the U. S. Naval Observatory. The data is given in Table 6 and is shown graphically in Figure 22. The actual position of the rocket is East of Churchill and varies during each flight and for the four different trajectories. The actual area of the disc (A) visible at the rocket at altitude (z) and time (t) is the same as that at Churchill at a greater height ($z + \Delta z$) and at an earlier time ($t - \Delta t$) in which Δz and Δt are given by

$$\Delta z = y \cot \chi$$

$$\Delta t = x/V$$

where x and y are distances defined in Figure 23, χ is the solar zenith angle and V is the velocity of the shadow along the path of totality, having the value 48 km/min.

Values calculated in this way for altitudes of 50, 100 and 150 km on the ascending and descending portions of the trajectories are given in Table 7 for the four rocket flights.

The ascending portion of the trajectory of 14.91 preceeds the minimum area by about 2 minutes. The descending portion and the remaining flights all follow the minimum area. The times are given in Table 8.

TABLE 6. Percentage Obscuration of Solar Disc at Altitudes above Churchill, Manitoba, 20 July 1963

UT	0 km	50 km	100 km	150 km	200 km
2000	4.1	4.0	3.9	3.8	3.6
2005	8.6	8.4	8.2	8.0	7.9
2010	14.0	13.7	13.4	13.2	13.0
2015	19.8	19.6	19.4	19.1	18.8
2020	26.5	26.2	25.9	25.5	25.2
2025	33.6	33.2	32.8	32.5	32.1
2030	41.0	40.6	40.2	39.8	39.4
2035	48.8	48.4	48.0	47.5	47.0
2040	57.0	56.5	56.0	55.4	54.9
2045	65.4	64.8	64.2	63.5	62.9
2050	73.8	73.1	72.4	71.7	70.9
2055	82.3	81.4	80.5	79.6	78.6
2100	90.1	89.0	87.9	86.7	85.5
2105	94.7	93.4	92.1	90.7	89.4
2110	90.8	90.1	89.4	88.6	87.7
2115	83.0	82.7	82.4	82.1	81.6
2120	74.4	74.3	74.2	74.1	74.0
2125	65.6	65.6	65.7	65.8	65.7
2130	56.9	57.0	57.2	57.3	57.4
2135	48.5	48.6	48.8	48.9	49.1
2140	40.0	40.3	40.6	40.8	40.9
2145	32.1	32.4	32.7	32.9	33.1
2150	24.6	24.9	25.2	25.4	25.6
2155	17.6	17.9	18.2	18.4	18.7
2200	11.3	11.6	11.9	12.1	12.3
2205	6.0	6.2	6.4	6.6	6.8
2210	1.8	2.0	2.2	2.3	2.5

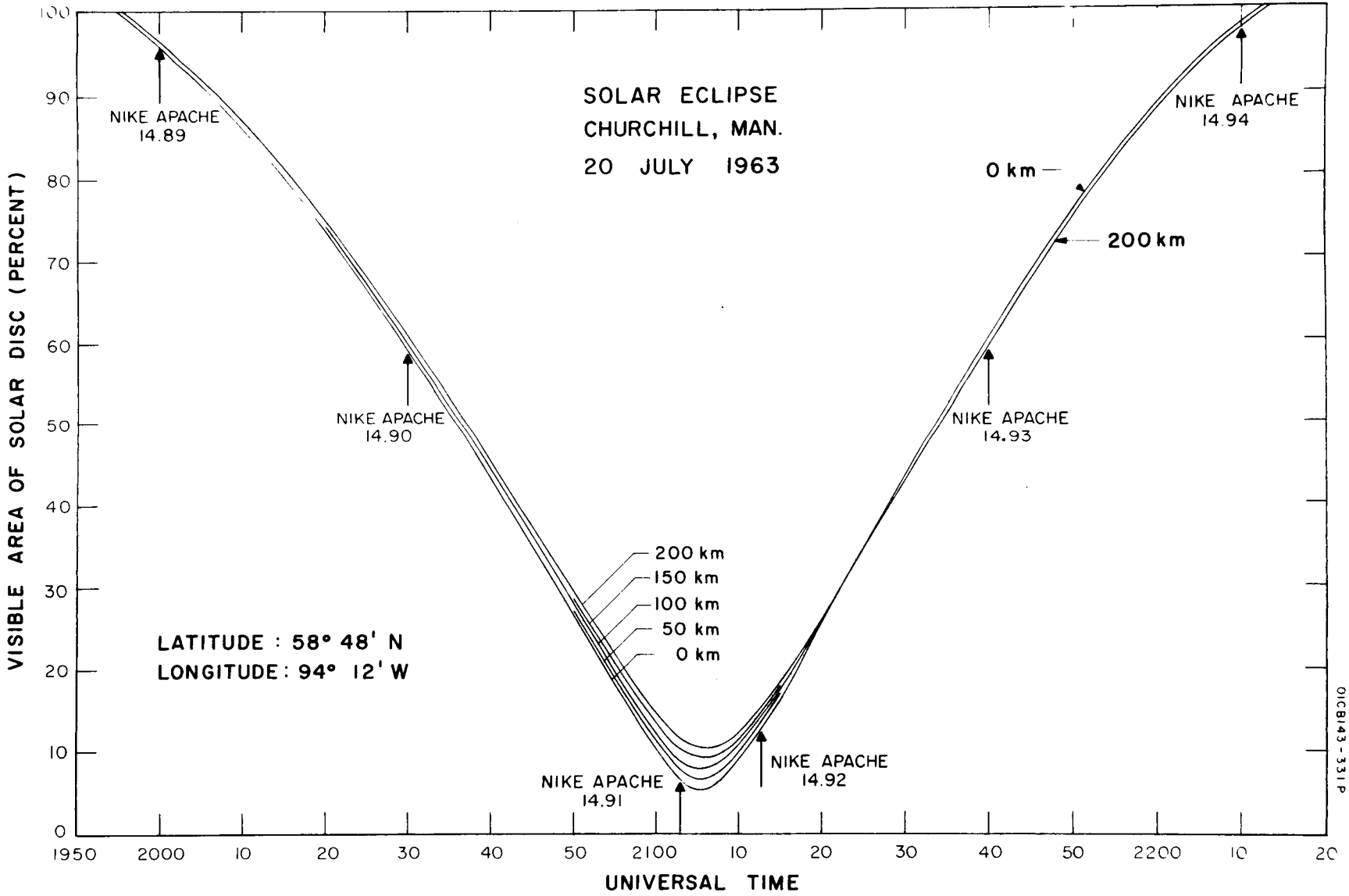

Figure 22. The variation of visible area of solar disc at altitudes up to 200 km above Churchill, Manitoba, 20 July 1963.

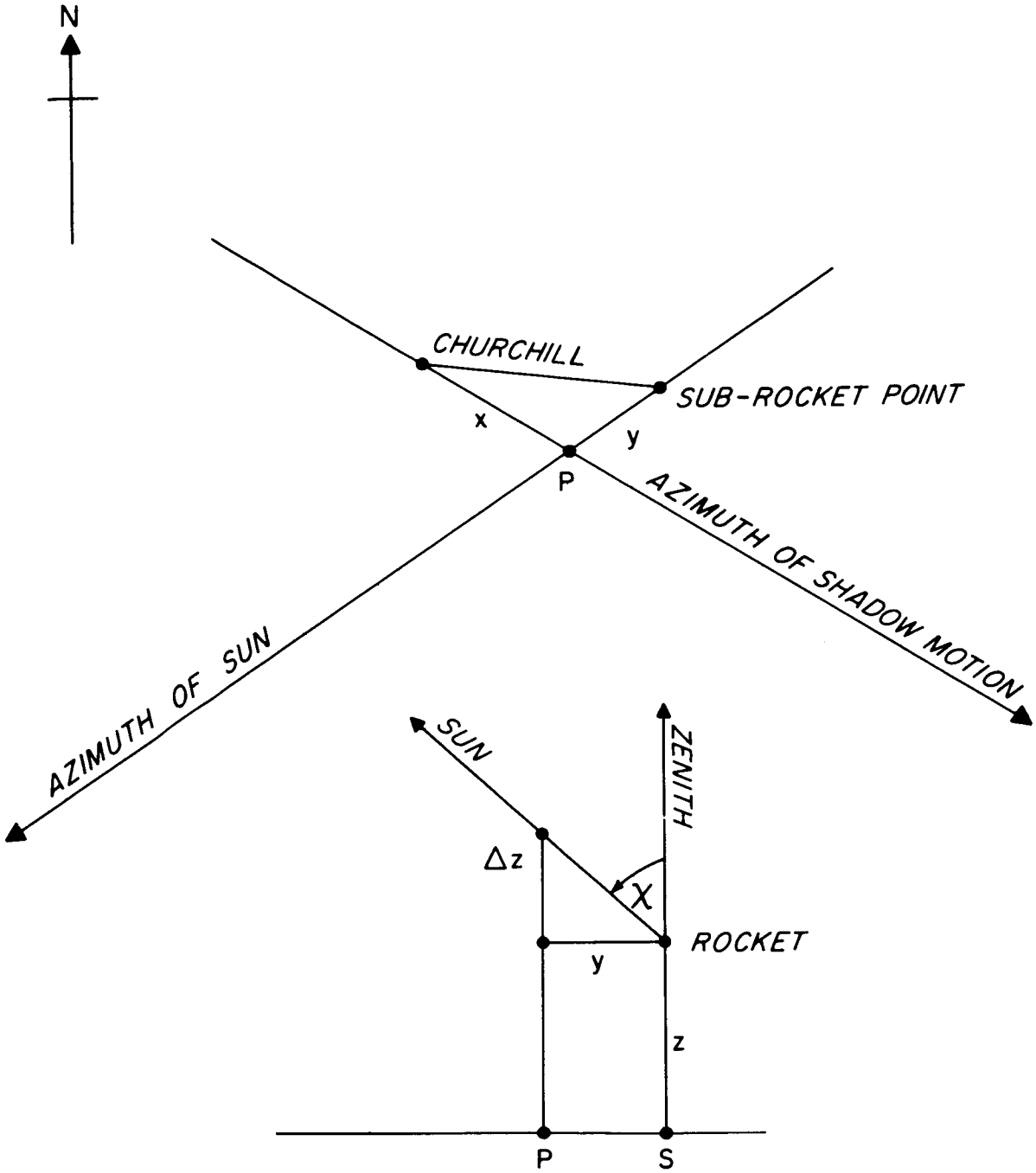

Figure 23. Position of rocket relative to Churchill, Manitoba.

TABLE 7. Percentage Area of Solar Disc Visible from Rocket

	50 km	100 km	150 km
14.91 ascending	7.5	8.6	9.7
14.91 descending	7.7	8.6	9.5
14.92 ascending	14.4	15.6	16.7
14.92 descending	21.3	20.8	20.4
14.93 ascending	60.0	60.7	61.5
14.93 descending	68.3	67.6	66.0
14.94 ascending	97.8	98.2	98.6
14.94 descending	100.0	100.0	100.0

TABLE 8. Time of Measurements Relative to Minimum Area of the Solar Disc

	50 km	100 km	150 km
14.91 ascending	-2m 17s	-2m 02s	-1m 49s
14.91 descending	+2m 07s	+1m 33s	+0m 49s
14.92 ascending	+7m 43s	+7m 58s	+8m 11s
14.92 descending	+12m 07s	+11m 33s	+10m 49s

A MINOR D-REGION EVENT*

On July 14, 1963, a Nike Apache rocket was launched at Fort Churchill, Manitoba for the purpose of establishing control data for a series of rocket flights designed to study the ionosphere during the solar eclipse of July 20, 1963. The rocket was instrumented with a DC probe for measuring electron density and temperature, a Geiger counter for measuring a narrow band of solar X-rays (44 to 60Å), two ion chambers for measuring ultraviolet radiation (1050 to 1240Å), a magnetometer and two solar aspect sensors for monitoring the orientation of the rocket. A more complete description of these instruments is presented elsewhere [6, 10]. The rocket failed to receive the proper spin stabilization in flight, resulting in an extreme precessional motion and a low apogee. Because of the resulting unfavorable aspect conditions seen by the solar radiation detectors, limited information on the X-ray and ultraviolet radiation was obtained. Fortunately, electron density profiles were obtained for both ascent and descent portions of the trajectory. The flight proved useful for a reason that was not originally anticipated. The electron density profiles were enhanced in the D- and lower E-regions compared with a profile obtained six days later. Also, the Geiger counter exhibited a background count rate well above the normal cosmic ray background.

Figure 24 shows the enhanced background count rate data obtained for both the ascent and descent portions of the flight. It is to be noted that the two profiles are not identical, suggesting either a spatial or temporal variability of the ionizing source. The count rates observed are low enough not to require significant dead time corrections (dead time for the counter was 135 microseconds).

Rocket experiments at high latitudes indicate that during time of auroral activity there is usually an associated corpuscular component [11,12,13,14]. In particular, the corpuscular radiation most often related to electromagnetic absorption in the D-region at auroral latitudes is electrons in the 10 to 100 kev range. Although the Geiger counter flown in the present experiment would not allow penetration of electrons of this energy over the entire cylindrical shell of the counter, the 0.25-mil thick mylar window (20-mil diameter) has a threshold for electron detection at approximately 25 kev. The possibility that the radiation observed might be attributable to protons does not appear likely. This is in part due to the fact that the data shows the radiation to be quasi-isotropic over the region scanned by the detector (30° above the nadir to 30° below the zenith); the isotropy appears more reasonable for

*This section is the text of a paper that has been accepted for publication in the Journal of Geophysical Research under the title "Probe and Geiger counter rocket measurements of a minor D-region event."

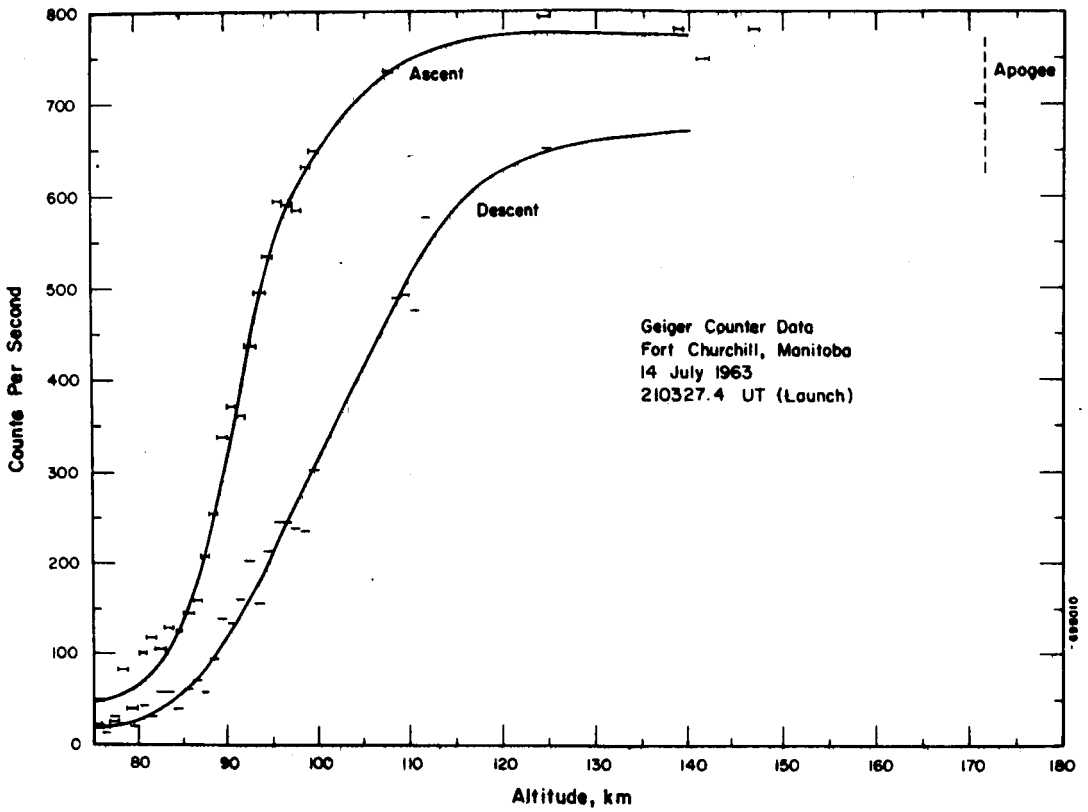

Figure 24. Count rate for corpuscular radiation measured during the flight of Nike Apache 14.88.

electrons rather than for heavier charged particles. In addition, the intensity at the top of the atmosphere of approximately 3.5×10^5 particles/cm^2/sec/sterad is somewhat higher than has been normally observed for protons for events of this type. This intensity is in general agreement with other measurements for electrons in the auroral zone.

The particle deposition rate due to ionizing collisions as a function of altitude for particles with energies greater than the detector threshold of 25 kev may be obtained by differentiating the data in Figure 24. The maximum deposition rate for these particles during both ascent and descent is found to occur in the 90 to 100 km region. The height where the maximum energy is deposited cannot be determined without prior knowledge of the energy spectrum of the particles. For the lower D-region, bremsstrahlung may play an important role in the ion production rate. Rees [15] has calculated the ionization production rate versus altitude for various energies and directional distributions of electrons. Using this information, the present data suggests that the average energy of the electrons is approximately 50 kev.

The electron density profiles for rocket ascent and descent on July 14, 1963 and for rocket ascent on July 20, 1963 are given in Figure 25. The profile for July 20 was measured at last contact of the solar eclipse. Other measurements made during the solar eclipse [6] show that the relaxation times in the lower ionosphere were small enough that the ionosphere at contact can be considered to have recovered from the eclipse. It is to be noted that the proportionality between the DC probe current and electron density is without theoretical justification below 90 km; however, a simultaneous comparison of this DC probe method with a propagation method has shown excellent agreement down to 75 km [16]. Therefore, the profiles of Figure 25 are considered to be reliable indications of the electron density down to at least 75 km. At lower heights there may be a systematic error in the electron density, but the differences between the various profiles are an approximate indication of the relative changes in electron density.

The curves illustrate very clearly the enhancement of ionization below the E-layer. Here again differences in the ascent and descent portions of the flight suggest either a time or spatial variability for the event. The maximum electron density increase is noted in the vicinity of 90 km agreeing approximately with the height of maximum particle deposition for particles of energies greater than 25 kev. From the collision frequencies shown in Table 9, the absorption of a 30 Mc/sec wave was calculated for the three electron density profiles in Figure 25. Based on Geiger counter data, the ionosphere at 2210 UT on July 20, 1963 is considered to be representative of conditions with no corpuscular radiation. The change in absorption on July 14 due to the presence of corpuscular radiation can then be determined. The results of these calculations are given in Table 10. 30 Mc/sec riometer data at Churchill, obtained from the Defence Research Telecommunications Establishment, Ottawa, indicates a 0.2 ± 0.1 db increase in absorption relative to quiet conditions

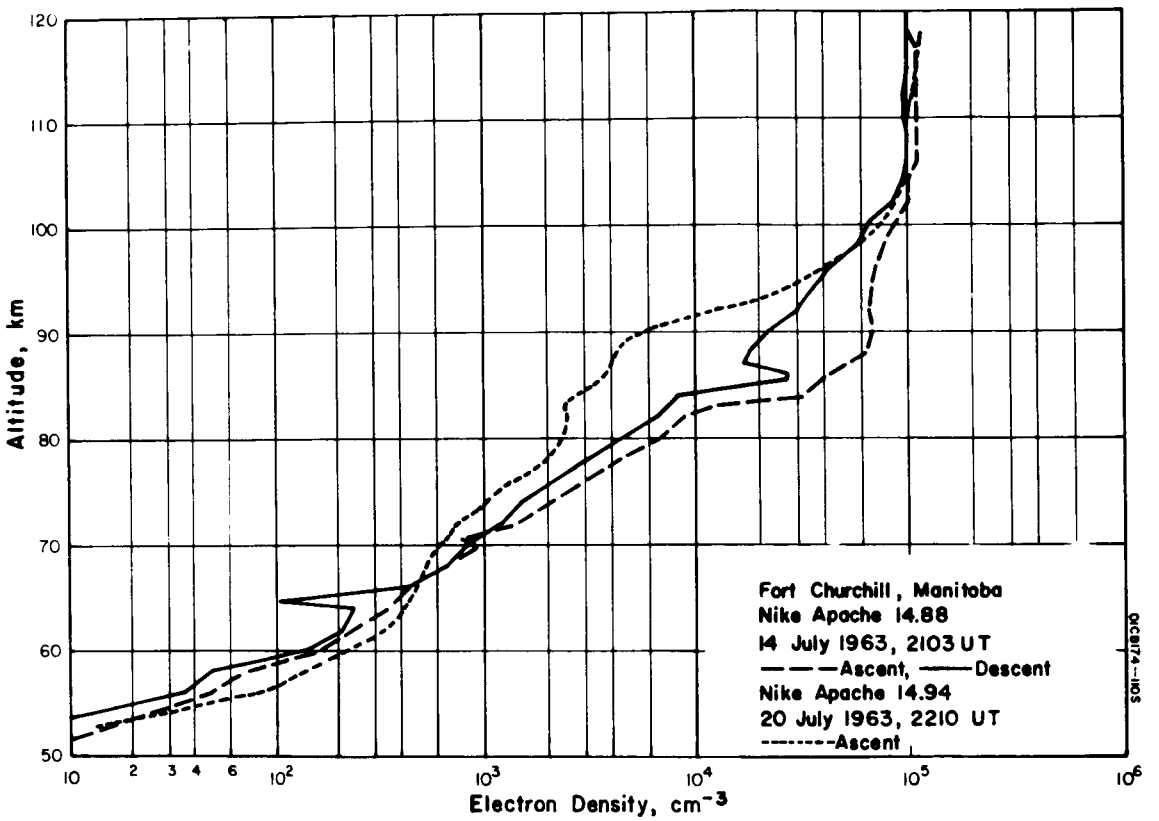

Figure 25. Electron density profiles obtained using the DC probe.

TABLE 9 Electron Collision Frequencies

h(km)	$\nu(\text{sec}^{-1})$
55	3.0×10^{7}
60	1.6×10^{7}
65	8.6×10^{6}
70	4.3×10^{6}
75	2.0×10^{6}
80	8.9×10^{5}
85	3.6×10^{5}
90	1.4×10^{5}
95	5.6×10^{4}
100	2.4×10^{4}

TABLE 10. Absorption at 30 Mc/sec

Identification	Date	Absorption (db)	Change in Absorption (db)
Nike Apache ascent	July 14,1963	0.33	0.18
Nike Apache descent	July 14,1963	0.21	0.06
Nike Apache ascent	July 20,1963	0.15	--
Riometer	July 14,1963	--	0.2 ± 0.1

at the time of the rocket flight on July 14. This is seen to be in approximate agreement with the calculated absorption change for the ascent electron density profile.

Conclusions

Both the Geiger counter and DC probe data reveal the presence of a corpuscular component, believed to be electrons, existing at Fort Churchill on July 14, 1963. An intensity of 3.5×10^5 particles/cm^2/sec/sterad and a mean energy of 50 kev are indicated by the Geiger counter data for a minor absorption event. The data suggests that more refined rocket measurements of both the spatial and energy distributions of particles causing enhanced ionization in the D-region, complemented by probe measurements of electron density would be useful in the investigation of the ionosphere at high latitudes.

THE ECLIPSE IN THE E AND F_1-REGION

Electron Density

The proportionality of probe current with electron density shows up clearly when the DC probe is compared with ionosonde data. The comparison is made at the peak of the E-layer, at an altitude of 105 km. The location of the ionosonde to the southwest of the launch site results in a time difference of about 20 seconds between the two measurements (the ionosonde preceding the probe). The ionosonde, which is 300 km from the path of totality, is 30 km closer than is the probe in penetrating the E-layer. This is offset by the "tilt" of the ionosphere due to the oblique angle of the penumbra so that the probe and ionosonde data can be compared without applying any corrections due to their slightly different location. The times at which the four rockets passed the altitude of 105 km are given in Table 11 together with the probe current (measured at 2.7 volt) recorded at that time. The uncertainty in the probe current is $\pm$ 3 percent. The simultaneous value of electron density is obtained from the E-layer critical frequency using

$$N = 1.24 \times 10^4 \ f^2 \ cm^{-3}$$

with f in mc/s. The uncertainty in the electron density is $\pm$ 5 percent.

The probe current is plotted against electron density in Figure 26. Three of the four flights show very good agreement with a linear relation through the origin, rather better than the experimental errors would indicate. The other (14.92) is in less good agreement. This measurement was made at a time of rapid change in f_oE and a timing error of 30 seconds would produce an error sufficient to account for the discrepancy. However, the differences may also be due to systematic errors (such as contact potential variation). Accordingly, electron density profiles are constructed using the separate scaling factors given in Table 11.

Comparison of the probe current at 180 km with the electron density obtained from the F_1 critical frequency does not give the linear relation found for the E-layer data. This is believed to be due to the effect of rocket outgassing; above 160 km the vehicle velocity is less than the mean thermal velocity of the ambient neutral particles.

The profiles of probe current in the E and F_1-regions up to rocket apogee are shown in Figure 27. The probe current increases by a factor of about three from 105 km to 180 km although the ionosonde data shows an increase of a factor of nearly two in electron density from the E-layer to the F_1-layer. This indicates that the scaling factor relating

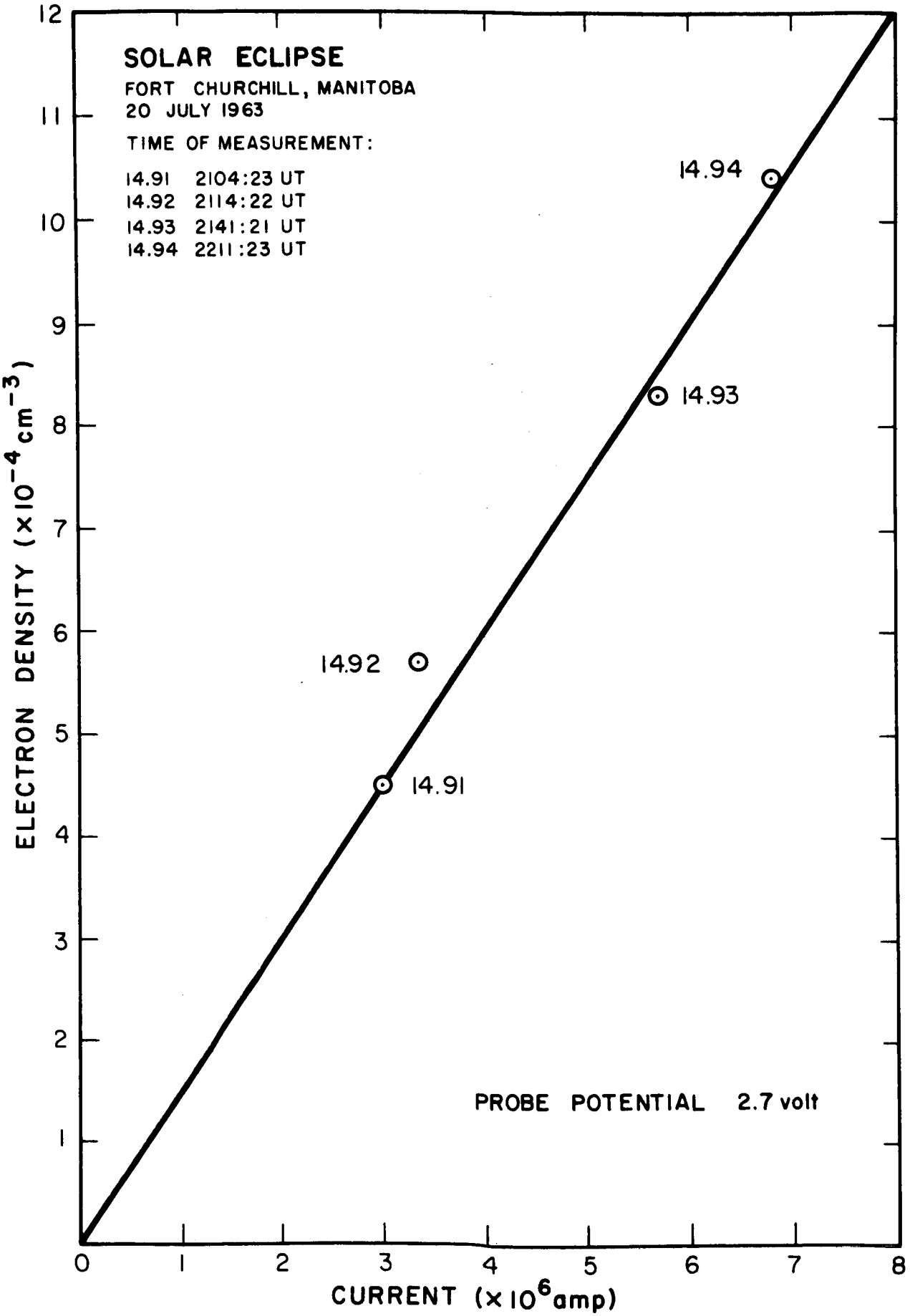

Figure 26. Comparison of DC probe and ionosonde at 105 km.

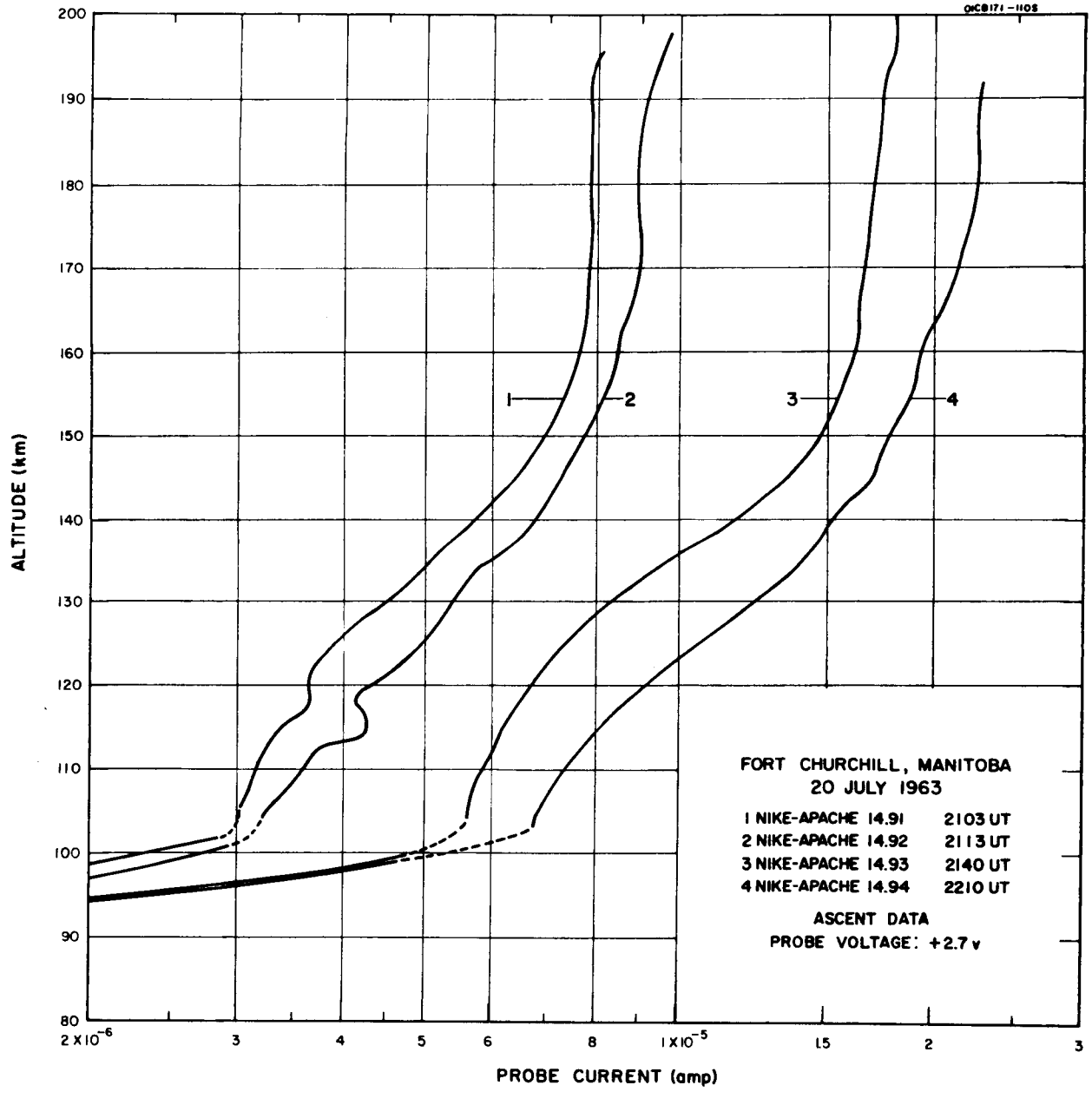

Figure 27. Profiles of probe current.

TABLE 11. Comparison of DC Probe with Ionosonde at 105 km

Nike Apache	Time at 105 km	Probe Current $I \times 10^{6}$ amp	Ionosonde Data $f_o E$ mc/s	Ionosonde Data $N \times 10^{4}$ cm^{-3}	$(N/I) \times 10^{-10}$ $cm^{-3} amp^{-1}$	Visible Area of Solar Disc (percent)
14.91	2104:23	3.0	1.90	4.5	1.50	8.6
14.92	2114:22	3.35	2.14	5.7	1.70	15.6
14.93	2141:21	5.7	2.58	8.3	1.45	60.3
14.94	2211:24	6.8	2.90	10.4	1.53	98.2

current to electron density is not independent of altitude. The profiles of current show that there was no significant change in the gross features of the profile during the eclipse. In particular the profiles did not develop the principal features of this region at night: the profile remained smooth and no deepening of the trough above the E-layer is observed. It is seen that the E and F_1-regions remain in equilibrium during the eclipse; that is, the electron density adjusts very quickly to changes in the photoionization rate (change in the solar obscuration).

Two interesting minor features of the profiles may be noted. An irregularity is observed between 115 km and 121 km on profile 1 and between 112 km and 118 km on profile 2 taken 10 minutes later. This may be a travelling disturbance of the type described by Bibl [17]. In addition all four profiles show a region of small-scale irregularities, indicated by the dashed portion of the profiles near 100 km altitude. The maximum excursion in the irregularities is $\pm$ 10 percent of the mean for profiles 1, 3 and 4 and is $\pm$ 18 percent for profile 2. The upper and lower boundaries of these regions are sharply defined, the thickness of the region is 3 to 4 km, and its location near 100 km suggest an association with sporadic E although no sporadic E was recorded by the ionosonde.

The relaxation time or "sluggishness" of an ionospheric layer is a very important quantity since, together with electron density data, it can be used to determine the effective recombination coefficient α according to the formula [18]

$$\alpha = \frac{1}{2N\ \Delta t} \quad ,$$

where N is the value of the electron density when the production rate is a minimum, and Δt is the time lag of the minimum electron density after the minimum production rate. The minimum production rate occurs during the maximum phase of the eclipse if it is assumed that the radiation from the sun is uniformly distributed. Consideration of the timing of the rockets and the profiles of Figure 27 shows that this time lag must be less than three minutes, and the ionosonde observations, Figure 28, with its better time resolution, shows that the time lag is one minute or less. It is found that the value of the effective recombination coefficient in the E-layer is then given by

$$\alpha_E \geq 1 \times 10^{-7}\ \text{cm}^3/\text{sec}.$$

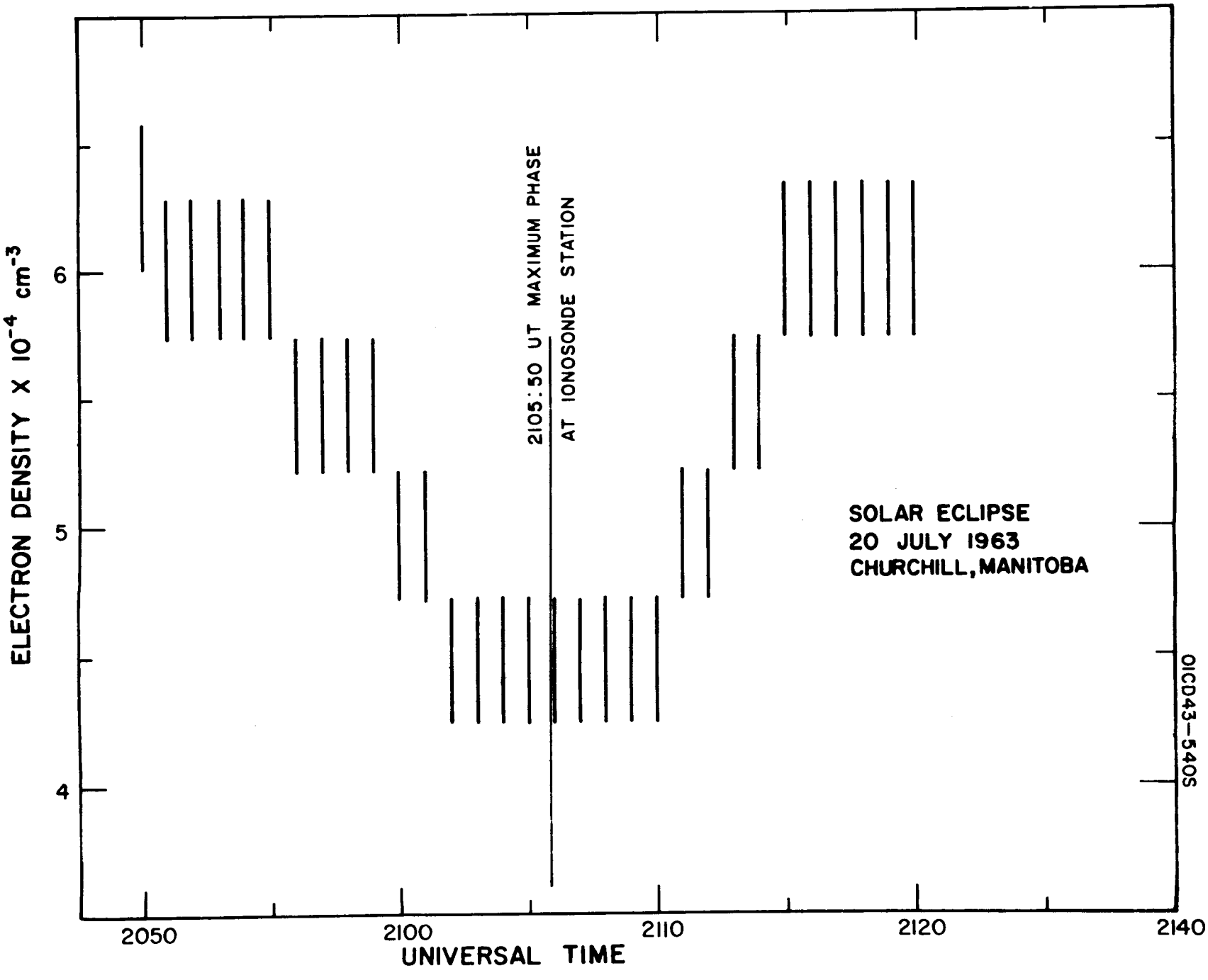

Figure 28. E-Layer ionosonde data.

The ionosonde records show that the time lag for the F_1-layer is one minute longer than the time lag for the E-layer; accordingly, the effective recombination coefficient for the F_1-layer is

$$\alpha_{F_1} \geq 4.6 \times 10^{-8} \text{ cm}^3/\text{sec}$$

Figures 29 and 30 exhibit the relative behavious of the E and F_1 critical frequencies during the eclipse. Although some systematic differences are seen, it is noted that the ratio of the critical frequencies is about the same at maximum phase as at first and last contacts, and that there is not a large deviation of one critical frequency with respect to the other at any time during the eclipse. This is in general agreement with the observed preservation of the profile shape noted earlier.

Electron Temperature

From the current-voltage characteristic of the probe, it is possible to deduce electron temperatures as a function of altitude. The procedure is not useful for heights lower than 110 km because the measured currents become too small to permit an accurate analysis of the current-voltage characteristic. It is seen in Figure 31 that, to within the experimental accuracy of $\pm 100^{\circ}$, there is no significant temperature variation during the eclipse period below a height of 160 km. Above this height up to 190 km, the temperature at the end of the eclipse appears to be significantly greater than during the first part of the recovery phase.

X-rays

The count rate data for a given view of the sun is obtained by averaging the number of counts in a 20 millisecond interval, during which the rocket spin turns the detector through an angle of 36°. This introduces an error of about 8% in the count rate. After deadtime corrections are made, 5 consecutive views are combined to obtain a single average count rate, corresponding to a given altitude with a 1 km height spread. The effect of the small aspect angles on the data is negligible.

In Figure 32, the normalized count rate data and its associated errors are given as a function of height for flights 14.91, 14.92 and 14.94. No solar radiation data was obtained from Nike Apache 14.93 due to failure of the door release mechanism. The data from flight 14.94 cannot be compared directly with the data from flights 14.91 and 14.92

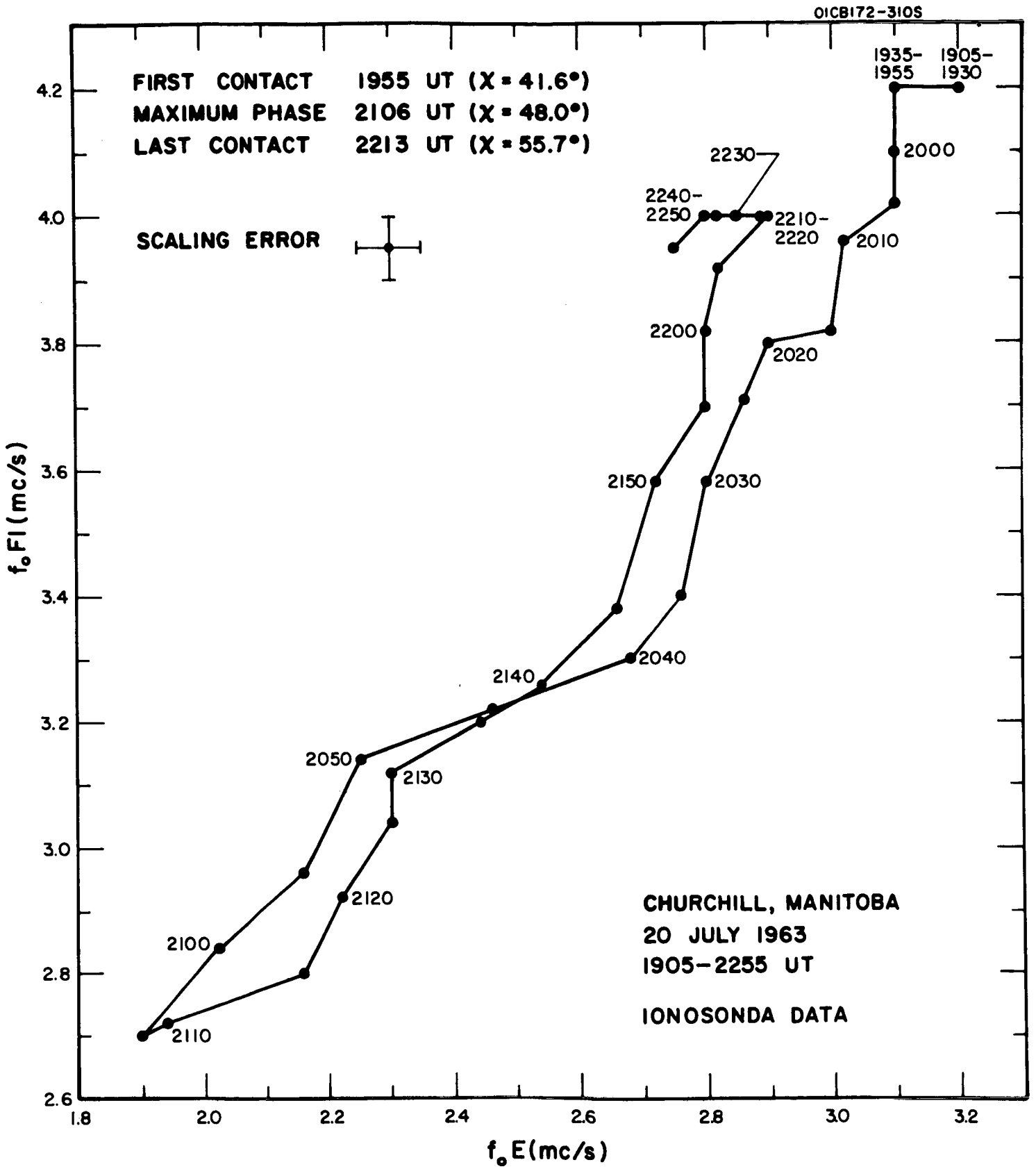

Figure 29. Variation of f_oE and f_oF_1 during the eclipse. Each point is the average of five readings taken at 1-minute intervals.

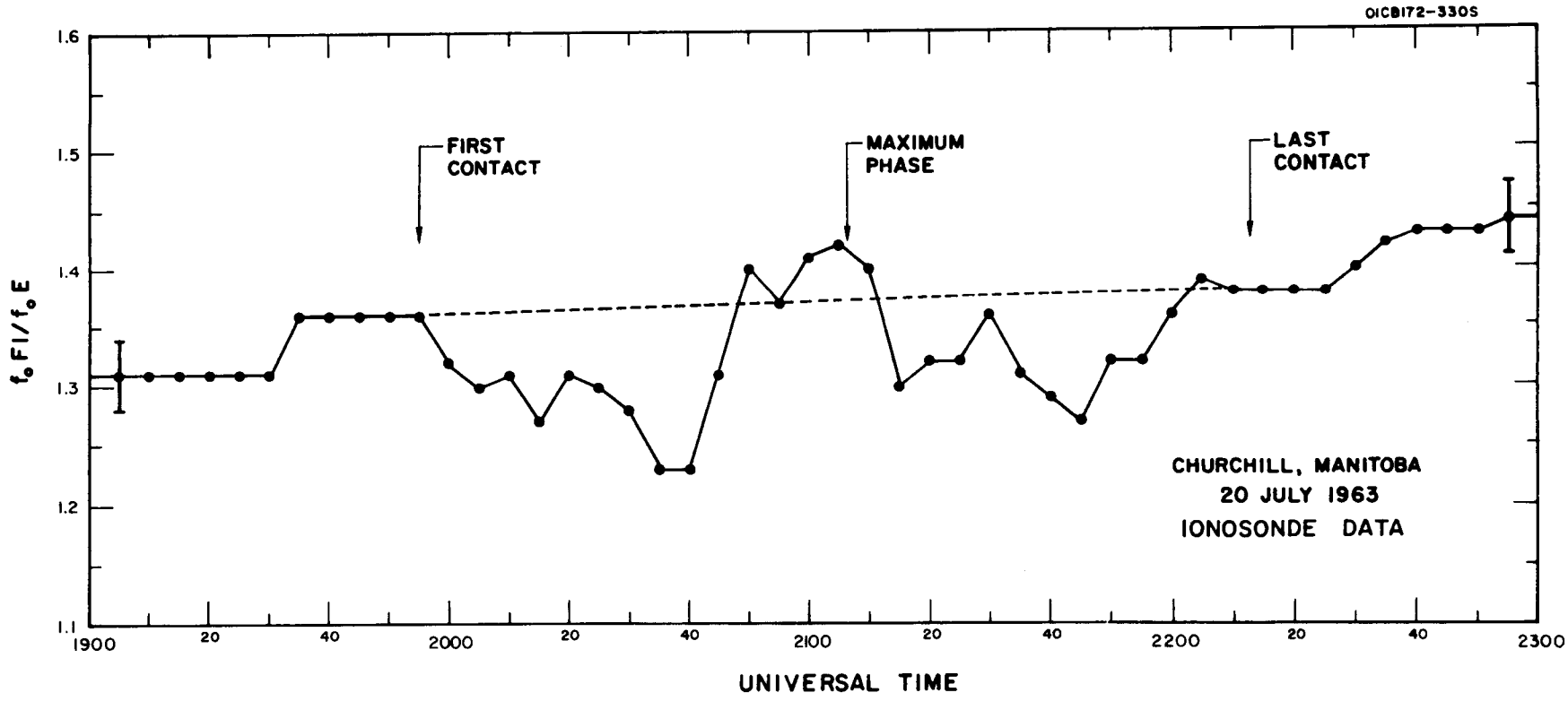

Figure 30. Variation of f_oF_1/f_oE during the eclipse. Each point is the average of five readings taken at 1-minute intervals.

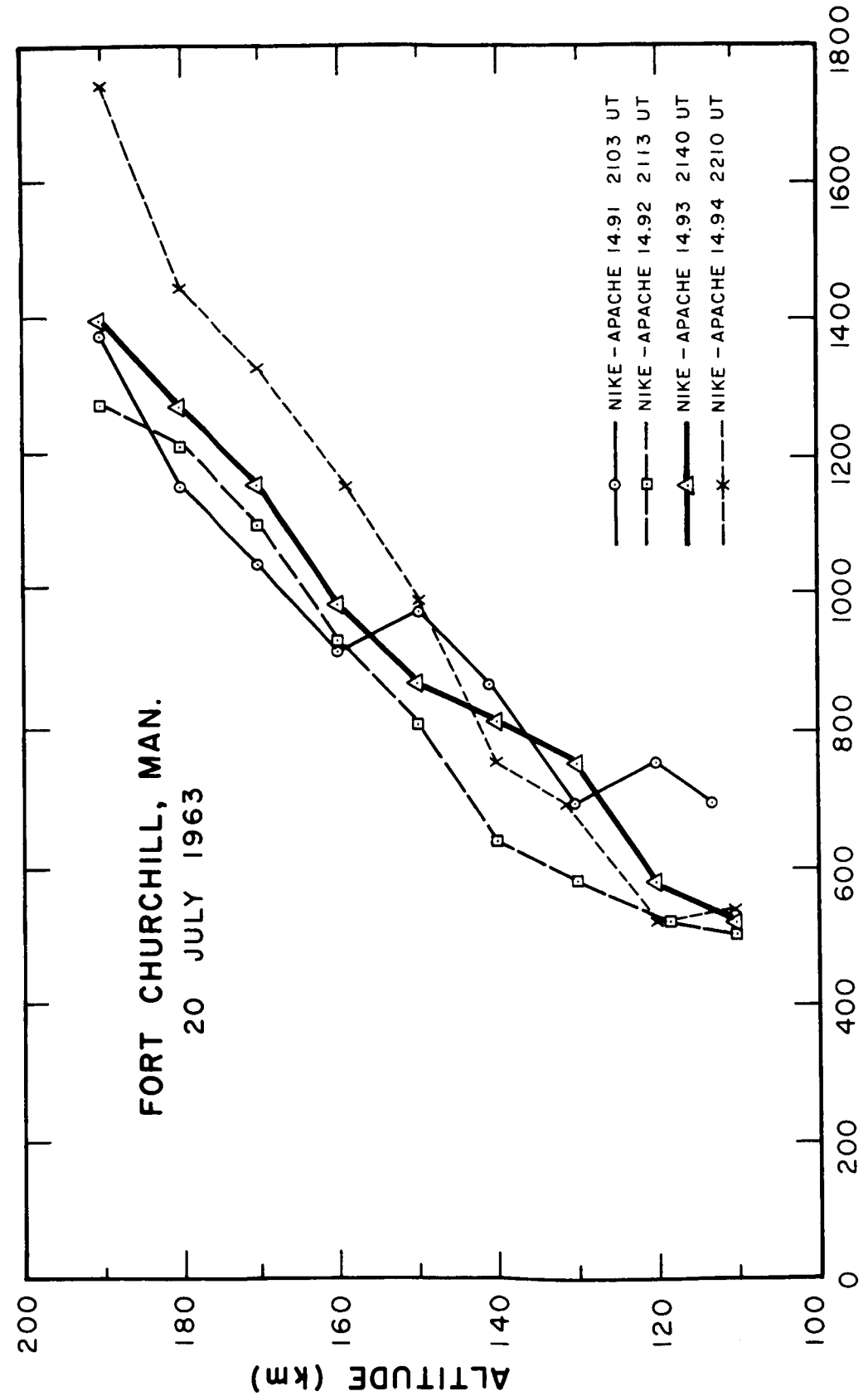

Figure 31. Electron temperature measured during the eclipse.

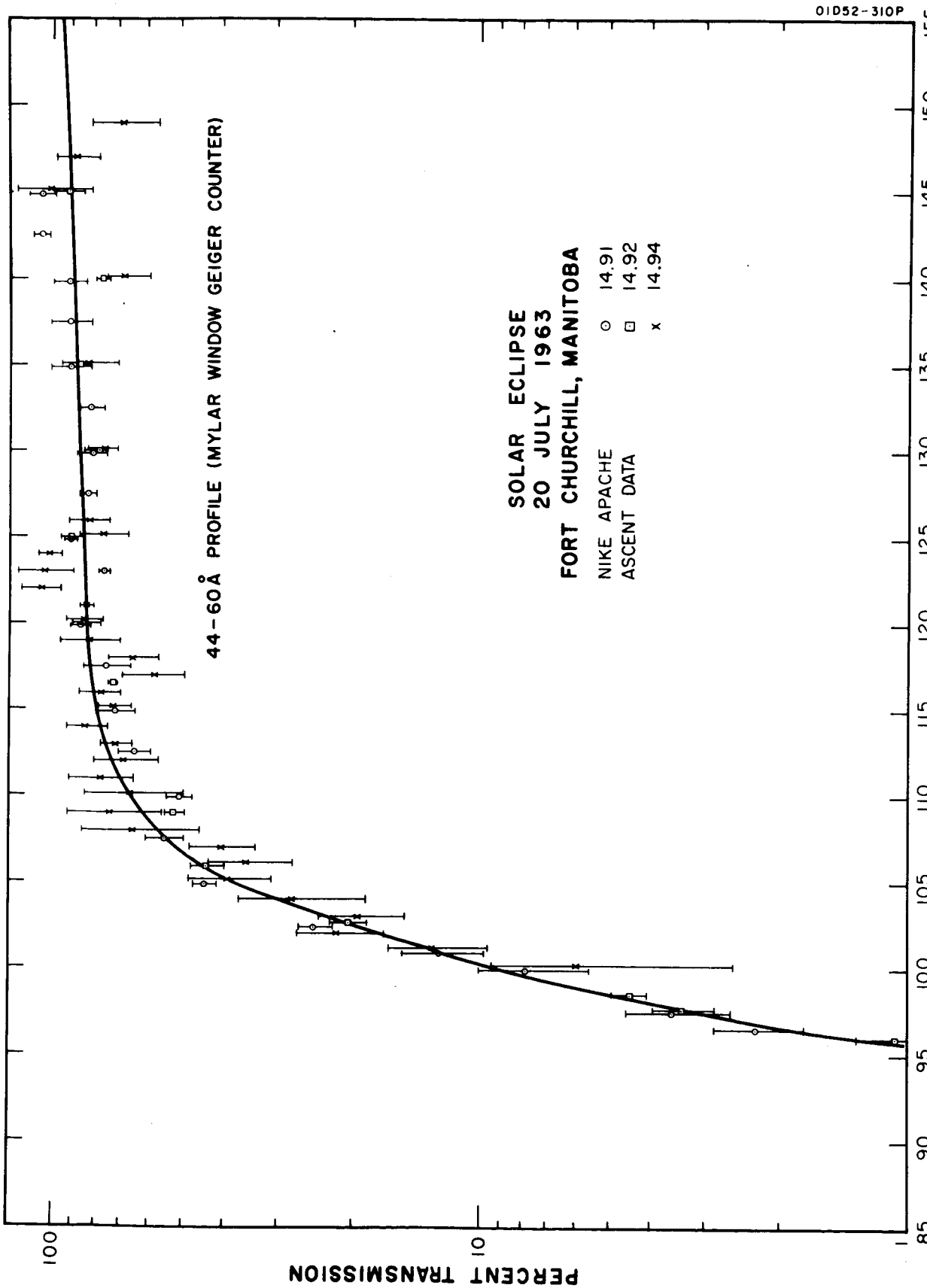

Figure 32. Absorption profiles of X-rays (44-60Å).

because of the zenith angle difference (48^{o} to 56^{o}); however, because of the large statistical errors, there is little change in the average profile if 14.94 data is included. The solid line in Figure 32 is a theoretical profile, which has arbitrarily been raised 1 km, based on the model of a single spectral line in that wavelength region for which 0, 0_2 and N_2 have been assigned absorption coefficients of 6.7 cm^{-1}, 13.4 cm^{-1} and 3.2 cm^{-1}, respectively. This profile is seen to be in good agreement with the data. Differentiation shows that the maximum energy loss and hence the maximum photoionization rate occurs near 104 km.

The absolute values of the flux shown in Table 12 have been obtained by correcting the count rate data for the appropriate window areas and taking a gray body distribution for a coronal temperature of 5×10^{5} ^{o}K. This method has been given in detail by Kreplin [2]. Analysis of the data for flight 14.94 (last contact) indicates a degradation of the Geiger counter sensitivity. For this reason, an incident flux at the top of the atmosphere during last contact was determined from the measurements made during the control flight 14.88 on July 14, at the same location and zenith angle. A summary of the Geiger counter measurements is given in Table 12.

From the incident flux of the unobscured sun, the percent of residual flux at two times during the eclipse was determined and is given in Table 13. For purposes of comparison, the percent of residual radiation as determined from the ionosonde critical frequency measurements is also shown in this table. Since the E-region was observed to react immediately to the eclipse conditions, the X-ray data and the ionosonde data can be compared at the same time. It is noted that the X-ray data is reduced much less than the area of the visible solar disc, due to a significant amount of coronal radiation. The interpretation of this data depends on the relation between critical frequency and ionization rate. If the loss process for the E-layer is taken to be recombination, as in most theoretical treatments, then $(f_o E)^4$ would be proportional to the flux of ionizing radiation. It would then be concluded that about half of the ionizing radiation is proportional to the area of the visible disc, and half is proportional to the measured band of X-rays. That is, the theoretical law is consistent with a model for which approximately half of the ionizing radiation is uniformly distributed over the visible solar disc and half is distributed in the same matter as X-rays in the band 44-60Å. However, although the fourth power law is frequently used in eclipse studies, it is not supported by observations, and, in fact, the diurnal variation of $f_o E$ shows that to a good approximation [19] $(f_o E)3$ is proportional to the flux of ionizing radiation. Taking this law to represent the real behaviour of the E-layer, a comparison with the X-ray data leads to a different conclusion: the ionizing radiation responsible for the E-layer is reduced during the eclipse in proportion to the measured band of X-rays.

TABLE 12. Summary of X-ray Geiger Counter Measurements

Flight	Date	Launch Time	Apogee	Zenith Angle	Window Area	Dead Time	Corrected Count Rate At Top of Atmosphere	44-60Å Flux (0.5×10^{6} °K)
14.88*	14 July 63	210327	171.6 km	48°	2.0×10^{-3} cm^2	135μ sec	2.47×10^{6} $\frac{\text{counts}}{\text{cm}^2\text{sec}}$	.074 ergs/cm^{2}sec
14.91	20 July 63	210300	196.0 km	48°	6.5×10^{-3} cm^2	140μ sec	5.47×10^{5} $\frac{\text{counts}}{\text{cm}^2\text{sec}}$	.016 ergs/cm^{2}sec
14.92	20 July 63	211300	198.8 km	49°	2.0×10^{-2} cm^2	130μ sec	1.05×10^{6} $\frac{\text{counts}}{\text{cm}^2\text{sec}}$	.030 ergs/cm^{2}sec
14.93**	20 July 63	214000	199.7 km	52°	8.3×10^{-2} cm^2	140μ sec	----------	----------
14.94***	20 July 63	22100	192.6 km	56°	2.0×10^{-3} cm^2	125μ sec	4.25×10^{5} $\frac{\text{counts}}{\text{cm}^2\text{sec}}$	.0120 ergs/cm^{2}sec

* Disturbed ionosphere, corpuscular component observed beginning approximately at 80 km.

** Geiger Counter not exposed to sun due to malfunction of door release. May provide cosmic ray data.

*** This counter evidences a reduced sensitivity.

TABLE 13. Comparison of X-ray and Ionosonde Data
Fort Churchill, Manitoba, 20 July 1963

X-ray (44 - 60 A)		
Nike Apache	14.91	14.92
Time (at 170 km)	2105:27 UT	2115:25 UT
Intensity	22 $\pm$ 2%	41 $\pm$ 4%
Area of Solar Disc	9.5%	17.0%
Ionosonde (E-Layer)		
Time	2109:00 UT	2115:00 UT
Area of Solar Disc (at 105 km)	9.5%	17.0%
f_oE	1.90 mc/s	2.15 mc/s
$(f_oE/3.0)^3$	25 $\pm$ 2%	37 $\pm$ 3%
$(f_oE/3.0)^4$	16 $\pm$ 2%	26 $\pm$ 3%

Discussion

The electron density profiles obtained from the DC probe support the earlier ionosonde measurements, which indicated rather small time lags between maximum phase and minimum electron density for the E and F_1 layers. Further, the overall regular behavior of the four probe-current profiles shows that there were no significant departures from the E and F_1 layer time lags over the height range 90-195 km; that is, the E and F_1 layers were generally typical of the E and F_1 regions during the eclipse.

Previous ionosonde studies on the E and F_1 layers have indicated that the sources of the ionization for these respective layers are distributed in the same way across the solar disc [20,21]. The rocket measurements support this conclusion since the profile shape is preserved without major change during the eclipse. This is difficult to explain on the basis of a model for which different parts of the spectrum are responsible for the E and F_1 layers. For example, coronal radiation below 100Å is considered important for the E layer, but the longer wave ultraviolet, important in the F_1 layer, is not coronal in origin.

Radiation measurements at various phases of an eclipse permit the relative contribution of this radiation from various sections of the solar disc to be determined and correlated with other solar indices. Other studies have suggested that the Ca K line and λ 5303Å may be indications of regions of enhanced X-ray emission [2,22]. The few successful rocket flights in this experiment were not sufficient for a complete study of the solar disc; however, the data in Table 13 suggests there may have been an uncovering of a radiation source on the west limb of the sun between the time of flight 14.91 and 14.92. Spectroheliograms of the sun in Ca K obtained from the McMath-Hulburt Observatory* show a plage also on the west limb, as well as several other plages. The rocket measurements indicate that the radiation responsible for the E layer is distributed across the disc in the same manner as the 44-60Å radiation.

In determining the effective recombination coefficient from the measured time lag between maximum phase and minimum electron density, it is assumed that the minimum ionization rate occurs during maximum phase. This will not be the case for a highly irregular distribution of radiation sources; however, on July 20, 1963 the sun was very quiet. The value obtained for the effective recombination coefficient in the E layer is somewhat larger than most eclipse determinations, but is in good agreement with some measurements [23,24]. The F_1 layer reconbination coefficient is also somewhat larger than most other eclipse values, but agrees well with Piddington [23], Meriau and Rawer [25], and Landmark [26]. The values for the time lags of the E and F_1 layers are consistent with observations of eclipse occurring, as does this eclipse, near the minimum of the solar cycle; however, at solar maximum the time lags are found to be much higher [1].

*The University of Michigan

Rydbeck and Wilhelmsson [27] have analyzed the variation of electron density during an eclipse. They assume that electrons are lost by recombination and that the ionizing radiation is proportional to the visible area of the solar disc. For a total eclipse of short duration with no change in solar zenith angle their analysis gives simple formulae relating the minimum electron density N_{min} and the time lag Δt between the time of totality and the time of minimum electron density to the effective recombination coefficient α. These formulae can be written

$$\left(\frac{N_{min}}{N_o}\right)^2 = 1.3\left(\frac{\Delta t}{t_o}\right) = \frac{0.46}{(\alpha N_o t_o)^{2/3}} \quad (\alpha N_o t_o > 3)$$

where N_o is the electron density at first contact and t_o the time between first contact and second contact. These formulae show that a reduction of electron density to one third of the normal value would require a time delay of 5 minutes while a reduction to one-half of the normal value would require a time delay of over 11 minutes. Such long delays are rarely found and have led to a search for another explanation. Further, it is found that for actual eclipse data, the formula which is most frequently used

$$\left(\frac{N_{min}}{N_o}\right)^2 = \frac{0.46}{(\alpha N_o t_o)^{2/3}}$$

gives a lower value for α than the formula

$$1.3\,\frac{\Delta t}{t_o} = \frac{0.46}{(\alpha N_o t_o)^{2/3}} \quad .$$

This inconsistency is probably due to the model that was used for the analysis. For example, if a significant fraction of the E layer ionization is produced by coronal radiation than the values of α obtained from the relation involving N_{min} will be too low. On the other hand, the values of α obtained from the relation involving Δt are very close to those obtained from the Appleton "sluggishness" formula, that was used in this analysis. It is believed that the larger values of α, i.e., as obtained from the time lag, are more nearly correct.

An attempt was made to attribute the nonuniform behavior of the critical frequency during the eclipse of February 1952 to a recombination coefficient that was changing as a result of a temperature variation [28]. The present measurements indicate that, at least as far as the E region is concerned, there is not a large enough temperature variation to produce this effect.

THE ECLIPSE IN THE D-REGION

Lyman-α

The Lyman-α ion chambers provided useful data on rocket flights 14.91, 14.92 and 14.94. A partial telemetry failure prevented any ion chamber data from being obtained during the descent portion of flight 14.91. Except during the time when the rocket tips over on descent, the aspect correction required for the A (60° position) ion chambers was small since the views were not more than 15° away from normal incidence. For the B (90° position) ion chambers, the aspect angles are significantly larger. Table 14 summarizes these aspect conditions. Because the rocket spin axis did not exactly coincide with the rocket axis, the aspect angles seen by the A and B ion chambers do not differ by exactly 30°. The corrections applied to the data for non-zero aspect angles take into account the reduction in flux incident on the aperture of the ion chambers and the increased radiation path in the lithium fluoride windows.

Corrected profiles show a maximum in the ion chamber currents at about 95 km heights on rocket ascent. The currents at greater heights eventually exceeded the values seen near 95 km, except for ion chamber No. 81 which exhibited a permanent sensitivity reduction at greater heights. The absence of any such features on the descent portion of the trajectories rules out the possibility of a physical effect external to the ion chambers responsible for this 95 km maximum. The magnitude of this peak current for a given flight is always greater for the ion chamber oriented at 60°, which is the detector that looks most directly at the sun. This suggests that the anomaly may result from a solarization or partial decomposition effect on the carbon disulfide gas fill due to the action of solar ultraviolet radiation, although a completely satisfactory explanation has not been found. On the basis of these results, it is felt that carbon disulfide is less suitable for ion chambers in rocket applications than is nitric oxide which, in other rocket flights, has been found to be well behaved. Fortunately this anomaly was not observed on the descent profiles, and except for ion chamber No. 81, these profiles were all in good agreement with theoretical calculations based on the 1962 US Standard Atmosphere, and an absorption coefficient of molecular oxygen at Lyman-α of 0.27 cm^{-1}, if the theoretical curve is arbitrarily raised by 1 km. It is unlikely that the rocket altitude was in error by this much and probably indicates a difference between the real atmosphere and the model. These profiles show that the maximum energy is deposited in the altitude range 80 to 82 km.

The absence of a systematic change in the profiles of the ion chamber currents above 72 km at various phases of the eclipse shows that the molecular oxygen density did not change by more than 16 percent above this height due to the eclipse.

TABLE 14. Ion Chamber Aspect Data

Rocket Number	Ion Chamber Number	Ion Chamber Position	Max. Aspect Angle Deviation from Normal Incidence	Variation in Aspect Angle due to Precession
14.91 A	60	60°	15°	10.5°
B	74	90°	44°	10.5°
14.92 A	82	60°	10°	11°
B	87	90°	31°	11°
14.94 A	81	60°	5°	6.5°
B	78	90°	21°	6.5°

*The aspect situation for the Geiger counters is identical to that of ion chamber A on the same vehicle.

Preflight laboratory calibrations of the ion chambers at 1215.7Å allow the Lyman-α flux in the D-region to be determined from the corrected currents. The most accurate profile of the Lyman-α flux was obtained from ion chamber No. 78, during last contact of the eclipse, and is shown in Figure 33. The uncertainties do not include possible changes in the sensitivity of the ion chamber subsequent to the preflight laboratory calibration, but such changes during flight are believed to be responsible for part of the difference seen between ascent and descent. The dotted portion of the descent profile indicates interpolated fluxes at heights where the rocket motion provided very unfavorable aspect angles for viewing the sun. In order to obtain the incident flux at the top of the atmosphere it was necessary to correct for the apparent sensitivity changes in the ion chambers taking place during rocket ascent. This was accomplished by extrapolating the currents measured on ascent at 90 km height to an incident flux from the measured attenuation at 90 km seen by ion chamber No. 78 on descent. In this way, more accurate estimates of the incident flux at the top of the atmosphere could be obtained for various phases of the eclipse. The reduction in incident flux at the middle of the eclipse is summarized in Table 15. The measured incident flux at last contact of 3.0 ± 0.3 ergs/cm^2/sec in the spectral range 1050 to 1240Å is about half the values obtained during the last solar maximum [29]. Further measurements during the IQSY will indicate if there is a significant solar cycle variation in the Lyman-α flux from the sun.

Since the measurements of Kreplin [2] during the total eclipse of 1958 showed that virtually all the Lyman-α radiation emanates from the visible solar disc, this measurement of a slightly enhanced emission at maximum phase shows that this enhancement must have originated from the exposed north sector of the visible disc. Work at NRL has suggested a close correlation between the location of CaK plages and Lyman-α plages on the solar disc [30]. However, spectroheliograms of CaK obtained from the McMath-Hulburt Observatory did not show any CaK plages on the north sector at the time of the rocket measurements.

Electron Density

Measurements of the electron density in the D-region obtained from the DC probe are shown in Figure 34. Profile (4), corresponding to last contact of the eclipse, shows interesting features of the normal D-region. The so-called C-layer (cosmic ray region) is observed from about 53 km to 70 km; above this, up to approximately 83 km is the Lyman-α region. The height of maximum deposited energy (maximum photoionization rate) at 80 to 82 km as determined from the ion chamber data, and the maximum ionization at 82 km, as seen from the probe data, is in good agreement. The change in curvature seen from 83 to 89 km indicates an additional source of ionization that cannot be accounted for by either cosmic rays or Lyman-α radiation. An interesting feature of this region is the small-scale irregularities observed from 84 to 89 km. This fine, irregular

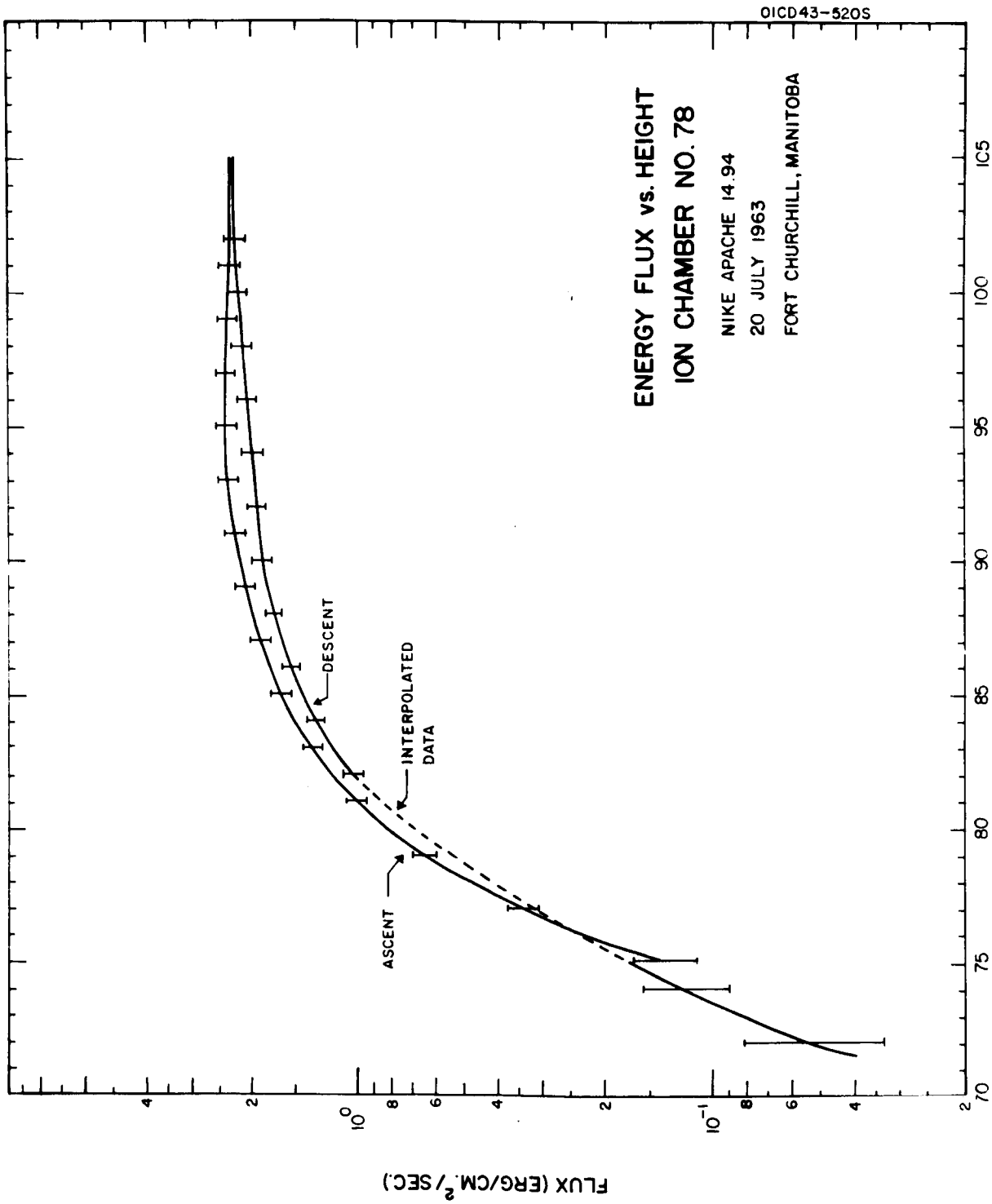

Figure 33. Absorption profiles of Lyman-α.

TABLE 15. Summary of Ion Chamber Data

Fort Churchill, Manitoba, 20 July 1963

Incident flux at last contact: 3.0 erg cm^{-2} sec^{-1}.
(Lyman-α flux estimated to be 80% of incident flux).

Nike Apache	14.91	14.92
Time (at 90 km)	2104:12 UT	2114:11 UT
Ion Chamber (60^{o})	10.6%	13.7%
Ion Chamber (90^{o})	9.2%	18.6%
Area of Solar Disc	8.4%	15.4%

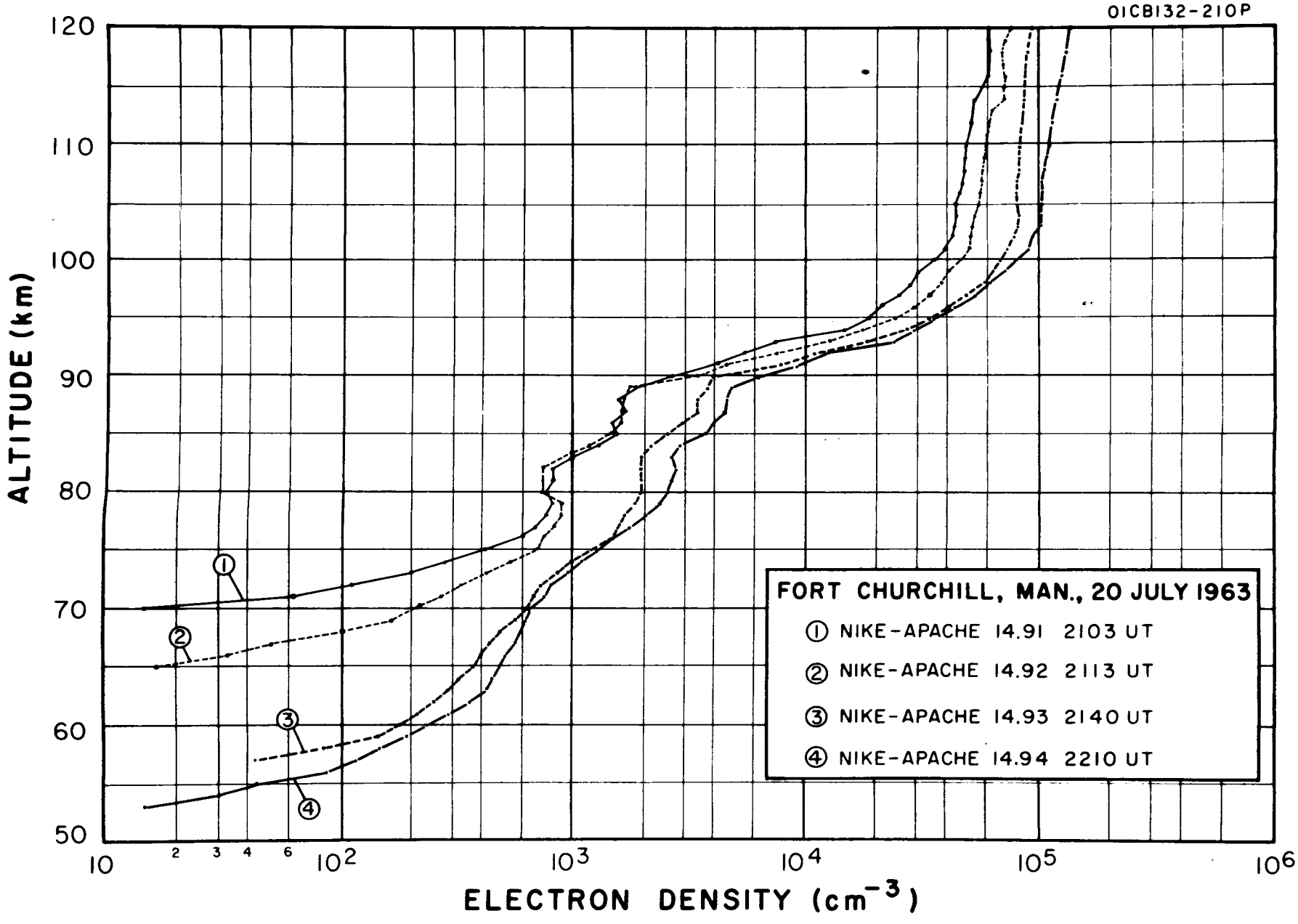

Figure 34. Electron density profiles in the D and lower E-regions.

structure is not apparent in Figure 34, where the data points are plotted at 1 km intervals, but it is clearly observable on the telemetry record.

The effect of the eclipse on the electron density is shown in profiles (1), (2) and (3) corresponding to about 8 percent, 15 percent and 60 percent exposure of the visible solar disc at D-region heights. The maximum ionization for the Lyman-α layer is seen to be about 79 km near maximum phase, in approximate agreement with the ion chamber data.

Considering the timing of rocket flights 14.91 and 14.92 with respect to maximum phase of the eclipse, it is found that the near equality of profiles (1) and (2) from 79 to 89 km indicates a time lag of the minimum electron density after the minimum area of the visible solar disc of about 3 minutes in this region of the ionosphere, and at the five heights where profiles (1) and (2) intersect, the time lag must have been 3 minutes. If it is assumed that the minimum area of the visible solar disc coincides with the minimum photoionization rate, the effective recombination coefficients during the maximum phase of the eclipse can be determined as was done for the E- and F_1-layers. The effective recombination coefficients thus determined at the five heights are given in Figure 35.

At lower, as well as at greater heights, the time lag is seen to be well under 3 minutes. The effect of the eclipse below 72 km is especially pronounced: the C-layer disappears completely near maximum phase of the eclipse (profiles (1) and (2)). The reduction of electron density in the lower D-region is also illustrated in Figure 36, where the electron density profiles are normalized to unity at 105 km. This figure also indicates the general complexity of the D-region, as evidenced by its features, contrasted to the rather regular behavior of the E-region during the eclipse.

Discussion

In a complete analysis of the D-region it is necessary to consider all the sources of ionization and the attachment and recombination rates for each ion species. In the recombination, the effect of ion-molecule charge exchange must also be taken into account. Because the various ion concentrations and their charge exchange and recombination rates are largely unknown, it is usually more convenient to use an effective recombination coefficient α for all ions, which can be defined in terms of the well known electron balance equation for the D-region: [30a]

$$\frac{dN}{dt} = \frac{q}{1+\lambda} - \alpha N^2 - \frac{N}{1+\lambda}\frac{d\lambda}{dt} \quad ,$$

where N is the electron density, q is the total photoionization rate, and λ is the ratio of negative ions to electrons. The effective recombination

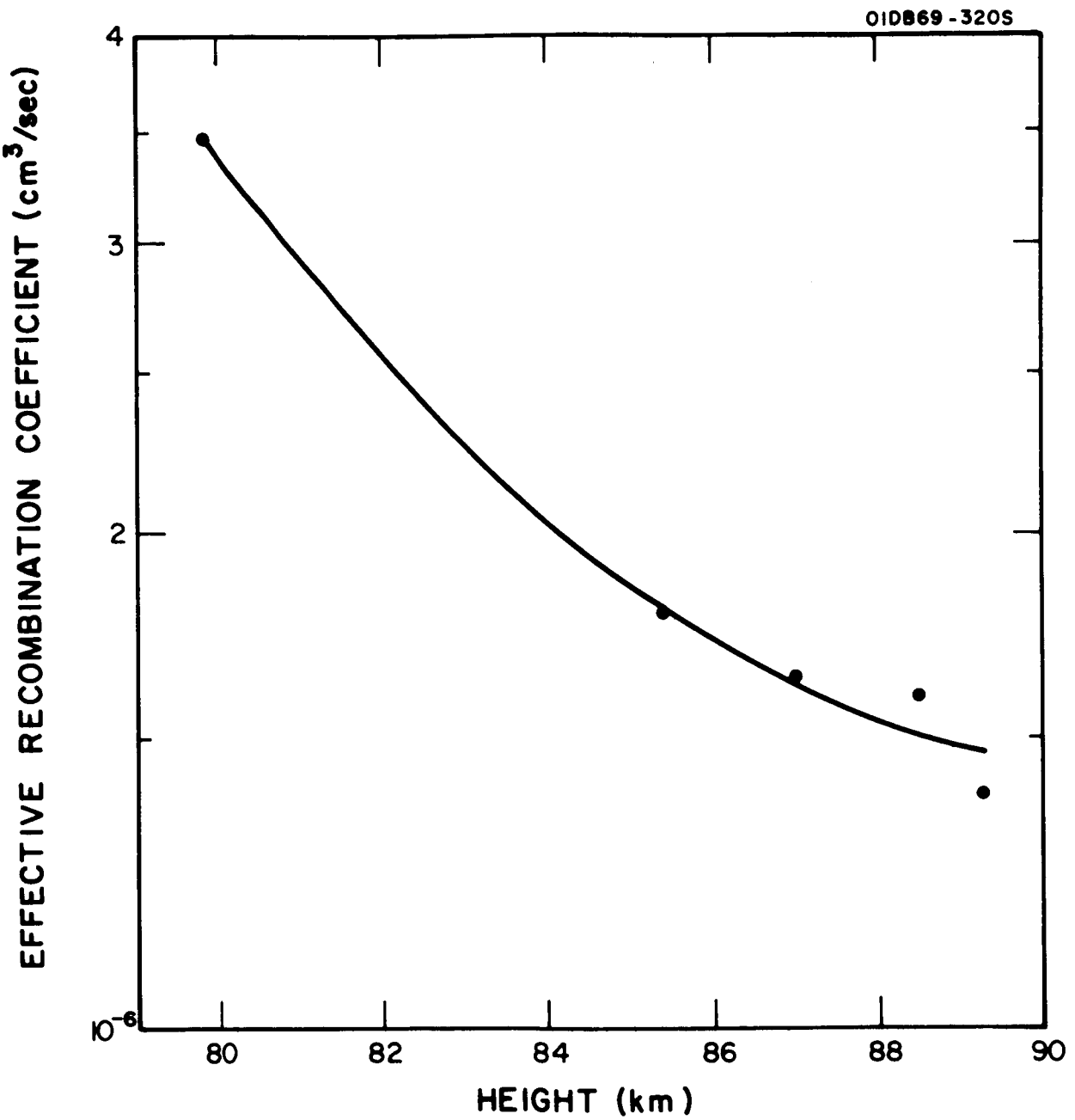

Figure 35. Effective recombination coefficient as a function of height.

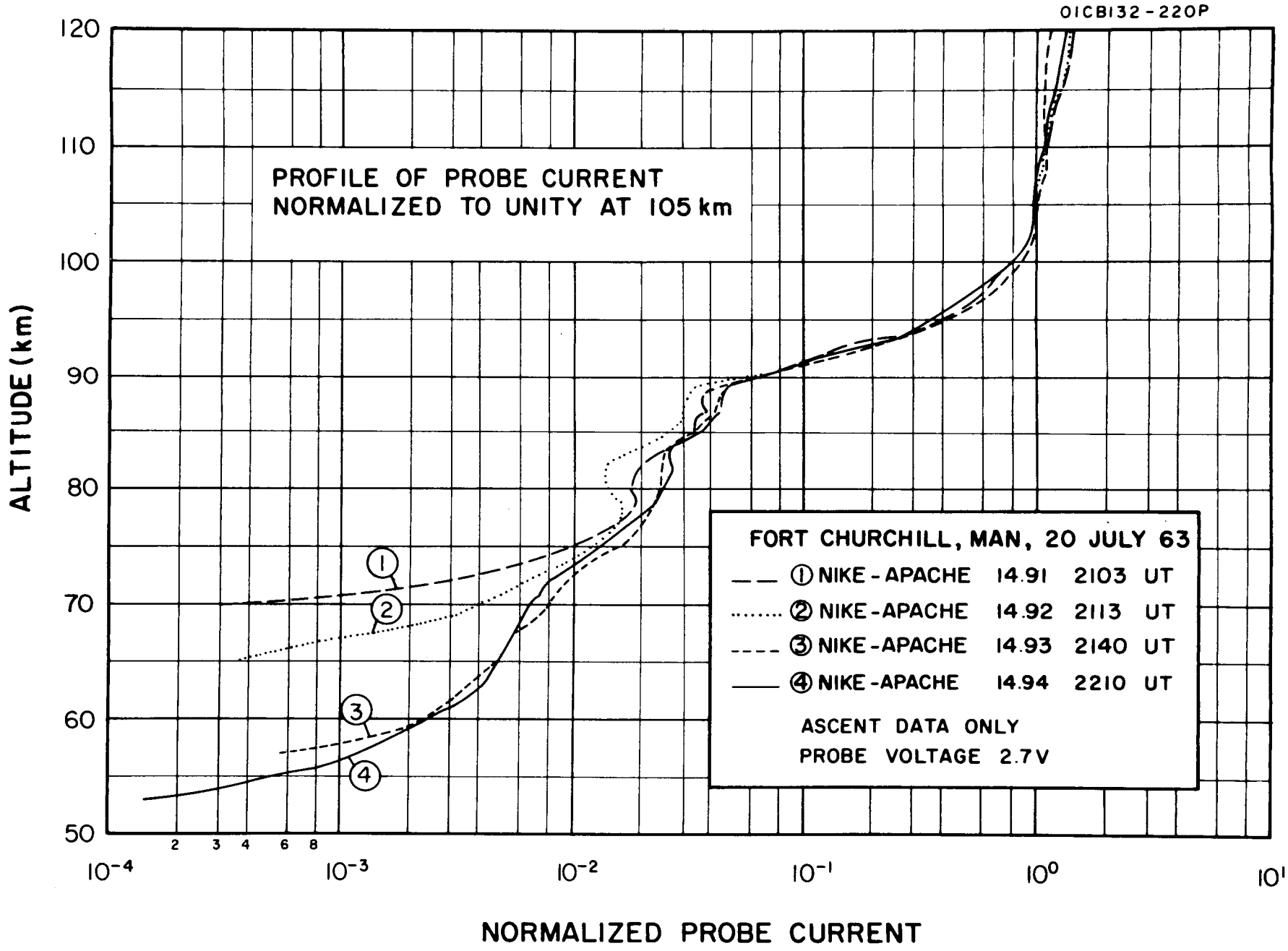

Figure 36. Profiles of probe current (proportional to electron density) normalized to unity at 105 km.

coefficient can be written

$$\alpha = \alpha_D + \lambda\alpha_i \quad ,$$

where α_D is the dissociative recombination coefficient and α_i is the mutual ionic neutralization coefficient.

The effective recombination coefficients given in Figure 35 pertain to conditions during the maximum phase of the solar eclipse. Because of the reduced photodetachment during the eclipse, the value of λ will be larger than during normal daytime conditions, and therefore the effective recombination coefficients will also be somewhat larger. If it can be assumed that α_D and α_i remain constant over the altitude range 80 to 90 km, and if it can be assumed that λ follows a straight line on a semi-log plot over this interval, e.g., λ proportional to the square of the molecular oxygen concentration, or to some other well-mixed constituent, then it is possible to separate from α the two terms α_D and $\lambda\alpha_i$. When this is done, for the data in Figure 35, it is found that the best straight line on a semi-log plot for $\lambda\alpha_i$ is obtained for $\alpha_D = 1.2 \times 10^{-6}$ cm^3/sec. For values of α_i ranging from 10^{-7} cm^3/sec to 10^{-8} cm^3/sec, estimates of λ as a function of height are given in Table 16. It is to be noted that these values of λ refer to eclipse conditions for which the percentage of the visible solar disc is 8 percent (on flight 14.91) to 15 percent (on flight 14.92).

Based on a model of molecular oxygen as the attaching agent in the D-region, the values of λ is Table 16 are large, even compared to a nighttime model for λ [31]. However, they are easier to explain if an agent having a larger attachment coefficient played an important role. The uncertainties in the values obtained for α_D and λ depend on the validity of the assumptions mentioned and may be quite large.

A model of the lower D-region was studied by means of a computer analysis. For this model the photodetachment coefficient ρ at any instant during the eclipse was taken to be proportional to the fractional area of the unobscured visible solar disc A:

$$\rho(t) = \rho_o \, A(t) \quad ,$$

where ρ_o represents the photodetachment coefficient at first (or last) contact. The following equation was used to define λ [32]

$$\frac{d\lambda}{dt} + \lambda^2[\rho + \gamma n + N(\alpha_i - \alpha_D)] + \lambda\,[\rho + \gamma n + N(\alpha_i - \alpha_D) + \frac{q}{N} - \beta m] = \beta m \quad ,$$

TABLE 16. Estimated Value for λ Near Maximum Phase of the Eclipse

h(km)	$\lambda\alpha_i$	λ $\alpha_i=10^{-7}$	$\alpha=10^{-8}$
90	2.10×10^{-7}	2.1	21.0
88	3.35	3.35	33.5
86	5.32	5.32	53.2
84	8.50	8.50	85.0
82	1.35×10^{-6}	13.5	135
80	2.15	21.5	215

where γn = collisional detachment coefficient and

βm = attachment coefficient.

The terms $N(\alpha_i - \alpha_D)$ and q/N turn out to be negligibly small. For specified values of γn, βm, and ρ_o, λ and $d\lambda/dt$ are computed at incremented times during the eclipse. The electron balance equation,

$$\frac{dN}{dt} = \frac{q}{1+\lambda} - (\alpha_D + \lambda\alpha_i)N^2 - \frac{N}{1+\lambda}\frac{d\lambda}{dt} \quad ,$$

for specified values of α_D and α_i, is then used to determine N and dN/dt for these times. This method was used to study the observed electron density variation at 65 km. At this height all the ionization was taken to be produced by cosmic rays, and constant production rates were used which would provide the measured value of electron density at last contact for the particular parameters considered. Values of λ at last contact ranging from 2.4 to 10 and values of α at last contact ranging from 10^{-7} cm^3/sec to 2.8×10^{-6} cm^3/sec were used. It was found that the terms $\frac{dN}{dt}$ and $\frac{d\lambda}{dt}$ were negligible and that the reduction in electron density was not nearly as great as was observed experimentally.

Although the electron densities measured in the lower D-region (below 75 km) may have significant systematic errors, as was discussed earlier, it is felt that the discrepancy between the measurements and the theoretical model is probably due to the presence of a constituent which had a much larger attachment coefficient than molecular oxygen, such as ozone or nitrogen dioxide. The presence of O_3^- or NO_2^- in significant numbers have been proposed to explain anomalies in riometer absorption of PCA events during sunrise and sunset [33,34,35]. It is also noted that a recent theoretical study has shown that the concentration of ozone will increase during a solar eclipse, especially in the D-region [36].

CONCLUSIONS

The eclipse of 20 July 1963 provides a very clear example of the behavior of the ionosphere up to 200 km. The sun was very quiet at the time of the eclipse. No sporadic E or other unusual phenomena other than possibly a small downward travelling disturbance was present in the ionosphere and excellent ionosonde records were obtained which complement the rocket observations in the E- and F_1-regions. In the D-region, not previously observed directly, a surprisingly large eclipse effect appeared below 75 km which has not been satisfactorily explained.

The rocket and ionosonde data taken together show that the ionosphere between 90 and 200 km remains essentially in equilibrium during the eclipse. The data indicate an effective recombination coefficient in the E-layer of no less than 1×10^{-7} cm^3 sec^{-1} and in the F_1-layer of no less than 4×10^{-8} cm^3 sec^{-1}. The time lag between maximum phase of the eclipse and the minimum electron density was much less than the five minutes required by the "sluggishness" hypothesis. The time lags of five minutes or more that have occasionally been reported are probably due to irregular distribution or temporal variation in the ionizing radiation.

The "residual radiation" hypothesis appears to provide a more satisfactory interpretation of the observed behavior of the ionosphere although some details remain to be explained. The rocket data confirm the existence of coronal radiation and point to X-rays as being a major part of the ionizing radiation of the E-layer. If, as is likely, the coronal radiation does not include a significant contribution in the extreme UV, then the interpretation of the F_1-layer during the eclipse presents a major problem. The rocket data shows that the electron density was reduced by the same factor over the altitude range 90 to 200 km which, if recombination is the only loss process for electrons, would imply that the photoionization rate was reduced by the same factor over this altitude. This is not acceptable in view of the changing spectral composition of the radiation as the sun is eclipsed.

The explanation of the behavior of the F_1-layer will probably depend on further knowledge of the photochemistry of the ionosphere and measurements of the spectral composition of the residual radiation at totality. The latter measurement need not wait on the occurrence of an eclipse as it is now quite feasible to investigate the solar corona from a sounding rocket or satellite by artificially eclipsing the solar disc.

The uniformity of behavior of the E- and F_1-regions is not found in the D-region which shows a more complex variation. The upper part of the region between 79 and 89 km shows a time lag of about 3 minutes and an effective recombination coefficient is obtained near maximum phase

which decreases from 3.5×10^{-6} cm^3 sec^{-1} at 79 km to 1.5×10^{-6} cm^3 sec^{-1} at 89 km. In the lower part of the D-region a smaller time lag is indicated.

The effect of the eclipse on electron density is more pronounced in the D-region below 72 km than at greater heights near maximum phase. In spite of some uncertainty at these altitudes in the value of electron density indicated by the probe the change in the lower D-region is larger than current theories allow and further investigation is required. The electron density profiles obtained permit the propagation characteristics of low frequency and very low frequency radio waves to be calculated. Further study of the present eclipse results should include such an analysis to provide quantitative comparisons with the results of radio wave measurements made during other eclipses particularly of the so-called absorption anomaly. The closely related phenomenon of the rapid change of radio absorption at sunrise and sunset offers additional opportunities for investigating the region.

It is very rarely that a total eclipse passes close to a permanent launch site. After the 20 July 1963 eclipse the next such occasion will be 7 March 1970 when the path of totality passes close to Cape Kennedy, Florida. Once or twice a year a total or annular eclipse occurs somewhere over the earth's surface and is accessible to a ship launch or, in some cases, to a temporary land-based launch site. Four eclipses occur in 1965 and 1966 as follows:

30 May 1965: South Pacific, Maximum duration of totality 5 minutes 16 seconds.

23 November 1965: India to the Pacific Ocean, Annular eclipse.

20 May 1966: Africa, Europe, Asia, Annular eclipse.

12 November 1966: South America and South Atlantic Ocean, Maximum duration of totality 1 minute 57 seconds.

The eclipses of 30 May 1965 and of 23 November 1965 are particularly valuable as they provide the possibility of examining the occurrence of the so-called $F_{1\frac{1}{2}}$-layer. It has been observed at ionosonde stations near the geomagnetic equator having dip angles less than 20 degrees and is characterized by a new critical frequency $f_oF_{1\frac{1}{2}}$ appearing between f_oF_1 and f_oF_2 during the eclipse. The central lines of both eclipses of 1965 cross the geomagnetic equator near local noon and provide excellent opportunities for investigation of the $F_{1\frac{1}{2}}$-layer. The eclipses of 1966 are more appropriate for mid-latitude studies and are suitable for rocket launches from a ship in the Mediterranean Sea and the South Atlantic Ocean, respectively.

It is important in future rocket programs to include the measurement of the positive ion mass spectrum. This is particularly significant if the detailed chemical reactions of the ionosphere are to be investigated. A minimum program for future eclipse investigations should include two rockets instrumented to measure electron density, X-ray flux (44 to 60Å) and positive ion mass spectrum. The first rocket would be launched at first contact and the second at maximum phase. A third rocket as a back-up would be highly desirable. A temporary land-based launch site is to be preferred to launches from a ship mainly because of the navigational problem of locating the exact position of the ship, but also because an ionosonde and other radio probing experiments can be coordinated with the rocket measurements. The ship does, however, allow greater flexibility in the selection of the actual launch position and is probably easier to instrument with telemetry and tracking support.

REFERENCES

1. Ratcliffe, J. A., "A Survey of Solar Eclipses and the Ionosphere," pp. 1-13, Solar Eclipses and the Ionosphere, Pergamon Press, New York, 1956.

2. Kreplin, R. W., "Solar X-Rays," Annales de Geophysique 17, 151-161 (1961).

3. Weeks, L. H., "Useful Ranges of Some Solar Detectors," GCA Tech. Rpt. No. 63-5-N (February 1963).

4. Accardo, C. A., Gross, H. G., and Weeks, L. H., "A Rocket-Borne 44-60Å Geiger Counter," GCA Tech. Rpt. No. 63-14-N (May 1963).

5. Weeks, L. H., "A Survey of the Lower Ionosphere during Solar Eclipses," GCA Tech. Rpt. No. 63-20-N (July 1963).

6. Smith, L. G., Accardo, C. A., Weeks, L. H., and McKinnon, P. J., "Rocket Measurements in the Ionosphere during the Eclipse of 20 July 1963," GCA Tech. Rpt. No. 64-11-N (May 1964).

7. Smith, L. G., "A DC Probe for Rocket Measurements in the Ionosphere," GCA Tech. Rpt. No. 63-19-N (June 1963).

8. McKinnon, P. J. and Smith, L. G., "A Solar Aspect Sensor for Sounding Rockets," GCA Tech. Rpt. No. 64-12-N (July 1964).

8a. Stober, A. K., "Ceramic Vacuum Ultraviolet Ion Chambers," NASA TN D-1180 (March 1962).

8b. Stober, A. K., "A Vacuum Ultraviolet Photoionization Chamber," NASA TN D-1715 (March 1963).

9. Smith, L. G., "A Simple Method of Trajectory Determination for Sounding Rockets," GCA Tech. Rpt. No. 63-9-N (March 1963).

10. Smith, L. G., "Langmuir Probes for Measurements in the Ionosphere," COSPAR Information Bull. No. 17, PP. 37-81 (February 1964) (Ed. K. Maeda).

11. Davis, L. R., Berg, O. E. and Meredith, L. H., "Direct Measurements of Particle Fluxes in and near Auroras," Space Res. 1, 721-735 (1960).

12. McDiarmid, I. B., Rose, D. C. and Budzinski, E., "Direct Measurement of Charged Particles Associated with Auroral Zone Radio Absorption," Canad. J. Phys. 39, 1888-1900 (1961).

13. McIlwain, C. E., "Direct Measurement of Particles Producing Visible Auroras," J. Geophys. Res. 65, 2727-2747 (1960).

14. O'Brien, B. J. and Taylor, H., "High-Latitude Geophysical Studies with Satellite Injun 3 for Auroras and Their Excitation," J. Geophys. Res. 69, 45-63 (1964).

15. Rees, M. H., "Auroral Ionization and Excitation by Incident Energetic Electrons," Planet. Sp. Sci. 11, 1209-1218 (1963).

16. Jespersen, M., Petersen, O., Rybner, J., Bjelland, B., Holt, O., Landmark, B., and Kane, J. A., "Electron and Ion Density Observations in the D Region during Auroral Absorption," Planet. Sp. Sci. 12, 543-552 (1964).

17. Bibl, K., C. R. Acad. Sci. Paris 235, 734-736 (1952). "Phénomènes Dynamiques dans les Couches Ionosphériques"; Z. Geophys. 19, 136-141 (1953). "Die Ionosphärenschichten und ihre Dynamischen Phänomene."

18. Appleton, E. V., "A Note on the 'Sluggishness' of the Ionosphere," J. Atmosph. Terr. Phys. 3, 282-284 (1953).

19. Ratcliffe, J. A. and Weekes, K., "The Ionosphere," Physics of the Upper Atmosphere (Ed., J. A. Ratcliffe) Academic Press, New York, 1960, P. 416.

20. Minnis, C. M., "The Effective Recombination Coefficients in the E- and F_1-Regions," Solar Eclipses and the Ionosphere (Ed., Beynon and Brown), Pergamon Press, New York, 1956, pp. 204-211.

21. Minnis, C. M., "The Interpretation of Changes in the E- and F_1-Layers during Solar Eclipses," J. Atmosph. Terr. Phys. 12, 272-282 (1958).

22. Blake, R. L., Chubb, T. A., Friedman, H., and Unzicker, A. E., "Interpretation of X-Ray Photograph of the Sun," Astrophys. J. 137, 3-15 (1963).

23. Piddington, J. H., "The Modes of Formation of the Ionospheric Layers," J. Geophys. Res. 56, 409-249 (1951).

24. Nestorov, G. and Taubenheim, J., "Untersuchungen an der Ionosphärischen E-Schict während der Totalen Sonnenfinsternis 15 February 1961," J. Atmosph. Terr. Phys. 24, 633-642 (1962).

25. Meriau, P. and Rawer, K., "Ionospheric Observations during the Eclipse of February 25, 1952 at Jibuti," Ann. Geophys. 10, 9-18 (1954).

26. Landmark, B., "Ionospheric Measurements in Norway during the Total Solar Eclipse of 30 June 1954," Solar Eclipses and the Ionosphere (Ed. Beynon and Brown) Pergamon Press, New York, 1956, pp. 54-56.

27. Rydbeck, O. E. H. and Wilhelmsson, H., "A Theoretical Investigation of the Ionospheric Electron De ity Variation during a Solar Eclipse," Trans. Chalmers Univ. Tech., No. 149 (1954).

28. Burkard, O., "Temperature-Controlled Variations of the Ionosphere during an Eclipse," Solar Eclipses and the Ionosphere (Ed. Beynon and Brown) Pergamon Press, New York, 1956, pp. 69-73.

29. Byram, E. T., Chubb, T. A., Friedman, H., Kupperian, J. E., Jr., and Kreplin, R. W., "Intensity of Solar Lyman-Alpha and Adjacent Ultraviolet Emission Lines," Astrophys. J. 128, 738-841 (1958).

30. Purcell, J. D. and Tousey, R., "Photography of the Sun in Lyman-Alpha and other Wavelengths," NRL Report 5608, Washington, D.C. (21 July 1961).

30a. Mitra, S. K., The Upper Atmosphere, The Asiatic Society, Calcutta, India, 1952, p. 313.

31. Aiken, A. C., "A Preliminary Study of Sunrise Effects in the D-Region," Electron Density Profiles (Ed.,B. Maehlum) Pergamon Press, New York, 1962, pp. 101-109.

32. Bates, D. R. and Massey, H. S. W., "The Basic Reactions in the Upper Atmosphere," Proc. Roy. Soc. London A187, 261-296 (1946).

33. Reid, G. C., "A Study of the Enhanced Ionization Produced by Solar Protons during a Polar Cap Absorption Event," Jounr. Geo. Res. 66, 4071-4085 (1961).

34. Reid, G. C. and Leinbach, H., "The Morphology and Interpretation of the Great Polar Cap Absorption Events of May and July 1959," Jour. Atmosph. Terr. Phys. 23, 216-228 (1962).

35. Reid, G. C., Bailey, D. K. and Leinbach, H., "On the Height Distribution of the Ratio of Negative Ions and Electron Densities in the Lowest Ionosphere," Jour. Atmos. Terr. Phys. 26, 145-147 (1964).

36. Hunt, G. B., Tech. Note PAD 84, Department of Supply, Australian Defence Scientific Service, Weapons Research Establishment, Salisbury, South Australia.